UNIVERSITÀ DEGLI STUDI FIRENZE

Da un secolo, oltre.

HR EXCELLENCE IN RESEARCH

PhD in
Chemical Science
cycle XXXVIII

COORDINATOR Prof. Anna Maria Papini

Electrochemical Strategies for Urea Quantification in Wastewater and Biological Fluids

Academic Discipline (SSD) CHEM-01/A

Doctoral Candidate
Dr. Lorenzo Quadrini

Supervisor
Prof. Ilaria Palchetti

Co-Supervisor
Prof. Anna Maria Papini

Co-Supervisor
Ing. Claudio Ciccone

Coordinator
Prof. Anna Maria Papini

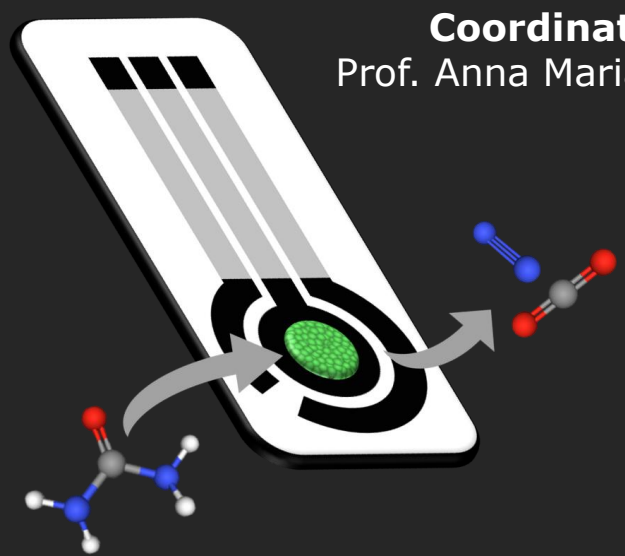

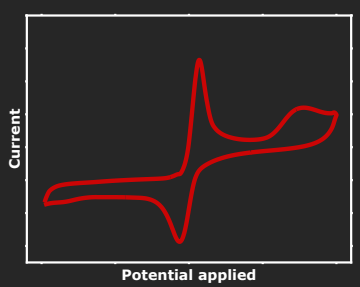

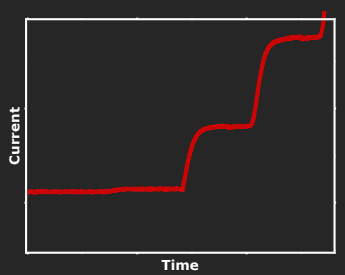

Finanziato dall'Unione europea NextGenerationEU
Ministero dell'Università e della Ricerca
Italiadomani
UNIVERSITÀ DEGLI STUDI FIRENZE

DOTTORATO DI RICERCA IN

Scienze Chimiche

CICLO XXXVIII - DM 352

Electrochemical Strategies for Urea Quantification in Wastewater and Biological Fluids

(topic: *Development of immersion and/or runoff measurement techniques for determining the concentration of Urea in water and organic liquids*)

Settore Scientifico Disciplinare

CHEM-01/A

Dottorando/a

Dott. Quadrini Lorenzo

Supervisore

Prof.ssa Palchetti Ilaria

Co-supervisore

Ing. Ciccone Claudio

Co-supervisore

Prof.ssa Papini Anna Maria

Coordinatore

Prof.ssa Papini Anna Maria

Contents

Preface 5
Abstract 6
Scientific Production 9
CHAPTER I 12
1. General Introduction: 13
1.1. History of urea 13
1.1.1. Background 13
1.1.2. First synthesis 14
1.2. Urea 14
1.2.1. Urea in humans 14
1.2.2. Urea in animals and plants 17
1.3. Industrial synthesis of urea 19
1.4. Environmental damage from fertilizers 25
1.5. Enzymatic catalysis 29
1.6. Urease 31
1.7. Biosensors 33
1.8. Electrochemical biosensors 34
1.9. Electrochemical methods for the determination of urea: Current trends and future perspective 36
1.9.1. Introduction 36
1.9.2. Direct electrochemical method for urea determination 40
1.9.3. Indirect electrochemical methods based on catalytic biosensors for urea determination 45
1.9.4. Potentiometric enzyme-based biosensors 47
1.9.5. Amperometric and impedimetric enzyme-based biosensors 53
1.9.6. Conclusions & further perspectives 60
CHAPTER II 62
2. Development of a flow biocatalytic-based platform for electrochemical monitoring of urea in wastewater 63
2.1. Introduction 64

2.2. Materials and methods 67
2.1.1. Reagents 67
2.1.2. Samples 68
2.1.3. Software 68
2.1.4. Measurements set-up & bioreactor assembly 68
2.1.5. Response Surface Methodology for parameters optimization 70
2.3. Results and discussion 71
2.2.1. NH_4^+-ISE sensor performances 71
2.2.2. Influence of the buffer composition 73
2.2.3. Reagent optimization by DoE in bioreactor assembly 75
2.2.4. Flow rate optimization 79
2.2.5. Calibration curves of urea in phosphate buffer 80
2.2.6. Application to real sample analysis 82
2.4. Conclusions 84
CHAPTER III 86
3. Industrial development and optimization 87
CHAPTER IV 91
4. Nanostructured Ni-based sensors for urea determination: a simple and novel approach for wastewater monitoring 92
3.1. Introduction 92
3.2. Materials and methods 95
3.2.1. Reagents 95
3.2.2. Measurement set-up 96
3.2.3. Samples 97
3.2.4. NiNPs synthesis 98
3.3. Results and discussion 100
3.3.1. NiNPs characterization 100
3.3.2. Analytical performance for urea determination 103
3.3.3. Interferents 105
3.3.4. Application to wastewater sample analysis 107
3.4. Conclusions 109

CHAPTER V 111
5. Final Conclusions 112
Bibliography 116

Preface

This doctoral research was conducted within an Industrial PhD program in collaboration with a private company operating in the field of wastewater treatment technologies. The primary objective of the project was to research, develop, and optimize innovative electrochemical sensing solutions for the quantitative monitoring of urea in complex aqueous matrices, with particular emphasis on continuous in-situ analysis. This industrial framework strongly shaped the research strategy, with an early focus on technological readiness, automation, device engineering, and scalability beyond laboratory-scale experimentation.

The multidisciplinary nature of the project, bridging analytical chemistry, electrochemical sensor technology, fluidic engineering, nanomaterials synthesis, and environmental applications, enabled the development of two complementary analytical platforms. The first relies on biocatalytic recognition by urease immobilized in a purpose-designed flow bioreactor, while the second exploits the electrocatalytic properties of nanostructured nickel-based materials to eliminate enzyme-related limitations. Both systems were optimized with respect to analytical robustness, operational sustainability, and real-sample applicability, ultimately contributing new technological knowledge and demonstrating viable industrial deployment routes.

Abstract

In the current scientific and technological landscape, the quantification of small organic molecules and metabolites plays a pivotal role across a variety of fields, ranging from clinical diagnostics to environmental monitoring. Among these compounds, urea occupies a unique position. In humans and animals, it represents the main product of nitrogen metabolism, making it an important biomarker for kidney and liver function as well as for the management of hemodialysis treatments. In parallel, urea is also one of the most widely produced industrial chemicals, largely employed as a nitrogen-based fertilizer in agriculture, in addition to applications in animal nutrition, cosmetics, and chemical manufacturing. However, excessive or mismanaged use of urea has severe ecological consequences, contributing to nutrient pollution, eutrophication, and harmful algal blooms in aquatic environments. The monitoring of urea levels is therefore of critical importance both in biomedical and environmental contexts.

Conventional analytical approaches, such as chromatographic or spectrophotometric methods, while accurate, are generally unsuitable for rapid, on-site monitoring due to their reliance on expensive instrumentation, time-consuming sample preparation, and limited portability. For this reason, electrochemical sensors and biosensors have emerged as promising alternatives, offering sensitivity, cost-effectiveness, and adaptability to miniaturized, portable, and even wearable devices. This Industrial PhD dissertation addresses the development of innovative electrochemical strategies for the quantification of urea in complex matrices, with particular

emphasis on wastewater monitoring, while providing a critical review of the state of the art and a perspective on future directions in the field.

Chapter I introduces the general framework of the thesis. It begins with a historical overview of urea, tracing its discovery, early isolation from urine, and the first laboratory synthesis by Friedrich Wöhler, which marked a milestone in modern chemistry. The chapter then discusses urea's physiological role in humans, animals, and plants, describing its centrality in the urea cycle and its relevance as a biomarker of renal dysfunctions and metabolic disorders. The industrial synthesis of urea is examined in detail, with particular attention to the Haber–Bosch and Bosch–Meiser processes, and the environmental burden associated with large-scale fertilizer use. Subsequently, the focus shifts to urease, the nickel-dependent enzyme that catalyzes the hydrolysis of urea, and its exploitation as a biorecognition element in biosensors. The chapter culminates in a comprehensive review of electrochemical methods for urea quantification, covering both direct approaches, based on the electrocatalytic oxidation of urea at suitable electrode materials, and indirect approaches, typically relying on urease-catalyzed hydrolysis and subsequent electrochemical detection of the reaction products. This critical review also highlights recent progress in electrode nanostructuration, microfluidic integration, and the application of artificial intelligence and machine learning to improve selectivity, data processing, and sensor optimization.

Chapter II is dedicated to the development of a biocatalytic-based flow platform for electrochemical monitoring of urea in wastewater. In this system, urease was immobilized within a bioreactor specifically designed for continuous operation, enabling real-time analysis of urea in complex aqueous matrices. A systematic optimization of the operating parameters was performed

using Response Surface Methodology (RSM) and Design of Experiments (DoE), with particular attention to buffer composition, reagent concentrations, and flow rate. The optimized platform was able to deliver reproducible and sensitive measurements with improved robustness compared to static systems. Crucially, its applicability was validated on real wastewater samples, demonstrating its potential as a reliable and practical tool for environmental monitoring. This work has been published in *Talanta (2025)*, providing one of the first examples of an integrated electrochemical biocatalytic platform specifically tailored for wastewater analysis.

Chapter III expands on the industrial optimization and system-integration aspects, trouble shooting, highlighting design choices enabling on-site operation, cartridge replacement strategies to compensate enzymatic degradation, and communication/control tools for Industry 4.0 deployment.

Chapter IV focuses on the design and characterization of a novel nickel-based electrochemical sensor. Nickel and its oxides are known for their remarkable electrocatalytic activity toward the urea oxidation reaction (UOR) under alkaline conditions, and represent a cost-effective alternative to noble metals such as platinum and palladium. In this study, nickel nanoparticles and nanostructured composites were synthesized and extensively characterized by dynamic light scattering, electron microscopy, and electrochemical techniques. The resulting nanomaterials provided high surface area, abundant active sites, and enhanced catalytic performance. The electrochemical behavior of the Ni-based sensors was evaluated in terms of sensitivity, linear range, limit of detection, and selectivity against common interferents. Application tests on real wastewater confirmed their practical feasibility. Importantly, these sensors do not rely on enzymatic components, thereby circumventing issues of enzyme stability, activity loss, and cost of biorecognition elements. The study,

submitted for publication, underlines the complementarity of enzymatic and non-enzymatic strategies and paves the way for new classes of non-enzymatic urea sensors.

Chapter V presents the general conclusions of the thesis. A comparative analysis between the two experimental strategies is offered: on one hand, the urease-based biocatalytic flow system, which provides high selectivity and biological relevance but suffers from the intrinsic limitations of enzyme stability; on the other hand, the Ni-based electrochemical sensor, which demonstrates robustness, lower costs, and freedom from biocatalyst-related issues, though at times challenged by selectivity. The strengths and weaknesses of both systems are critically discussed, together with their possible fields of application. Future perspectives include the integration of these sensors into microfluidic and lab-on-chip platforms, the development of wearable and point-of-care devices for real-time monitoring, and the use of artificial intelligence to improve data handling, predictive modeling, and interference correction. Beyond environmental applications, the methodologies developed in this work hold promise for clinical diagnostics, food quality control, and industrial process monitoring.

Overall, this dissertation advances the field of electrochemical sensing of urea by combining enzymatic and non-enzymatic approaches within innovative platforms. It provides both a thorough review of the state of the art and original contributions to the design, optimization, and validation of new sensing strategies. By addressing the challenges of sensitivity, selectivity, stability, and applicability in real matrices, this work demonstrates the feasibility of developing reliable, cost-effective, and versatile tools for urea monitoring. The outcomes contribute not only to bioanalytical chemistry but also to broader goals of sustainability, healthcare, and industrial innovation.

Scientific Production

Publications on the topic of the PhD project

- **Lorenzo Quadrini**, Serena Laschi, Claudio Ciccone, Filippo Catelani, Ilaria Palchetti; Electrochemical methods for the determination of urea: Current trends and future perspective; *TrAC Trends in Analytical Chemistry*, 168, 2023, 117345, ISSN 0165-9936, **DOI**:/10.1016/j.trac.2023.117345.
- **Lorenzo Quadrini**, Serena Orlandini, Serena Laschi, Claudio Ciccone, Filippo Catelani, Ilaria Palchetti; Development of a flow biocatalytic-based platform for electrochemical monitoring of urea in wastewater; *Talanta*, Volume 289, 2025, 127755, ISSN 0039-9140, **DOI**:10.1016/j.talanta.2025.127755.
- **Lorenzo Quadrini**; Novel Ni-based sensor for monitoring of urea in wastewater; TBD, 2025, IN PREPARATION.

Nonincluded publications

- Gina Elena Giacomazzo, Luca Conti, Daniele Paderni, Patrick Severin Sfragano, **Lorenzo Quadrini**, Eleonora Macedi, Camilla Andreini, Chiara Donati, Caterina Bernacchioni, Gloria Mulas, Barbara Valtancoli, Ilaria Palchetti, Luca Giorgi, Vieri Fusi, Francesca Cencetti, Claudia Giorgi; Ruthenium(II) Polypyridyl Complexes with Benzoxazole Derivatives and Non-Innocent Ligands as Effective Antioxidants in Human Neuroblasts; *Chemistry–A European Journal*, 2024, 30.38, e202400834, **DOI**:10.1002/chem.202400834.
- **Lorenzo Quadrini**, Emma Salvadori, Serena Laschi, Margherita Verrucchi, Alessio Gnerucci, Andrea Cagnini, Ilaria Palchetti;

Characterization of corrosion products on contemporary bronze artwork by using voltammetry of microparticles and PCA; *Microchemical Journal*, 200, 2024, 110330, ISSN 0026-265X, **DOI**:10.1016/j.microc.2024.110330.

- Andrea Revilla-Cuesta, Irene Abajo-Cuadrado, **Lorenzo Quadrini**, Sara Failli, Andrea Rodríguez-Rubio, José V. Cuevas, Carla Hernando-Muñoz, José García-Calvo, Tomás Torroba; Chemical speciation of methylmercury and mercury(II) cations in fish by new fluorogenic naphthalimide alkynyl gold complexes: The ultimate test for detecting fish contamination; *Sensors and Actuators B: Chemical*, 421, 2024, 136492, ISSN 0925-4005, **DOI**:10.1016/j.snb.2024.136492.

CHAPTER I

This chapter provides a general introduction and an overview of the state of the art in electrochemical sensors for the quantification of urea in matrices of different origins.

1. General Introduction:

1.1. History of urea

1.1.1. Background

Urea, also known as carbamide, is the diamide of carbonic acid with the chemical formula $CO(NH_2)_2$. It has a molar mass of 60.06 g/mol. Due to the presence of a carbonyl group, urea is a polar molecule; it is highly soluble in water as a result of its ability to readily form hydrogen bonds, while maintaining an overall neutral charge [1].

The first documented isolation of urea dates back to the early 18th century and is attributed to Herman Boerhaave (1688–1738), a Dutch botanist and chemist from Leiden. In his seminal work *Elementa Chemiae* (published in 1732), Boerhaave provided a detailed description of the procedures to demonstrate the actual presence of urea in urine, presenting a study based on the urine of a healthy individual.

In 1773, Hilaire-Marin Rouelle (1718–1779), a natural scientist, succeeded in isolating urea once again, and he is more commonly recognized as the true discoverer of this compound. A few decades later, in 1808, Antoine-François de Fourcroy (1755–1809) and Louis Nicolas Vauquelin (1762–1829), both prominent figures in 19th-century chemistry, assigned the name “urée” to the substance, emphasizing its specificity to urine. Subsequently, in 1817, Joseph Frédéric Bérard (1789–1828) refined the characterization of urea’s chemical composition, building upon the earlier work of Fourcroy and Vauquelin in France. He reported that urea derived from urine contained 43.4% nitrogen, 19.4% carbon, 10.8% hydrogen, and 26.4% oxygen [2].

1.1.2. First synthesis

Almost one century after Boerhaave's pioneering observations, the German chemist Friedrich Wöhler (1800–1882) achieved the groundbreaking result of synthesizing urea in the laboratory [1]. Interestingly, Wöhler's original intention was not to produce synthetic urea. His discovery occurred unexpectedly while combining lead cyanate with ammonia and water, which resulted in the formation of ammonium cyanate and lead hydroxide (Reaction 1):

$$Pb(OCN)_2 + 2NH_3 + 2H_2O \rightarrow Pb(OH)_2 + 2NH_4(OCN) \quad (1)$$

Upon heating ammonium cyanate, Wöhler realized that the resulting product exhibited the same properties as urea [1]. This accidental synthesis not only marked a turning point in the study of urea but also represented a milestone in the history of chemistry, as it challenged the prevailing vitalist theories by demonstrating that an organic compound could be produced from inorganic precursors.

1.2.Urea

1.2.1. Urea in humans

Nitrogen is abundantly present in the atmosphere as molecular nitrogen (N_2), in organic forms within soil, and as ionic species in plants and microorganisms. In living organisms, non-protein nitrogen primarily occurs in the form of ammonia. Since ammonia is the precursor molecule used to incorporate nitrogen into animal tissues, it plays an essential role as a substrate in the biosynthesis of amino acids, proteins, and nucleic acids. However, despite its importance in metabolism, an excess concentration of ammonia (around 50

μM) can be toxic, thereby requiring regulatory mechanisms to control its flux within organisms [3].

In ureotelic organisms, including humans, mammals, and certain amphibians—urea is synthesized as part of the urea cycle, primarily from amino acid oxidation or directly from ammonia. This process occurs continuously in the liver [4], urea thus represents a non-toxic, nitrogen-containing organic end product of protein metabolism and accounts for the elimination of approximately 80–90% of nitrogen from the human body [5].

The urea cycle was discovered in 1932 by Hans Krebs (1900–1981) and Kurt Henseleit (1907–1973) and is recognized as the first metabolic cycle ever described. Within this cycle, urea is produced through a sequence of reactions in which the amino acid ornithine serves as a carrier for the various intermediates formed. The reactions of the urea cycle occur predominantly in the mitochondria and cytosol of cells [1], with arginase being the key enzyme responsible for the hydrolytic cleavage of arginine into urea and ornithine.

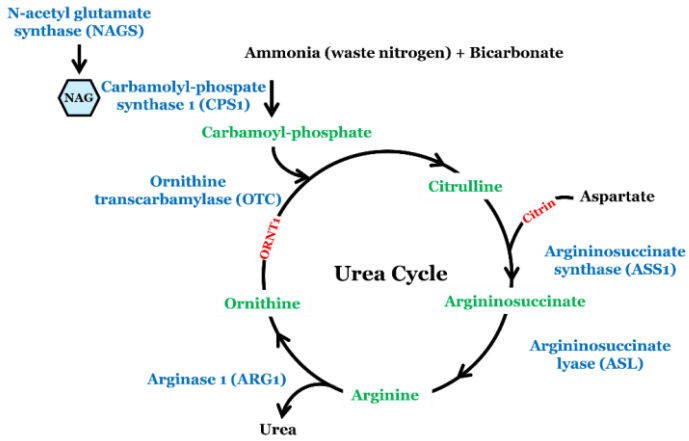

Figure 1. *Reactions of the urea cycle.*

The reactions involved in the urea cycle are illustrated in **Figure 1**, but they can also be summarized into a single overall reaction (2):

$$NH_4^+ + HCO_3^- + Asp + 3ATP \rightarrow Urea + fumarate + 2ADP + AMP + 2Pi + PPi \quad (2)$$

Most of the urea formed in the human body is excreted in urine, with approximately 400 mmol eliminated daily, while only a small fraction is lost through perspiration [6].

To assess blood urea nitrogen (BUN), clinical examinations are performed, providing valuable information about renal function [7]. Normal serum/plasma levels of urea range between 15 and 40 mg/dL. Elevated concentrations of urea are associated with a wide variety of pathological conditions, including indigestion, acidity, ulcers, cancer, renal dysfunction, renal failure [8], urinary tract obstruction, dehydration, circulatory collapse, burns, and gastrointestinal hemorrhage. Conversely, abnormally low levels of urea may indicate hepatic insufficiency, nephrotic syndrome, or cachexia [8]. Additionally, reduced blood urea levels may reflect inadequate protein intake or excessive alcohol consumption [9].

A number of diseases are therefore linked to urea, particularly those related to impaired elimination of nitrogenous waste products generated by normal metabolic processes. These conditions are referred to as urea cycle disorders, in which the pathological accumulation of urea in the blood can result in severe intoxication of the central nervous system. Deficiencies in specific enzymes, each of which plays a critical role in the conversion of ammonia to urea, underlie the individual types of urea cycle disorders.

In general, these disorders manifest in the neonatal period, but the initial symptoms are often nonspecific. Most affected infants are born at a normal

weight and appear healthy, but within hours, sometimes less than 24, they may develop vomiting, irritability, loss of appetite, and other vague symptoms. This can subsequently progress to secondary complications, including impaired liver function, and if untreated, may result in death due to cerebral or pulmonary hemorrhage [10].

Urea is also commonly used as a biomarker for the severity of chronic kidney disease (CKD). For many years, urea was regarded as a relatively inert and non-toxic compound; however, recent studies have contradicted this assumption [11]. Patients with CKD experience a progressive decline in renal function, losing the ability to excrete potentially toxic compounds in urine. These retained solutes are known as “uremic retention solutes,” and when they are biologically active, they are referred to as “uremic toxins.” Their accumulation negatively affects multiple physiological systems, particularly the cardiovascular system. Moreover, recent evidence has shown that elevated urea levels directly impair intestinal epithelial permeability and barrier integrity, thereby promoting the production and absorption of uremic toxins as well as altering the gut microbiota [11].

1.2.2. Urea in animals and plants

Not all living organisms rely on the urea cycle to eliminate nitrogenous waste. Depending on their habitat, animals have evolved two main alternative strategies:

- Ammoniotelic, characteristic of aquatic species, in which ammonia is directly excreted.
- Uricotelic, typical of birds and reptiles, involving the excretion of uric acid [12].

Aquatic organisms excrete nitrogen primarily as ammonia despite its high toxicity, since ammonia is highly soluble in water and can be safely eliminated at low concentrations [12].

In most mammalian species, urea is considered the main nitrogenous waste product, derived from the detoxification of ammonia. However, ruminants have evolved the ability to recycle urea within the gastrointestinal tract, particularly through ruminal microflora. This recycling mechanism is essential for maintaining nitrogen balance in these species [13].

In monogastric animals, the precursors for urea synthesis mainly originate from tissue nitrogen metabolism. In contrast, in ruminants, more than 60% of plasma urea nitrogen can be derived from ruminal ammonia. In these animals, urea and ammonia, together with amino acids, peptides, and microbial crude proteins, play a key role in nitrogen digestion and metabolism. Although the liver is the principal site of urea production, other tissues also possess enzymatic activity necessary for its synthesis. Once released into the bloodstream, urea can either be excreted in urine or diffuse back into the digestive tract, either through saliva or directly across the intestinal wall [14].

The extent of urea production, excretion, and recycling depends strongly on dietary composition and animal intake. Depending on these factors, between 19% and 96% of endogenous urea production may be recycled in the intestine, with 15–94% of this recycled fraction transferred into saliva, and 25–90% degraded in the post-ruminal digestive tract. Urinary urea excretion accounts for approximately 25–60% of endogenous production in goats, sheep, cows, and cattle [14].

In plants, urea also plays an important role, as it accumulates in plant cells as a result of secondary nitrogen metabolism. Two major biochemical pathways

can lead to the synthesis of urea: the urea cycle itself, and the degradation of purines or ureides. For instance, leguminous species use ureides for long-distance nitrogen translocation, thereby introducing larger amounts of nitrogen through urea into their storage tissues.

Since urea accumulation is particularly high in senescing leaves and germinating seeds, it has been suggested that it primarily reflects nitrogen recycling from protein catabolism, especially that of arginine, supported by elevated levels of arginase relative to total seed proteins [15].

At least three key enzymes are involved in urea metabolism in plants: arginase, urease, and glutamine synthetase. Most ureolytic organisms employ urease, a nickel-dependent metalloenzyme (nickel-urease), which catalyzes the hydrolysis of urea to form ammonia and carbon dioxide. Specifically, the hydrolysis of one urea molecule releases two molecules of ammonia and one molecule of carbon dioxide. The principal role of urease is to enable the organism to exploit urea, whether produced internally or absorbed externally, as a nitrogen source [16].

Only certain algae, fungi, and bacteria employ an alternative urease-independent pathway that involves two distinct enzymatic reactions. Nonetheless, urease activity is widespread in plants, if not universal, and is present in various tissues, including potato and soybean [17].

1.3. Industrial synthesis of urea

From an industrial perspective, the first commercial production of solid synthetic urea began relatively late, in November 1935, in the United States. Nevertheless, the synthetic route that underpins industrial production was proposed much earlier: in 1868, Alexander I. Basaroff described the synthesis

of urea from carbon dioxide and ammonia by heating ammonium carbonate in a sealed glass tube, thereby laying foundational knowledge for subsequent industrial processes [18].

Over time, urea production has expanded dramatically. Today, the principal producing countries include Russia, Canada, Saudi Arabia, and several Middle Eastern states such as Iran and Iraq. Global demand has steadily increased: world urea production reached approximately 183.82 million tons in 2022, compared with 147 million tons in 2009 [19].

The industrial manufacture of urea typically comprises two main integrated processes: ammonia synthesis and subsequent urea synthesis, the latter using ammonia and carbon dioxide [20,21].

Ammonia is produced industrially by the Haber–Bosch process, named after Fritz Haber (1868–1934) and Carl Bosch (1874–1940). Haber patented the modern method for ammonia synthesis in 1905, and Bosch extended it to industrial scale in 1910; the process remains the backbone of industrial ammonia production [1,21].

The process begins with hydrogen generation, typically via steam reforming of methane or other natural gases. At elevated temperature and pressure, hydrogen is reacted with atmospheric nitrogen over an iron-based catalyst to yield ammonia. These conditions (high pressure, high temperature, catalyst) are energetically demanding but effective for large-scale NH_3 production [1].

The produced Ammonia by Haber–Bosch is then employed in the industrial synthesis of urea via the Bosch–Meiser process (**Figure 2**), developed in 1922 and currently the dominant industrial rout [22]. The mechanism comprises two principal steps:

1. Formation of ammonium carbamate (exothermic):

$$CO_2 + 2NH_3 \longrightarrow NH_2COONH_4 \quad (3)$$

2. Dehydration of ammonium carbamate to urea (endothermic):

$$NH_2COONH_4 \longrightarrow NH_2CONH_2 + H_2O \quad (4)$$

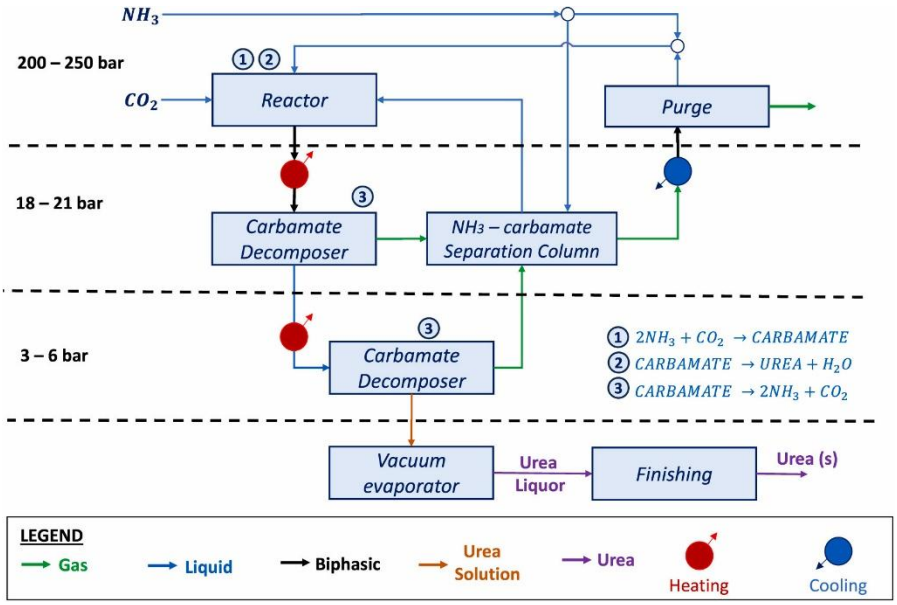

Figure 2. *Diagram of a Bosch–Meiser plant for urea production [23].*

The first reaction is strongly exothermic and proceeds rapidly at roughly 135–200 °C, provided that the system pressure exceeds the decomposition pressure of ammonium carbamate at the operating temperature. The reaction medium must be essentially anhydrous; the presence of free water molecules favors the formation of ammonium carbonates and generates a metastable, complex aqueous system.

By contrast, the second (dehydration) step is endothermic and kinetically sluggish, limiting urea yield. It is never complete under practical conditions and therefore requires recycling and dissociation stages. Kinetic barriers

include the formation of the second C–N bond in urea and the cleavage of the C–O bond in the carbamate. Various catalysts and promoters have been investigated to accelerate this step, including water and ammonia as homogeneous promoters, soluble metal complexes, and cerium dioxide. The reaction rate increases markedly above ~160 °C [24]. Because ammonium carbamate is relatively volatile at these temperatures, synthesis must be carried out under elevated pressure to maintain the desired liquid-phase regime. The overall liquid-phase product is therefore a complex mixture of water, urea, unconverted ammonium carbamate, and ammonium carbonates [25].

From an operational viewpoint, the urea production cycle can be divided into three stages: (i) raw-material preparation, (ii) synthesis, and (iii) effluent/waste treatment. In the preparation stage, natural resources are processed and supplied to the plant as feedstock. In the synthesis stage, ammonia is produced (from coal or natural gas) and then reacted with CO_2 to produce urea. In the waste-treatment stage, flue gases, wastewater, and solid residues are managed and disposed of appropriately [20].

Several issues complicate industrial urea manufacture. First, the requirement for high temperature and pressure makes the process highly energy-intensive and a significant source of CO_2 emissions. Second, ammonium carbamate is highly corrosive toward steel and other construction materials; thus, unconverted carbamate must be decomposed back to the original reagents for recycling and to limit reactor damage. Thermal control is also critical because formation of ammonium carbamate is highly exothermic and can generate hot-spots if not properly managed [22,23].

Unwanted side reactions further complicate product quality. One important parasitic reaction is biuret formation, which results from the condensation of two urea molecules with the release of ammonia:

$$2H_2CONH_2 \leftrightarrow C_2H_5N_3O_2 + NH_3 \quad (5)$$

Biuret is toxic and must be removed; its formation is minimized by shortening residence time in process zones favorable to its formation, controlling temperature and maintaining an excess of ammonia to shift equilibria toward urea.

Another undesirable pathway is urea decomposition to isocyanic acid:

$$H_2CONH_2 \leftrightarrow HNCO + NH_3 \quad (6)$$

Again, operating with ammonia in excess moves the equilibrium back toward urea and mitigates this decomposition [26].

Urea production is central to multiple industrial and agricultural sectors due to its chemical properties and versatility. The largest application (>75% of global use) is as a nitrogen fertilizer. Non-fertilizer uses are also significant and growing.

In agriculture, aside from direct fertilizer application, urea is used as a feed additive for ruminants (approximately 10% of non-fertilizer uses). This practice aims to stimulate ruminal microflora and enhance microbial protein synthesis; urea can be applied directly to forages (e.g., wheat or rice straw) or blended with molasses to create “urea–molasses licks” or multi-nutrient blocks for sheep, cattle, buffalo, and horses [27]. Feeding strategies that supply adequate degradable rumen protein are crucial for meat and milk production; however, modern intensive systems often provide protein in excess of the animal’s productive response, so a substantial fraction of dietary nitrogen is

excreted in urine and feces. This excreted nitrogen becomes an environmental issue if soil absorption and reuse capacities are exceeded, a problem increasingly evident with livestock intensification [13].

Urea derivatives are also employed as agrochemicals: substituted urea (particularly trisubstituted urea) such as Fenuron, Monuron and Diuron (**Figure 3**), function as herbicides by inhibiting photosynthesis in target weeds [13]. Despite their effectiveness and synthetic accessibility, these compounds raise environmental and human-health concerns: less than 1% of applied pesticides typically reach the intended target, while the majority disperses into aquatic environments via runoff and leaching, making some urea-derived pesticides common organic contaminants in natural waters [28].

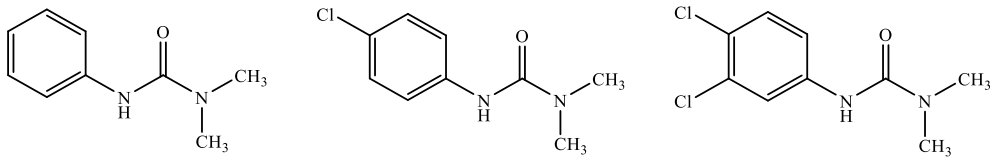

Figure 3. *Structural formulas in order, of the pesticides Feuron, Monuron, and Diuron.*

In the chemical industry, urea is a key precursor for producing complex organic materials such as urea–formaldehyde resins (UF), melamine–formaldehyde, phenol–formaldehyde and melamine–urea–formaldehyde (MUF) resins. These polymers are widely used in laminates, coatings, industrial adhesives, and insulating materials [29]. Classic urea–formaldehyde resins have desirable mechanical properties and low cost but suffer from formaldehyde emissions; accordingly, melamine-modified UFM resins, offering lower formaldehyde release, durable bonding, and moisture resistance, have attracted interest [30].

Pharmaceutically and cosmetically, urea is valued for keratolytic, humectant and permeation-enhancing properties. Emulsions containing 5% urea have been shown to increase skin water-holding capacity, and urea is commonly

included in topical treatments for psoriasis, atopic dermatitis and hyperkeratosis [31]. It is also widely used in cosmetic formulations for skin and hair care due to its moisturizing benefits [32].

A further major application is in transportation: urea is the active component of AdBlue, an ultra-pure aqueous urea solution (~32.5% urea w/w in demineralized water) used in modern diesel vehicles to reduce NO_x emissions via selective catalytic reduction (SCR). AdBlue is injected into exhaust gases where urea decomposes to generate ammonia, which then reacts over a catalyst to convert NO_x to N_2 and H_2O [33].

1.4. Environmental damage from fertilizers

As introduced previously, the major field of application for urea is in nitrogen fertilizers, since nitrogen is the most widely used element in soil fertilization. It is estimated that nitrogen-based fertilizers are responsible for feeding 48% of the global population and that 80% of the nitrogen present in human tissues originates from such compounds [34]. Among nitrogen fertilizers, urea is today the most important for global agriculture [35] because it contains 46% nitrogen, is inexpensive, and is easy to apply [36]. Moreover, urea can be administered to soil in solid or solution form, or even as foliar sprays for certain crops, while presenting negligible fire and explosion hazards. In addition, it is unique that its transformation to ammonium and its utilization efficiency are governed by the enzymatic activity of urease (Reaction 7) [36].

Urea-based fertilizers range from dry, granular urea, which can be mixed with $Ca(H_2PO_4)_2$ and K_2CO_3 like products, to blended fertilizers containing urea and other nitrogen, phosphate, or potassium sources. The most common nitrogen mixture is liquid urea–ammonium nitrate solution (UAN) [37].

Once applied to soil, urea undergoes a series of chemical, physical, and biological transformations to generate plant-available nutrients, according to the following reactions:

$$(NH_2)_2CO + 2H_2O \xrightarrow{\text{Urease}} (NH_4)_2CO_3 \quad (7)$$

$$(NH_4)_2CO_3 + 2H^+ \xrightarrow{\text{Ammonification}} 2NH_4^+ + CO_2 + H_2O \quad (8)$$

$$2NH_4^+ + 3O_2 \xrightarrow{\text{Nitrosomonas/Nitrosococcus}} 2NO_2^- + 2H_2O + 2H^+ + \text{Energy} \quad (9)$$

$$2NO_2^- + O_2 \xrightarrow{\text{Nitrobacter}} 2NO_3^- + \text{Energy} \quad (10)$$

$$NO_3^- \xrightarrow{\text{Microorganisms/}O_2\text{ deficit}} N_2 + N_2O \quad (11)$$

$$NH_4^+ \xrightarrow{\text{Urease/basic soil pH}} NH_3(g) + H^+ \quad (12)$$

Reactions (8) and (10) yield the essential nutrients required by plants. However, since plants require only limited amounts of nutrients during their growth, excess nitrogen is lost by leaching [38], which occurs when free nitrate is washed away from the root zone during heavy rainfall. This phenomenon is not only inefficient but also environmentally hazardous. Conversely, in reactions (11) and (12), nitrogen is emitted into the atmosphere in gaseous form [38].

The rapid hydrolysis of urea to ammonium carbonate by soil urease presents several complications [36]. First, if the soil pH is significantly higher than 7, substantial amounts of ammonia may form due to the equilibrium:

$$NH_4^+ \rightleftharpoons NH_3 + H^+ \quad (13)$$

Ammonium ions themselves are generally retained by soil and absorbed by plants, without gaseous losses. In contrast, ammonia is volatile and toxic to plants and animals at elevated concentrations.

The concentration of ammonia formed in soil depends on multiple factors:

- Soil urea concentration: higher concentrations accelerate hydrolysis and thus increase ammonia production.
- Soil pH: elevated pH shifts the equilibrium toward ammonia formation.
- Rate of urea hydrolysis: rapid hydrolysis limits the diffusion time of urea and ammonium deeper into soil, resulting in localized accumulation, elevated pH, and enhanced ammonia volatilization. Hydrolysis rates are further influenced by soil urease activity, temperature, and moisture content [39].

High levels of organic matter and crop residues further enhance hydrolysis and ammonia volatilization, largely because urease is produced by microorganisms whose activity increases in organic-rich soils compared to mineral soils [40].

Another significant issue is the accumulation of nitrite (NO_2^-) in urea-fertilized soils, which can cause nitrogen losses as gaseous products from nitrite decomposition, as well as groundwater contamination by nitrates [35]. When excessive fertilizer is applied relative to plant demand, urea is not fully absorbed, and residual nitrates dissolve in water, entering surface and groundwater flows. In compact or waterlogged soils, nitrates can undergo microbial denitrification, returning nitrogen to the atmosphere as N_2 or nitrous oxide (N_2O) [41].

Additionally, numerous studies indicate that urea fertilizers can negatively impact seed germination, early plant development, and growth. These effects are largely attributed to ammonia generated via urease-mediated hydrolysis, as well as impurities in commercial fertilizers such as biuret or cyanuric acid, and nitrite accumulation during nitrification [35].

To address these challenges, several strategies have been developed, including the addition of polymers, sulfur, calcium salts, and particularly urease inhibitors [42]. The latter have shown the greatest success, as they slow urea hydrolysis [36], allowing more time for soil infiltration and subsequent mineralization, while stabilizing nitrogen in soil exchange complexes or making it more readily available for plant uptake [42].

Despite its benefits in agriculture, urea remains an environmental contaminant of concern, both as fertilizer and in other applications such as animal feed and pesticides. Excess nitrogen and phosphorus, major nutrients also present in wastewater, can reach rivers, lakes, and marine environments, where they promote eutrophication [27].

Eutrophication is driven by uncontrolled algal and plant growth due to nutrient enrichment. Its most evident effect is the proliferation of phytoplankton blooms, which reduces water clarity, diminish light penetration, and damage aquatic ecosystems. Excessive photosynthesis depletes dissolved inorganic carbon and drives pH to extreme levels. When algal blooms eventually die, microbial decomposition consumes dissolved oxygen, creating anoxic conditions that cause massive mortality among aquatic organisms [43].

Moreover, algal proliferation can release toxins harmful to human health, contaminating drinking water and food resources [43].

One of the primary reasons why urea remains largely unmonitored is that it is highly biodegradable and undergoes rapid transformation into ammonium and nitrate in aquatic systems. This dynamic behavior makes it difficult to trace urea back to specific sources of nitrogen surplus, since the original molecule often disappears before detection. Furthermore, the temporal and spatial variability of urea loading, especially via agricultural runoff or urinary inputs,

requires rapid, in situ detection methods rather than conventional low-frequency sampling. Together, these factors highlight the critical need for monitoring and regulatory frameworks that support on-site, real-time sensing of urea and its rapid derivatives to adequately address nitrogen-driven eutrophication and nutrient pollution. This highlights the urgent need to monitor and regulate urea concentrations in aquatic systems to protect ecosystems, safeguard water resources, and promote sustainable agricultural practices. Enforcement of European, national, and regional regulations is essential to mitigate these environmental impacts.

1.5. Enzymatic catalysis

Life depends on a multitude of chemical reactions, some of which are too slow to sustain biological processes without assistance. To overcome this limitation, nature has evolved biocatalysts known as enzymes. These macromolecules, primarily proteins, are capable of accelerating biochemical reactions by up to 10^{17}, fold by lowering the energy barriers required for the conversion of substrates into products [44].

Proteins are biopolymers composed of 22 proteinogenic amino acids, encoded directly by the universal genetic code. Amino acids are linked via peptide bonds, amide linkages formed between the carboxyl group of one amino acid and the amino group of another, releasing one molecule of water. These bonds are rigid and planar, forming the backbone of the polypeptide chain, while the variable side chains (residues) provide chemical diversity [45].

Protein architecture is organized into four structural levels: (i) the primary structure, a linear sequence of amino acids; (ii) the secondary structure, local conformations stabilized by hydrogen bonding (α-helices and β-sheets); (iii) the tertiary structure, the three-dimensional arrangement governed by side-

chain interactions; and (iv) the quaternary structure, the functional assembly of multiple polypeptide subunits [45].

For a protein to be defined as an enzyme, several features must be satisfied: it must not be consumed in the reaction; it must act effectively at low concentrations; and it must display substrate specificity, catalyzing only particular chemical transformations [44]. Enzymes achieve catalysis through their unique three-dimensional conformations, which optimize substrate alignment, facilitate bond formation or cleavage, and contribute to thermodynamic stability.

The catalytic process involves the formation of an enzyme–substrate (ES) complex, which then transitions into an enzyme–product (EP) complex before releasing the final product (P) and regenerating the enzyme (E):

- Uncatalyzed reaction: $S \rightleftarrows P$
- Catalyzed reaction: $E + S \rightleftarrows ES \rightleftarrows EP \rightleftarrows E + P$

Notably, only a small fraction of the enzyme, the *active site* (≈10–20% of the structure), interacts directly with the substrate. The classical *lock-and-key model* proposed by Emil Fischer in 1894 explains enzyme specificity through structural complementarity between enzyme and substrate [46]. Interactions at the active site can include electrostatic forces, hydrogen bonds, van der Waals interactions, and hydrophobic effects.

However, this model does not account for conformational flexibility. In 1958, Daniel E. Koshland Jr. proposed the *induced-fit model*, whereby the enzyme undergoes a conformational change upon substrate binding, achieving complementarity only during ES complex formation [45]. This duality

suggests that enzymes are both preformed for specific substrates (lock-and-key) and adaptable (induced fit).

Some enzymes require cofactors to function. Cofactors may be small organic molecules, metal ions, or metal complexes. The protein alone, termed an *apoenzyme*, is catalytically inactive; the active form, including both apoenzyme and cofactor, is called a *holoenzyme*. Organic cofactors, known as *coenzymes*, temporarily bind to enzymes, often mediating electron transfer in redox reactions. In contrast, *prosthetic groups* are tightly or covalently bound cofactors, either metal-containing or non-metal-containing, that remain integral to the enzyme [44].

1.6. Urease

Urease, also known as urea amidohydrolase, is a cytosolic metalloenzyme containing nickel [47]. It catalyzes the hydrolysis of urea into ammonia and carbamate; the latter is unstable and spontaneously decomposes into a second ammonia molecule and carbonic acid. Because the final products exist in equilibrium with their protonated and deprotonated forms, the reaction causes an increase in pH [48].

Urease was the first enzyme to be crystallized (from *Canavalia Ensiformis*, Jack Bean) in 1926, providing the first proof of the protein nature of enzymes and highlighting the essential role of nickel in biological catalysis.

Ureases are widely produced across species except Animalia, accelerating the urea-to-ammonia conversion rate by at least 10^{14} times compared to uncatalyzed reactions, making them among the most efficient enzymes known. In plants, urease prevents urea accumulation from arginine degradation and

facilitates nitrogen mineralization. The pH changes induced by urease activity also help certain microbial pathogens, such as *Helicobacter pylori*, survive and colonize specific host environments like the human stomach [47,48].

Most urease isoforms share conserved active-site structures and amino acid sequences, although overall quaternary structures, chain topologies, and oligomeric assemblies are variable. Each enzyme contains multiple binding sites corresponding to its functional monomers [49].

The active site generally consists of two nickel ions (Ni^{2+}) coordinated by four histidines (His), an aspartate (Asp), and a carbamylated lysine (Lys). The Ni^{2+} ions are bridged by the carbamylated lysine and a hydroxide ion, with only one Ni^{2+} additionally coordinated by the aspartate. Before urea binding, three water molecules coordinate the Ni^{2+} ions, forming a tetrahedral water cluster with hydrogen bonding (**Figure 4**)[50]. Despite decades of study, the precise position of the nickel ions within the metal center and their role in urea binding remain debated [47].

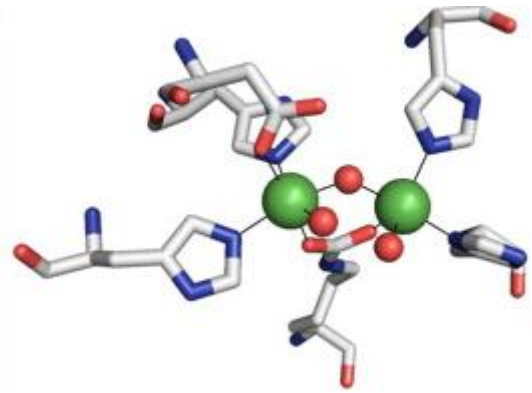

Figure 4. *Urease active site [50].*

Urea binding involves the carbonyl oxygen interacting with one Ni^{2+}, inducing a conformational change in a 30-amino-acid mobile flap that closes over the

754 active site during catalysis. Subsequently, one of the urea nitrogen binds the
755 second Ni^{2+}, forming a bidentate interaction that makes the urea carbon more
756 susceptible to nucleophilic attack by a nearby hydroxide ion or water molecule
757 [47].

758 Given the extensive biochemical and structural studies conducted on urease,
759 and its unique catalytic role in urea hydrolysis, this enzyme has been widely
760 exploited as a biorecognition element. Its robust activity and well-
761 characterized mechanism have made urease one of the earliest and most
762 studied enzymes in the development of biosensors for urea detection.

763 1.7. Biosensors

764 Biosensors is device that uses specific biochemical reactions mediated by
765 isolated enzymes, immunosystems, tissues, organelles or whole cells to detect
766 chemical compounds usually by electrical, thermal or optical signals [51].
767 Their defining feature is the incorporation of a biorecognition element, often
768 termed a biochemical receptor, bioreceptor, or biorecognition molecule, that
769 selectively interacts with the target analyte. This interaction is converted by a
770 transducer into a measurable signal, which is then processed and displayed as
771 analytical output [52].

772 Based on their operating principles, biosensors can be broadly divided into two
773 main classes: catalytic biosensors, which rely on biocatalytic reactions and
774 measure the concentration of species produced or consumed over time [53],
775 and affinity biosensors, which detect physicochemical changes resulting from
776 the binding of an analyte to its complementary receptor [54].

Further classification is determined by the transduction mechanism employed and the nature of the bioreceptor [52,55,56]. Examples include:

i. magnetic biosensors, which detect phenomena such as magnetoresistance or giant magnetoresistive effects;
ii. calorimetric biosensors, which measure heat generated or absorbed during biochemical reactions;
iii. micromechanical biosensors, based on the deflection of cantilevers coated with bioreceptors, and their function relies on surface stress changes or mass variations upon analyte binding;
iv. piezoelectric and microgravimetric devices, where oscillating crystals register frequency shifts upon mass loading and they detect analyte binding through resonance frequency shifts caused by added mass;
v. optical biosensors, exploiting changes in optical properties of molecules after analyte interaction, with or without labeling;
vi. electrochemical biosensors, which measure electron transfer processes at electrode interfaces, either through electroactive analytes or mediator species.

This work will primarily focus on electrochemical biosensors, due to their versatility and widespread application in bioanalytical chemistry.

1.8. Electrochemical biosensors

Electrochemical biosensors represent a major branch of modern bioanalytical sensing, offering several advantages such as high sensitivity, low cost, and strong compatibility with portable and point-of-care platforms [57]. Depending on the type of bioreceptor employed, they can be designed for

either catalytic or affinity-based detection. Binding or catalytic events occurring at the electrode surface result in measurable electrical signals.

Several transduction strategies exist, each suited to different analytical requirements:

- Potentiometric biosensors, which measure potential differences between working and reference electrodes under zero-current conditions [58].
- Amperometric biosensors, which quantify currents arising from redox reactions at a fixed applied potential; the resulting current is proportional to analyte concentration [59].
- Voltammetric biosensors, which employ potential sweeps to record current responses, enabling both qualitative and quantitative analyte analysis through diverse waveforms [60].
- Impedimetric biosensors, which monitor changes in impedance at the electrode–solution interface upon biorecognition [61].
- Conductometric biosensors, which measure conductance variations between two electrodes under alternating potential [62].
- Field-effect transistor (FET)-based biosensors, which convert biochemical or ionic interactions directly into amplified electronic signals proportional to analyte concentration [63].

In addition to the transduction approach, electrochemical biosensors can operate in label-based or label-free formats. Label-based methods involve coupling analytes with electroactive tags, while label-free systems detect intrinsic changes at the electrode interface upon recognition events.

1.9. Electrochemical methods for the determination of urea: Current trends and future perspective

Urea is the final product of nitrogen metabolism in mammals. In human beings, it is a main indicator of liver and kidney activity and a marker for hemodialysis treatments. Furthermore, urea is used in many industrial processes, in agriculture and in the farm industries. Thus, it is important to evaluate the level of this compound in biological fluids, in environmental matrices and in food samples. Electrochemical sensors represent an interesting tool for simple, rapid, in-situ, in-flow monitoring of urea. This review focuses on the recent advancements in electrochemical sensors and biosensors for urea determination. An overview of the existing electroanalytical approaches for urea determination is presented, and some new strategies are discussed, particularly those based on nanostructuration of the electrode surface. Finally, a brief description of the role that Artificial Intelligence could have in overcoming selectivity issues and speed of the analysis is also discussed.

1.9.1. Introduction

Urea, also known as carbamide, is an organic compound with the chemical formula $CO(NH_2)_2$. In human beings, urea is a product of protein catabolism and helps in preventing acidosis or ionic decompensation caused by NH_4^+ [64]. Under normal conditions, the bloodstream concentration of urea varies from 15 to 40 mg/dl (2.5–7.5 mM) [8]. Monitoring the amount of urea has always been of primary interest to the whole clinical diagnostic, since urea is a main

indicator of liver and kidney activity and a marker for hemodialysis treatments. Some examples of commercial point-of-care analyzers of urea in clinical settings are reported in **Table 1**. Whereas, in **Table 2** are reported the concentration range of urea in some biological fluids.

Table 1. *Examples of commercial devices for urea quantification in clinical settings.*

Supplier	Commercial name	Transduction	Reference
ESAMED	SDI	Optical	[65]
Lifetest Vet Equipment ApS	InSight Minichem Analyzer	Optical	[66]
Hangzhou Lysun Biotechnology Co., Ltd	Lysun	Optical	[67]
Abbott Point Of Care Inc.	i-Stat	Electrochemical	[68,69]
Siemens Healthineers	epoc® Blood Analysis System	Electrochemical	[70]
Edan Instruments	EDAN i15	Optical	[71]
Radiometer Medical ApS	ABL90 FLEX PLUS blood gas analyzer	Electrochemical	[72,73]

Table 2. *Average concentration ranges of urea in biological fluids.*

Matrix	Urea Range (mM)	Reference
Blood	2.5–7.5	[8]
Urine	215–360	[74]
Saliva	1.2–7.8	[75]
Sweat	0–50	[76]

Matrix	Urea Range (mM)	Reference
Milk	3.0–6.6	[8,77]

Apart from its physiological role in mammals, urea is a compound with significant industrial applications. It is used in agriculture in combination with other nitrogenous fertilizers to increase the productive capacity of a soil [78–80]. Urea is also used as a component in skin care products [81], in cleaning products, in certain medicines, in urea–formaldehyde plastics or as a supplement in the diet of animals on intensive livestock farms [82]. The market demand for urea is expected to grow at 2% per annum, reaching 211.5 million metric tons by 2026 [83]. The main sources of urea in the environment are municipal, industrial, and agricultural waste and sewage systems, including the waste from intensive livestock farms [84]. The fact that urea ends up in water reservoirs and watercourses creates eutrophication problems [27] and it is correlated with the outbreaks of several harmful algal blooms in several estuarine environments [85]. There is a general consensus to fix the maximum acceptable concentration of urea in wastewater at 12 mM in wastewater [86], but this value drops to 0.16 mM in water for human consumption [87].

Thus, even though the analytical methods reported in literature for the determination of urea have largely focused on clinical applications, there is a growing demand for reliable, robust, instrumentation and methodologies for the determination of urea in food and environmental samples. Indeed, a wide variety of analytical techniques have been developed for urea determination, including spectrophotometric, chromatographic, and electrochemical methods, with no single technique dominant in all areas, because of the diversity of applications [88]. These methods can be briefly classified as indirect methods

879 or direct methods. Enzymatic hydrolysis with urease (EC 3.5.1.5) is generally
880 performed and then ammonia and carbon dioxide can be optically [89] or
881 electrochemically [90] measured to stoichiometrically determine indirectly the
882 urea concentration. Direct methods for urea determination are instead
883 commonly based on urea complexation with a ketone or an aldehyde (such as
884 xanthydrol or diacetyl monoxime), under strong acidic conditions to form a
885 product which is then measured either colorimetrically or by using an HPLC-
886 based method [91,92]. The use of electrochemical sensor and biosensor
887 technology for urea measurement is an interesting approach which possesses
888 technical simplicity, low cost, and suitability for in-field analysis.
889 Electrochemical sensors and biosensors can be taken to the sampling sites,
890 having results in real time [93–95]. The first electrochemical urea biosensor
891 was reported by Guilbault and Montalvo [96]. In that approach a glass
892 electrode was used to detect ammonium ion activity by urease-catalyzed
893 hydrolysis [97–101]. Over the time, neutral carrier-type ion-selective
894 ammonium (NH_4^+) electrodes [102,103], gas-permeable ammonia [104] or
895 carbon dioxide (CO_2) [100] electrodes, replaced the first employed glass
896 electrode. Nowadays, different electrical and electrochemical transducers have
897 been reported including Field Effect Transistor (FET) [105], potentiometric all
898 solid-state electrodes, and amperometric transducers [106]. Also in this case,
899 both direct and indirect electrochemical methods can be carried out. In the case
900 of direct electrochemical measurements, a quantification of urea can be
901 performed by measuring the current density resulting from its direct oxidation
902 reaction [107–110], whereas in the case of indirect quantification
903 electrochemical measurements can be carried out by monitoring the urea
904 hydrolysis reaction. A plethora of novel electrode materials has been proposed
905 for both direct and indirect electrochemical urea measurements [90].

Several reviews have been published recently on electrochemical sensors and biosensors technology for the detection of urea, but these are mainly focused on clinical applications [111] and on potentiometric transducers [8,90]. Thus, the aim of this review is to provide an updated revision of the literature in the last 5 years showing the current trends and future perspective (beyond the solely potentiometric and enzymatic biosensors) in terms of electrochemical transducer materials and sensor formats for urea electrochemical (bio)sensors assembly. Different examples of direct and indirect electrochemical methods for urea determination are here described. Moreover, the role of AI in improving the analytical performance of the sensors and in the optimization of working parameters is also discussed.

1.9.2. Direct electrochemical method for urea determination

Direct electrochemical measurement means that the analytical signal can be directly correlated with the concentration of urea in the sample. These methods are mainly based on amperometry or voltammetry and are related to the urea redox reaction at the electrode surface. The redox reaction is driven by an applied potential and leads to a current density value proportional to the concentration of urea in the bulk of the solution. This type of measurement is generally performed by using selected electrode materials or by modifying traditional electrode surfaces with innovative nanomaterials. Indeed, the nanostructuration of the electrode surface, increases the surface area of the electrode, improving the analytical signal [112]. In recent years, it has been shown that Ni is an excellent catalyst for urea oxidation reaction (UOR), with a low cost compared to Pt and Pd [113]. The catalytic oxidation process promoted by nickel-based materials has been studied with a particular focus

on alkali conditions [107–110] (**Figure 5**). The surface area of the nickel electrode is firstly chemically oxidized to $Ni(OH)_2$ by the alkaline solution; then the $Ni(OH)_2$ undergoes oxidation to its active NiOOH form due to the high potential value applied at the electrode during the urea adsorption step, as shown in **Figure 5**; then, the NiOOH oxidizes urea to regenerate $Ni(OH)_2$; the total balance of the reaction is (14):

$$CO(NH_2)_2 + 6OH^- \rightarrow N_2 + 5H_2O + CO_2 + 6e^- \quad (14)$$

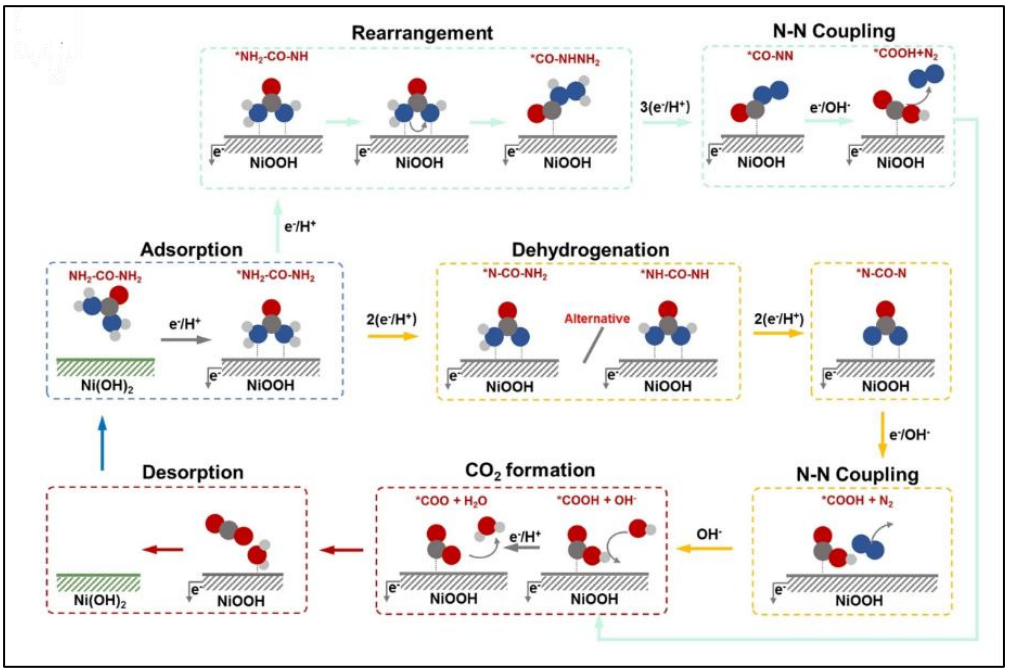

Figure 5. *Scheme of a proposed electrochemical urea oxidation under alkali conditions. (Reproduced with permission from Ref. [114])*

Hence, NiOOH acts as the catalytic active form. However, the current density is generally low because of the unavailability of NiOOH active sites. To overcome these problems, attempts have been made to develop different kinds of nanomaterials, because, as it is well known, the surface area of nanomaterials are larger than those of macro counterparts. This property

contributes to the increase of the number of active sites, and thus to a more efficient catalytic behavior.

In addition to enhancing the catalytic activity and specific surface area, it's worth noting that expediting the desorption of CO from the electrode surface is crucial since it is the slow step of the reaction. Therefore, there is an interest in developing alternative nanomaterials or nanocomposites for accelerating this process.

Different examples of Ni nanocomposites, i.e. nanofibers [115], nanoneedles [116] nanobelts [117], nanorods [118] nanotubes [119] have been reported in literature as shown in **Table 3** and in **Figure 6**.

Table 3. *Some examples of direct urea electrochemical sensors and their analytical performances.*

Materials	Electroanalytical method	Linearity Range (M)	Detection Limit (M)	Real Sample	Reference
Polyvinylidene Fluoride-co-Hexafluoropropylene (PVdF-HFP)/Ni-Co nanofiber/	Amperometric	2×10^{-5} – 2.0×10^{-3}	1.2×10^{-5}	Urine	[115]
$NiCo_2O_4$ NNs/GCE	CV	1×10^{-5} – 5×10^{-3}	1.0×10^{-6}	Urine	[116]
Nafion/ (Ni-MOF)NBs/GCE	LSV	1×10^{-5} – 7.0×10^{-3}	2.23×10^{-6}	Urine	[117]
NiOOH/Ag/Carbon paper	Amperometric	2×10^{-4} – 26.0×10^{-3}	5.0×10^{-6}	Urine	[118]
Ni NTs/Stainless Steel Electrode	Amperometric	3×10^{-6} – 2×10^{-2}	3×10^{-6}	Tap Water	[119]
NiS/Graphene Oxide/GCE	DPV, Impedimetric	1×10^{-4} – 1.0×10^{-3}	3.79×10^{-6}	Milk	[120]

Materials	Electroanalytical method	Linearity Range (M)	Detection Limit (M)	Real Sample	Reference
NiS/GO/CPE	Amperometric	1×10^{-4} – 6.0×10^{-3}	7.02×10^{-6}	Saliva	[75]
$LaNi_{0.6}Fe_{0.4}O_3$-CeO_2 (LNF-C)/MWCNT/ITO	Amperometric	25×10^{-6} – 670×10^{-6}	1×10^{-6}	Urine	[121]
Ni-metal organic framework/MW CNT/ITO	Amperometric	1×10^{-5} – 1.12×10^{-3}	3×10^{-6}	Urine	[122]
Graphene-PANI	Amperometric	10×10^{-6} – 200×10^{-6}	5.88×10^{-6}	Tap Water Milk	[123]

NNs: nanoneedles; NBs: nanobelts; NTs: nanotubes; MWCNT: Multi-Walled Carbon Nanotubes; ITO: Indium Tin Oxide; CNT: Carbon Nanotubes; PPY: PolyPirrole; PANI: Polyaniline; SPE: Screen Printed Electrode; CV: Cyclic Voltammetry; DPV: Differential Pulse Voltammetry

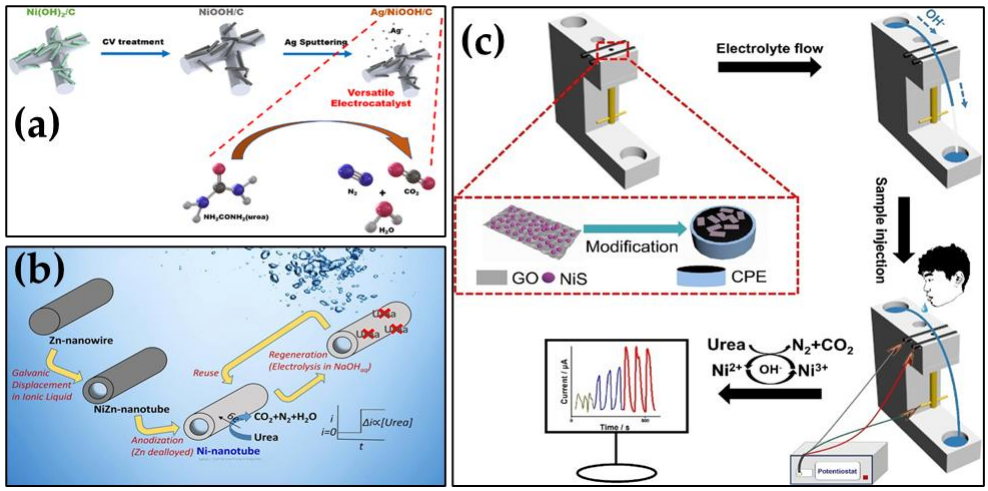

Figure 6. *Different examples of Ni-nanocomposites for urea detection. a) Silver (Ag)/NiOOH nanorods prepared by a cyclic voltammetry treatment of the $Ni(OH)_2$ precursor and sputter deposition of Ag (Reprinted with permission from Ref. [118]. Copyright 2020 American Chemical Society.); b) Overall process of modification of a stainless-steel electrode modified with ZnNi-Nanotubes and urea measurement (Reproduced with permission from Ref. [119]); c) Schematic illustration of thread-based microfluidic electroanalytical device (μTED) for detecting urea. The μTED consists of a carbon paste electrode (CPE) modified by NiS/Graphene Oxide (GO) and cotton threads as microfluidic channels (Reproduced with permission from Ref. [75]).*

A nanostructured Ni-based sensor for urea monitoring in milk sample was reported in Ref. [120]. In this case a graphene stabilized nickel sulfide electrode was used. Nickel Sulfide/Graphene Oxide (NiS/GO) nanocomposites were obtained by a superficial hydrothermal process on a modified Glassy Carbon Electrode (NiS/GO/GCE). A LOD and LOQ of 3.79 and 12.6 μM, respectively, were found. Moreover, NiS/GO/GCE demonstrated robustness for the detection in real sample with a recovery percentage of 98.6–99.4%.

Recently, a NiCu(OOH)/Polystyrene (PS) electrode was used for the development of a wearable biosensor [124]. PS provided a porous structure, leading to an enough number of active sites, easy access to reactants, and adequate water wettability for effective charge transfer. The modified surface was obtained through co-sputtering of Ni-Cu alloy as catalyst.

A microfluidic electroanalytical device, allowing the quantification of urea in saliva is reported in Ref. [75]. A Cotton thread pad was used as microfluidic sampling channel and a NiS/GO/Carbon Paste Electrode (CPE) was developed as urea-sensitive sensor. Two graphite rods (Ø = 3.0 mm) were used as auxiliary electrode and pseudo-reference electrode, respectively, together with NiS/GO/CPE as working electrode. The system is shown in **Figure 6c**. This amperometric sensor allowed to detect urea in the concentration range from 0.1 mM to 6.0 mM.

As reported in literature, direct amperometric measurement of urea is an interesting approach, as there is no need for an enzymatic component that may undergo a change in activity with time (stability issue) or may increase the cost of the measurements. By contrast the selectivity, in absence of the biocatalyst, could be compromised. The interference from other electroactive species could also be a major issue, leading to inaccurate results. From this point of view

chemometric methods, machine learning (ML), and Artificial Intelligence (AI) could help in overcoming selectivity issues [125,126]. Critically analyzing the literature, it has to be highlighted that the analytical performances of the reported systems are basically compatible with clinical (see **Figure 6**) or environmental requirements. By contrast, in some cases, the complexity of the surface modification is not well explained and the role of the different nanocomposites and their morphologies in achieving the required analytical performance.

1.9.3. Indirect electrochemical methods based on catalytic biosensors for urea determination

Indirect urea determination can be performed by using both potentiometric and amperometric biosensors.

The most common bioreceptor for urea determination is the enzyme urease, a nickel-containing metalloenzyme [127] that hydrolyzes urea into CO_2 and NH_4^+ ions, following the scheme reported in **Figure 7**.

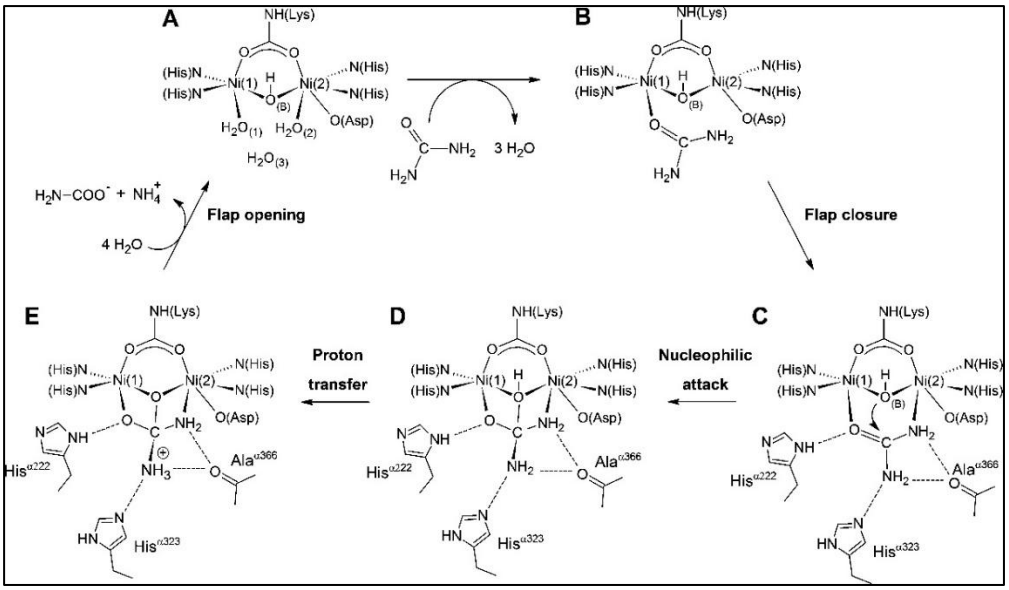

Figure 7. *Scheme of the catalytic mechanism of urease. The neutral imidazole side chain of the active site conserved histidine residue, moving nearer the active site upon closure of the flap, stabilizes the nascent C-NH_3^+ group (5E). The distal C–N bond is broken, ammonia is released, and the resulting carbamate decomposes into NH_4^+ and bicarbonate. The flap opening could facilitate the release of products and allow bulk water to rehydrate the active site to yield the native state of the enzyme (5A). These steps could occur in a concerted manner. This mechanism agrees with all kinetics data, in particular the pH-dependence of the enzyme activity and the noncompetitive inhibition by fluoride, thought to replace the bridging hydroxide. (Reprinted with permission from Ref. [127]. Copyright 2011 American Chemical Society).*

Many examples of potentiometric urease-based biosensors are reported in literature. Coupling a potentiometric measurement with the enzymatic catalysis means that high selectivity can be achieved due to the high affinity and selectivity that the enzyme possesses for the substrate and to the fact that potentiometric transducers, such as the ion-selective electrodes (ISEs) for NH_4^+, very selectively detect the products of the enzymatic hydrolysis reaction. Nevertheless, potentiometric urea biosensors face interference from competing species such as uric acid, Na^+ K^+ and Ca^{2+} ions, which results in high detection limits and slow response times [128]. Coupling urease-based catalysis with an amperometric measurement is also feasible and some examples are reported in literature. Furthermore, other bioreceptors have been

recently explored such as aptamers and Molecular Imprinted Polymers (MIPs) [129,130].

In the following sections, indirect urea determination is reviewed as enzymatic-based electrochemical biosensors and non-enzymatic electrochemical biosensors. Literature is revised considering the electroanalytical technique used (i.e., potentiometry vs amperometry).

1.9.4. Potentiometric enzyme-based biosensors

As already mentioned, urease catalyzes the conversion of urea to NH_3 and CO_2, which then dissociates to NH_4^+ and bicarbonate HCO_3^- ions in solution. Thus, urea measurement can be performed through NH_3, CO_2, NH_4^+, and pH variations.

The NH_4^+ ions are detected using various type of potentiometric transducers (**Figure 8**), including conventional liquid-membrane, all solid-state and gas-permeable membrane ISEs [128,129]. Conventional liquid membrane ISEs use ionophores embedded in a hydrophobic membrane to selectively bind NH_4^+ ions, generating a potential variation proportional to the NH_4^+ activity [131,132]. Liquid-membrane ISEs contain liquid contacts (typically referred to as inner filling solutions) that separate the sensing membrane from the inner reference electrode [131]. All solid-state ISEs employ an electron-conducting layer, such as conductive polymers, metal oxides or porous carbon, that interacts with NH_4^+ ions, causing a change in electrical properties measured potentiometrically against a reference electrode [133]. In all solid-state ISEs, a solid contact is formed between the sensing membrane and an electron-conducting layer to replace the liquid contact, serving as an ion-to-electron transducer. Note that all-solid-state ISEs are not to be confused with ISEs that

comprise a solid-state ion-selective membrane (such as the fluoride electrode based on LaF_3) [134].

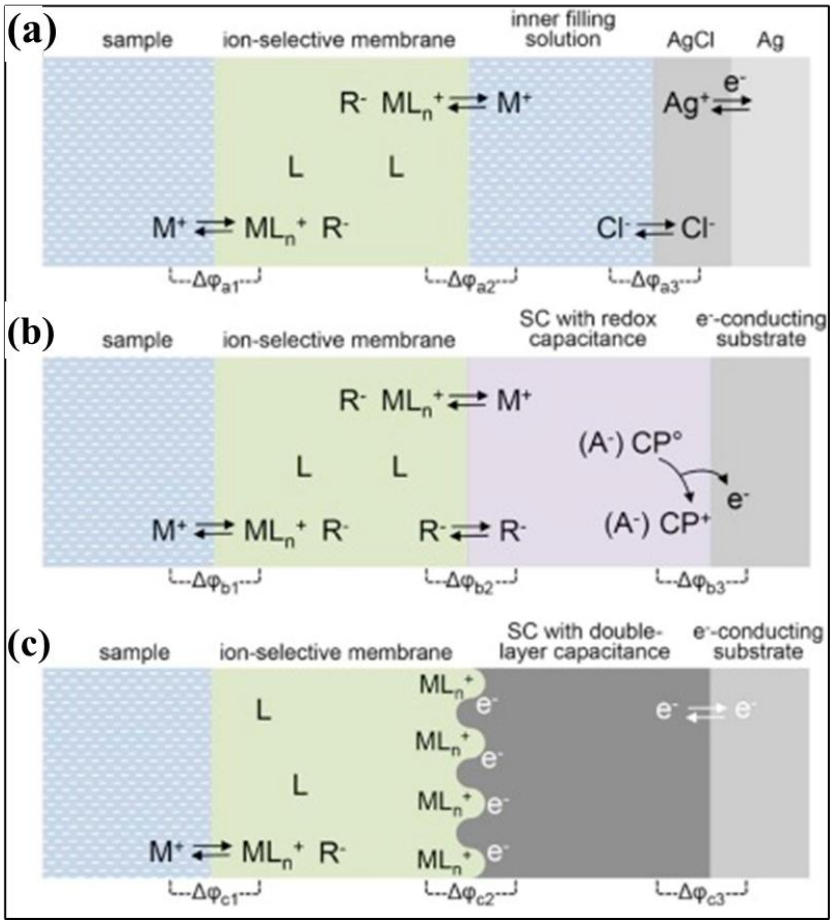

Figure 8. *Schematic representation of all relevant interfaces within different types of ISEs with cation (M^+) selective membranes that contain an electrically neutral ionophore (L) and anionic sites (R^-): a) a conventional ISE with an inner filling solution; b) an all-solid-state ISE based on an anion (A^-, R^-) doped-conducting polymer (CP) solid contact (SC) with a high redox capacitance; c) an all-solid-state ISE based on a high-surface-area SC exhibiting a high double layer capacitance. (Reproduced with permission from Ref. [134]).*

Gas-permeable membrane ISEs convert NH_4^+ to NH_3 gas, which diffuses across a selective gas membrane and reacts with a sensing solution, altering the pH in a concentration-dependent manner. Then, the variation in pH is measured by a pH sensitive glass electrode [135]. CO_2 is commonly measured

by a Severinghaus-type electrode, based on normal pH-glass electrode with a bicarbonate-electrolyte around the tip, separated from the sample by a gas-membrane permeable to CO_2. The pH of bicarbonate resets according to the local pCO_2 and can be measured with the pH-sensor. In all cases, for gas permeable ISEs a temperature-compensation is needed.

Potentiometric transducers offer simple, selective, inexpensive means of detecting the products of the urease reaction to determine urea concentrations and for this reason potentiometric urease-based biosensors have demonstrated to be a robust platform for urea detection. Some commercial instrumentations that take advantage of potentiometric urease-based biosensors are reported in **Table 1** [136].

Many procedures have been developed over the years for the fabrication of urease-based biosensors. Nowadays, new approaches based on thick- and thin-film technologies are used to mass produce miniaturized, cost-effective, reproducible, calibration-free transducers [137] that fit quite well with the requirements of point-of care or point-of needed analyzer. A thick-film sensor comprises layers of special pastes (thickness 10 - 50 μm) deposited onto an insulating substrate; the method of film deposition is the screen-printing technique [138]. Thin-film electrochemical transducers are built up by the successive deposition and patterning of dielectric and conductive materials, on top of an optically flat and polished substrate. The deposition of the thin metallic films (thickness 10 - 200 nm) is generally carried out by classical evaporation or sputtering of a solid metal source; then, photolithography and other techniques can be envisaged to pattern the electrode material. Using these technologies, disposable microfabricated arrays of sensors and biosensors have been developed.

The potential usefulness of nano- and micro-structured materials and composites in potentiometric applications (both as transducers and receptor phases in ion-selective electrodes) continue to be deeply explored [139–166]. In one of these approaches as an example, urea detection was facilitated by a four-layer structure containing a poly(3,4-ethylenedioxythiophene) polystyrene sulfonate (PEDOT:PSS) conductive layer, a NH_4^+-selective layer, an enzymatic layer (urease/chitosan) and a Nafion (Nf) layer [107]. This flexible device can be conformally and harmlessly attached to the skin surface, and was used to the simultaneous quantification of glucose, lactate, pH, Cl^- and urea, **Figure 9a**. The reported LOD for the urea was 1.3 mM with a sensitivity of 31.4 mV per decade of concentration.

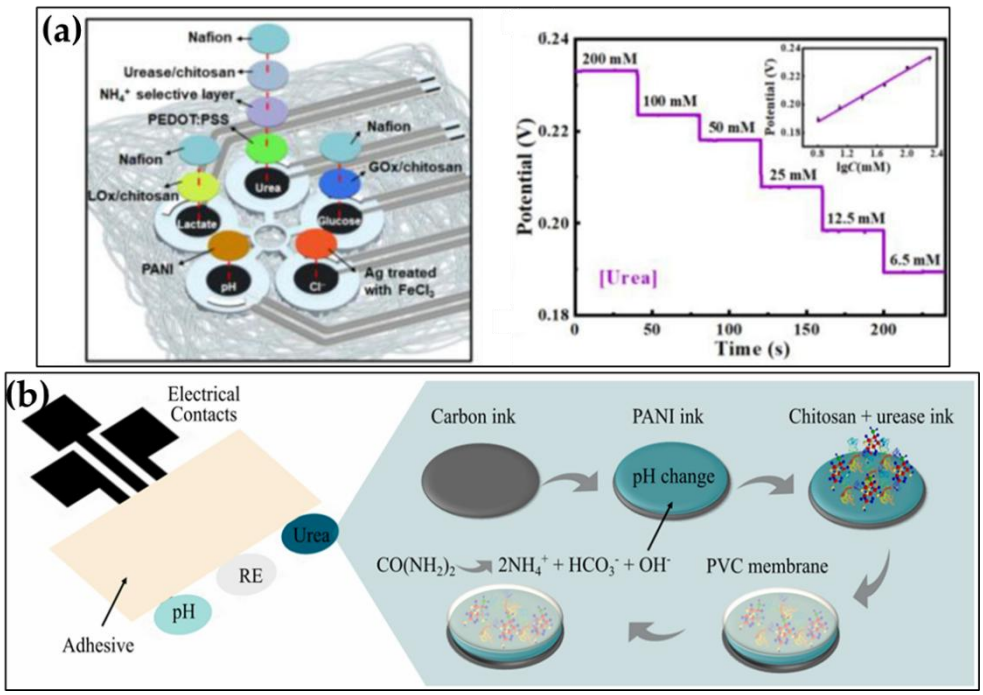

Figure 9. *a) Schematic illustration of the multilayer assemblies in an exploded view, including glucose, lactate, Cl^-, urea and pH sensing units and Open Circuit Potential response for relevant levels of urea (Polyaniline (PANI), Graphene Oxide (GO), poly(3,4-ethylenedioxythiophene) polystyrene sulfonate (PEDOT:PSS) (Reproduced with permission from Ref. [167]), b) Representation of the potentiometric sensors for pH monitoring and detection of urea in sweat and schematic treatment of the electrode surface*

(PANI, Polyvinyl chloride (PVC), Reference Electrode (RE)) (Reproduced with permission from Ref. [168]).

Ibáñez-Redín et al. [168] developed a wearable potentiometric biosensor for urea sensing in sweat. The sensor is based on a screen-printed carbon electrode modified with polyaniline ink, urease bioink and a polyvinylchloride membrane (**Figure 9b**). Urea detection was performed in a wide concentration range (from 5 to 200 mM), encompassing urea levels in human sweat. The biosensor had a 5 min response time and did not show interference from other substances in sweat. Some other examples of enzyme-based potentiometric biosensors are also shown in **Table 4**.

Table 4. *Some examples of indirect urease-based potentiometric sensors recently reported in literature with the kind of real samples analyzed and the reported analytical features.*

Materials	Measure	Linearity Range (M)	Detection Limit (M)	Real Sample	Response Time (sec)	Stability (days)	Ref.
Urs-Chitosan-encapsulated/PANI-grafted ZnO	Potentiometric	3×10^{-4} – 8×10^{-3}	5×10^{-4}	Blood	180	56	[139]
Urs-Poly(2-hydroxyethyl methacrylate-glycidyl methacrylate) nanoparticles	Potentiometric	1×10^{-5} – 5×10^{-1}	7.7×10^{-7}	Artificial Serum	30	90	[142]
Urs-COO-PVC(Nonactin)	Potentiometric	10^{-4} – 10^{-2}	1.0×10^{-4}	Urine	60 to 120	20	[145]
Recombinant Urs-PVA/Styrylpyridinium (SbQ) photopolymer	Potentiometric	5×10^{-4} – 1.5×10^{-2}	1×10^{-4}	Blood	60 to 120	150	[148]
Urs- γ-Al_2O_3	Potentiometric	3.0×10^{-5} – 1.4×10^{-2}	10×10^{-6}	Urine	120 to 240	90	[149]

Materials	Measure	Linearity Range (M)	Detection Limit (M)	Real Sample	Response Time (sec)	Stability (days)	Ref.
Urs-PVA & polyacrylamide (PAA)	Potentiometric	1×10^{-3} – 1	1×10^{-3}	Blood Serum	120	–	[150]
Urs-Imprinted TiO_2	Potentiometric	8×10^{-6} – 3×10^{-3}	5.0×10^{-6}	Urine	25	30	[151]
Urs-Fullerene-Poly(n-butyl acrylate)-Hydrogen Ionophore	Potentiometric	4.2×10^{-5} – 1.2×10^{-3}	–	Urine	<120	140	[153]
Urs-Nylon	Potentiometric	1.6×10^{-5} – 3.3×10^{-4}	–	Sugar Cane Vinasse	900	70	[154]
Urs-Poly(acrylonitrile–methylmethacrylate–sodium vinylsulfonate)	Potentiometric	1×10^{-3} – 1×10^{-1}	3×10^{-4}	Milk	120	70	[156]
Urs-Fe_3O_4 Paramagnetic Particles-Polyelectrolyte Microcapsules	Potentiometric	3×10^{-5} – 1×10^{-1}	3×10^{-5}	Milk	30 to 150	30	[157]
Urs-Chitosan	Potentiometric	5×10^{-4} – 10^{-2}	1×10^{-4}	Serum	30 to 120	60	[158]
Urs-Polypyrrole/Carbon Paper	Potentiometric	1.22×10^{-6} – 3.85×10^{-3}	1×10^{-6}	Serum	60 to 100	>30	[159]
Urs-Tetraphenylborate doped Polyaniline	Potentiometric	–	20×10^{-6}	Serum Milk	–	60	[160]
Urs-Poly(carbamoylsulphonate) (PCS) + polyet	Potentiometric	–	2.5×10^{-5}	Milk	30 to 40	8	[164]

Materials	Measure	Linearity Range (M)	Detection Limit (M)	Real Sample	Response Time (sec)	Stability (days)	Ref.
hyleneimine (PEI)							
Nafion-Urease + Chitosan-PEDOT.PSS/NH_4^+ selective layer	Potentiometric	6.4×10^{-3} – 200×10^{-3}	1.3×10^{-3}	Sweat	900	28	[167]
PVC-Chitosan + Urease-PANI-Screen Printed Electrode	Potentiometric	5×10^{-3} – 200×10^{-3}	---	Sweat	150	<10	[168]

Urs: Urease; PVC: Polyvinyl Chloride, PANI: Polyaniline; PVA: Polyvinyl Alcohol; NC: Nitrocellulose; GO: Graphene Oxides; PET: Polyethylene Terephthalate, PVC: Polyvinyl Chloride, MWCNT: Multi-Walled Carbon Nanotubes; ITO: Indium Tin Oxide; BSA: Bovine Serum Albumin; EDC: 1-Ethyl-3-[3-dimethylaminopropyl]carbodiimide hydrochloride; NHS: N-hydroxysulfosuccinimide; CNT: Carbon Nanotube.

1.9.5. Amperometric and impedimetric enzyme-based biosensors

As for the potentiometric-based biosensors, recent advances in nanomaterials, conductive polymers, electrode modifications, and immobilization techniques have significantly improved the performance of amperometric urease-based biosensors, enhancing their sensitivity, selectivity, and stability. Among other nanomaterials, graphene [169,170] and carbon-nanotubes [171] have been frequently used. Thus, in comparison to few decades ago, when potentiometric transducers were solely used, nowadays different examples of amperometric biosensors are reported in literature, with analytical performances not far from the potentiometric counterpart.

Dervisevic et al. [172], developed a biosensor using ferrocene-poly(amidoamine) (Fc-PAMAM) dendrimers combined with MWCNTs and urease. In this approach the electrochemical signal is related to the electron transfer of ferrocene linked in the dendrimer. The polymer can change its spatial conformation depending on the pH that is locally modified on the electrode surface during the urea hydrolysis process. The biosensor exhibits a linear range of 0.2 - 1.8 mM with a LOD of 0.05 mM. This biosensor was used to detect urea in human blood.

Iron-based nanoparticles were largely used to indirect urea quantification, due to their chemical stability, mechanical hardness and low toxicity. As an example, Fe_3O_4/MWCNT/PANI-Nafion (Nf) nanocomposites [173] or Fe_3O_4/Cu/PANI-Nf [174] were coupled to urease for the modification of GCEs (**Figure 10a**). In these two approaches the biocatalytic process of urea hydrolysis generates NH_4^+ ions on the surface. The NH_4^+ ions bind to PANI. The electroactive species then is the PANI-NH_4^+ that gives an amperometric signal that could be correlated to the concentration of urea in the solution. In the case of Fe_3O_4/Cu/PANI-Nf/urease nanocomposite a LOD of 0.17 μM and a wide linear range of 0.5 - 45.0 μM were obtained.

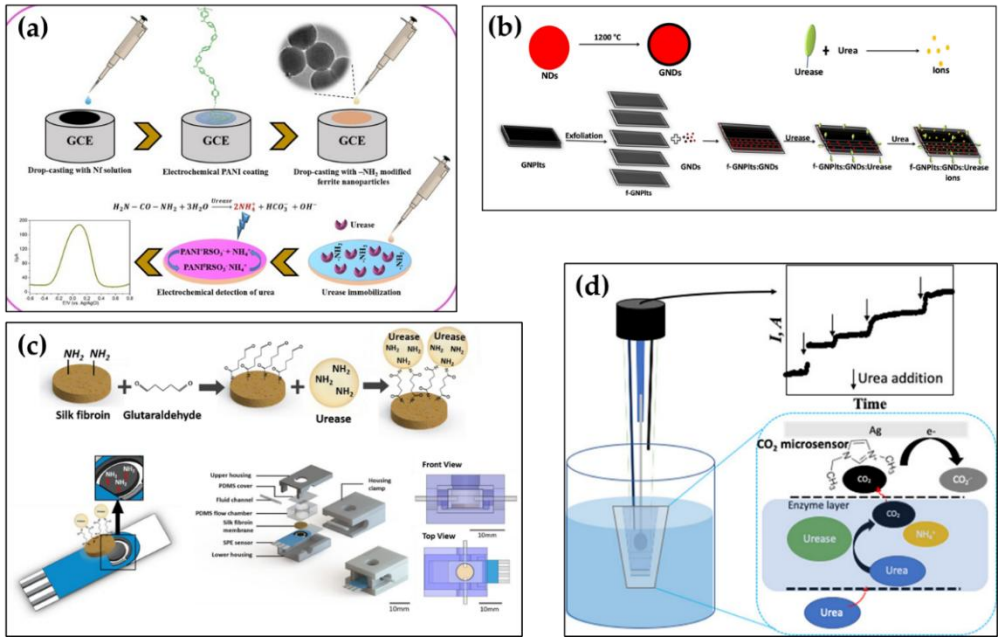

Figure 10. *a) Procedure for Urease/CuF/PANI/Nf(GCE biosensor preparation and a schematic illustration of NH_4^+ detection mechanism (Reproduced with permission from Ref. [174]), b) Schematic for the graphitization of nanodiamonds (NDs) by heating at 1200 °C in the presence of argon, hydrolysis of urea into ions by the urease, incorporation of graphitized nanodiamonds (GNDs) into layers of exfoliated f-GNPlts and the capture of ions onto the composite surface upon the hydrolysis of urea. (Reproduced with permission from Ref. [175]), c) Schematic diagram of the principle of immobilization of urease on the silk fibroin (SF) membrane, the amination of the surface of the carbon electrode, and the configuration of the sensor system (Polydimethylsiloxane (PDMS), Screen-printed electrodes (SPEs)) (Reproduced with permission from Ref. [176]), d) Schematic representation of the urea microsensor based on the CO_2 microsensor. The CO_2 produced from urea hydrolysis diffuses through the gas permeable membranes of the CO_2 microsensor and is detected through reduction at an Ag cathode. (Reproduced with permission from Ref. [177]).*

Kumar and his group [175] (**Figure 10b**) developed a graphene nanoplatelet (GNPlts)/Graphitized Nanodiamonds (GNDs)/Urease using a self-organization process. The ions generated by the addition of urea, thanks to the urease immobilized on the surface of the nanocomposite, alter the electron transport parameters (e.g., the mobility of electrons, conductivity, and Dirac point shifting). Changes in these parameters led to the appearance of a current.

Urease, immobilized onto Silk Fibroin (SF) scaffolds mounted in a polydimethylsiloxane (PDMS) sensor housing, as shown in **Figure 10c**, was

proposed by Kim et al. [176] for urea measurement in flow conditions. This urea biosensor elicited a linear current-concentration response in a range from 0.1 to 20 mM.

Fapyane et al. [117] reported the possibility of fabricating an urea amperometric biosensor by monitoring the CO_2 that is released from the urease in presence of the substrate. The system is based on a CO_2 microsensor equipped by a gas permeable membrane with a gap filled with a buffer solution containing urease and a sensing Ag wire dipped in an ionic liquid (**Figure 10d**). An external silicon membrane is in contact with the sample solution. In this condition, urea can migrate in the urease-buffer solution; the produced CO_2 diffuse through the gas permeable membrane to the ionic liquid medium; in this water free environment, the Ag microsensor can reduce the CO_2 to $CO_2^{\bullet-}$. The reported urea biosensor has a linear range from 0 to 1000 μM with a LOD of 0.94 μM.

Another electroanalytical approach used for urea detection is based on Electrochemical Impedance Spectroscopy (EIS) [178]. A disposable copper tape-based electrode, covered with layers of wax, urease, and poly(methyl methacrylate) (PMMA) was developed by Bose et al. [179] for non-faradaic impedimetric sensing of urea. In this set-up, a wax layer keeps a paper–dielectric sensor dry, even in aqueous media. During the measurement, the sensor is dipped into the urea solution. The enzymatic hydrolysis of urea produces ammonium and carbonate ions, reducing the solution resistance and creating a measurable variation in impedance, useful to quantify total urea. A working range of 0.16 - 175 mM (corresponding to 1 - 1050 mg/dL) is reported [179]. An example of faradaic impedance measurements is described in Ref. [180] and shown in **Figure 11**. The analytical signal is due to the redox reaction of NH_3 at the Urs/Nano-ZnO/TiO_2/Fluorinated-Tin Oxide (FTO) electrode

surface. The TiO_2 substrate promotes electron transfer between ZnO to FTO electrode, by the formation of heterojunctions with ZnO.

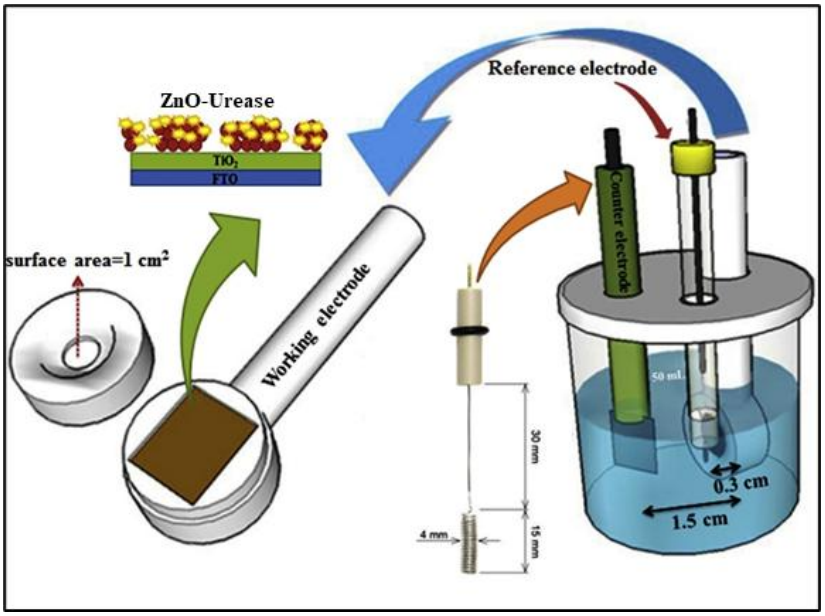

Figure 11. *Examples of EIS-urea biosensor: Schematic representation of the measurement setup and the Urease/Nano-ZnO/TiO_2/Fluorinated-Tin Oxide (FTO) working electrode (Reproduced with permission from Ref. [180]).*

Other examples of enzyme based amperometric assays are shown in **Table 5**.

Table 5. *Some examples of indirect urease-based voltammetric/amperometric sensors with the reported analytical features and the type of real samples analyzed.*

Materials	Measure	Linearity Range (M)	Detection Limit (M)	Real Sample	Response Time (sec)	Stability (days)	Ref.
Urs - (MWCNTs)-Ferrocene-poly(amidoamine)- Pencil graphite electrode (PGE)	Amperometric	2×10^{-4} - 1.8×10^{-3}	5×10^{-5}	Blood	3	3	[172]
Urs-Nafion-MWCNT-	CV, DPV, CA	1.0×10^{-3} - 2.50×10^{-2}	6.7×10^{-5}	Milk	–	60	[173]

Materials	Measure	Linearity Range (M)	Detection Limit (M)	Real Sample	Response Time (sec)	Stability (days)	Ref.
PANI-Fe_3O_4-GCE Urs-CuF-PANI-Nafion-GCE Urs-CoF-PANI-Nafion-GCE Urs-NIF-PANI-Nafion-GCE Urs-ZnF-PANI-Nafion-GCE	DPV	5×10^{-7} - 4.5×10^{-5} 5×10^{-7} - 4.5×10^{-5} 5×10^{-7} - 4.5×10^{-5} 5×10^{-7} - 4.5×10^{-5}	1.7×10^{-7} 2.3×10^{-7} 3.7×10^{-7} 4.2×10^{-7}	Soil Milk	–	7	[174]
Urs-Graphitized nanodiamond-Graphene nanoplatelet-Screen Printed Electrodes (SPEs)	Amperometric	1.6×10^{-3} - 15×10^{-3}	8×10^{-5}	Milk	20	15	[175]
Dyalisis membrane/Urs solution/Ionic Liquid/Ag	Amperometric	0 - 100×10^{-5}	1×10^{-6}	Blood Plasma	120	<14	[177]
Urs-Nano ZnO-TiO_2-FTO	Impedimetric	5×10^{-4} - 3.4×10^{-2}	3×10^{-4}	Serum	4	28	[180]
Urs-Polyaniline-Sulfonated Graphene-ITO	Amperometric	1.2×10^{-4} - 1.23×10^{-2}	50×10^{-5}	Urine	5	15	[181]
Urs-Clinoptilolite Zeolite modified Electrode	Conductimetric	0 - 64×10^{-3}	10^{-6}	Urine Blood	40 to 70	150	[182]
Urs-ZnO-MWCNT-ITO	CV	1.6×10^{-3} - 1.6×10^{-2}	2.3×10^{-4}	Serum	4	120	[183]

Materials	Measure	Linearity Range (M)	Detection Limit (M)	Real Sample	Response Time (sec)	Stability (days)	Ref.
Urs-PVA conducting hydrogel membrane-PANI grafed polyacrylamide-GCE	DPV, EIS	1.5×10^{-6} - 1×10^{-3}	6×10^{-8}	Milk Urine Serum Soil Puffed Rice	10	60	[184]
Urs-ZnO-F-doped SnO_2	Impedimetric	1.3×10^{-3} - 1.8×10^{-3}	8.3×10^{-4}	Serum	10	21	[185]
Urs-Nano ZnO-FTO	Impedimetric	8.3×10^{-4} - 2.32×10^{-2}	4.0×10^{-4}	Serum	4	42	[186]

Urs: Urease; ITO: Indium Tin Oxide; PANI: Polyaniline; MWCNT: Multi-Walled Carbon Nanotubes; GCE: Glassy Carbon Electrode; SF: Silk Fibroin; PVA: Polyvinyl Alcohol; FTO: Fluorinated-Tin Oxide; EIS: Electrochemical impedance spectroscopy; CV: Cyclic voltammetry; CA: Chronoamperometry; DPV: Differential pulse voltammetry.

Examples of non-enzymatic quantification of urea are also reported. Liu et al. [130], developed a flexible biosensor for the indirect quantification, monitoring the signal decrease of the redox species Fe^{2+}/Fe^{3+}, using a Molecular Imprinted Polymers (MIPs) sensing layer. In this approach, the electropolymerization of 3,4-ethylenedioxythiophene (EDOT) was used for MIP layer development. The reported linearity range was between 1 and 100 mM and the LOD was 0.1 mM.

An alternative strategy for the determination of urea through an enzyme-free, indirect approach was proposed by Vasconcellos et al. [187] and it takes advantage from the presence of Cl^- ions in solution. In this case a suitable electrode material could be used to generate chlorine from the electrochemical oxidation of chloride following reaction (15) [114]. Evolved chlorine quickly dissociates in water yielding hypochlorous acid according to reaction (16), in which speciation is defined by the acid-base equilibria of reaction (17).

$$2Cl^- \rightarrow Cl_2 + 2e^- \quad (15)$$

$$Cl_{2(aq)} + H_2O \rightarrow HClO + Cl^- + H^+ (4) \quad (16)$$

$$HClO \leftrightharpoons ClO^- + H^+, \text{ pKa} = 7.55 \quad (17)$$

Electrogenerated active chlorine species from reactions (15 - 17) react with urea yielding N_2 (18).

$$(NH_2)_2CO + 3ClO^- \rightarrow N_2 + CO_2 + 3Cl^- + H_2O \quad (18)$$

The chemical reaction that consumes electrogenerated active chlorine species can be used to quantify the concentration of urea in solutions [187]. This method can allow urea quantification with a LOD of 1.83×10^{-6} M and a linear range of 6.66×10^{-6} to 3.33×10^{-4} M.

1.9.6. Conclusions & further perspectives

In this work different methods for direct and indirect electrochemical determination of urea have been revised. Indirect electrochemical methodologies exhibit intriguing features for various applications, offering high selectivity due to the reliance on the enzymatic reagent but also leading to stability issues over time. By contrast, direct electrochemical methods show interesting features in terms of stability and cost-effectiveness but suffer in selectivity. AI-based methodologies have the potential to facilitate the creation of smart sensors capable of adapting to dynamic environments and delivering instantaneous feedback. Additionally, AI-based approaches can aid in optimizing sensor performance and offer real-time feedback from the identified analyte. Recent advancements in AI and ML have proven useful in data processing for real sample analysis, enhancing biosensor development. AI and ML techniques analyze large datasets, identify patterns, and optimize experimental conditions for increased sensitivity and selectivity [188]. AI-based biosensors hold potential for simultaneous detection of multiple

substances using electrodes with different analyte response characteristics. AI can also optimize parameters in industrial chemical processes, as demonstrated in a study on ceramic-based microbial fuel cells (CMFCs) [189] or in the monitoring and prediction of blood urea and glucose in Chronical Kidney Disease Patients [190], in environmental science with studies about the urea release as fertilizer [191].

By leveraging the capabilities of nanomaterials and AI-based approaches, it could be possible to push the boundaries of sensor technology and renewable energy solutions, leading to more efficient, cost-effective, and environmentally friendly solutions for urea detection.

CHAPTER II

This chapter presents the study and the development of system for urea quantification in continuous based on potentiometric measurements and urea quantification.

2. Development of a flow biocatalytic-based platform for electrochemical monitoring of urea in wastewater

Talanta
Volume 289, 1 July 2025, 127755

The early evaluation of urea content in water and wastewater is of utmost importance for preventing pollution and improving remediation technologies, also related to urea conversion into a valuable energy product. In this work, a customized urease-based potentiometric platform for the detection of urea in wastewater samples was developed. Amino-functionalized glass beads were used as support material for urease immobilization in a customized bioreactor; then, using an online flow measurement setup, the NH_4^+ produced by the enzymatic reaction was measured by means of a potentiometric sensor housed in a customized flow cell. Operational and analytical parameters were optimized to achieve the best bioreactor performance. An in-depth study of the composition of the measurement buffer was also carried out; its influence on the sensitivity and detection limits was investigated, demonstrating that a careful selection of its concentration needs to be performed based on the type of samples to be analyzed (LOD = $8.9 \cdot 10^{-6}$ M). Finally, at the optimized operative conditions, the full system was applied to the determination of urea in spiked wastewater samples. Using the standard addition method, an average percentage of recovery of 102 ± 5 % was obtained for the analyzed samples despite the interferents present, demonstrating a possible application of the developed setup for remote online urea monitoring in wastewaters.

2.1. Introduction

The ever-increasing demand for cultivated products and the subsequent intensification of farming practices have made the use of urea-based fertilizers more widespread than ever [192]. As a result, significant amounts of urea inevitably seep into water systems via agricultural runoff, ultimately contaminating receiving water bodies [193]. This contamination has harmful consequences for aquatic ecosystems, as urea contributes, together with other ammonium-based fertilizers, to eutrophication, a process that promotes excessive algal blooms, leading to oxygen depletion and significant ecological damage [27,194]. Furthermore, urea is present in high concentrations in mammals' urine. Thus, beyond agricultural runoff, urea also enters water systems through municipal wastewater and animal waste streams, making it a prominent contaminant in both industrial and domestic effluents. Rapid detection methods are crucial for effective real-time monitoring and quantification of urea levels in aquatic environments [195], for preventing pollution and improving remediation technologies, also related to H_2 production [196–198]. Indeed, the electrooxidation of urea, present at high concentration in wastewater, converts urea into a valuable energy product (i.e. H_2). Recently, the utilization of urea-rich wastewater for producing useful fuel has been gathering increasing attention due to society's need for alternative energy sources. Thus, for this reason, there is the need to characterize the wastewater on its content in urea [199–201].

At present, several analytical techniques are employed for the quantification of urea [202], including HPLC-based methods [88]. While these methods provide accurate results, they are often resource-intensive, requiring costly equipment and highly trained personnel. Furthermore, they are typically

unsuitable for in situ and online monitoring, as they involve complex sample preparation procedures and laboratory-based analyses. These limitations highlight the necessity for developing alternative methodologies that enable real-time, on-site quantification of urea and other contaminants in water systems [95,203].

By contrast, colorimetric kits and urease-based potentiometric biosensors can be used in decentralized analysis and have been used in clinical settings for many years. Different types of colorimetric kits are commercially available: some of them employ urease and glutamate dehydrogenase [204], and some others are based on the formation of a colored complex of urea with a chromogenic reagent [205]. These kits, however, are prone to issues related to interference, such as ammonium naturally present in wastewater samples, as well as samples characterized by high turbidity levels or inherent coloration. Potentiometry is less prone to being affected by turbidity and the presence of interferences in the samples, but it has been scarcely applied to wastewater analysis [202]. Indeed, only a few examples of potentiometric biosensors have been tested for urea environmental analysis so far (**Table 6**).

Table 6. *Overview of various potentiometric urease-based sensors and their analytical performance. The table summarizes the linearity range, limit of detection (LOD), stability over time, type of sample tested, and relevant citations for each material used in urea detection applications.*

Material	Linearity Range (M)	LOD (M)	Time Stability	Real sample	Ref.
Polyaniline-LbL-Urease	$1.0x10^{-5}$ - $1.0x10^{-3}$	Not reported	21 days	Synthetic urine	[206]
Urease-fullerene nanomaterial on SPE with membrane hydrogen ionophore	$4.2x10^{-5}$ - $1.2x10^{-3}$	Not reported	140 days	Urine	[207]

Material	Linearity Range (M)	LOD (M)	Time Stability	Real sample	Ref.
Urease immobilized chitosan membrane	$1.6x10^{-6}$ - $1.0x10^{-4}$	$1.2x10^{-6}$	280 s	Urine	[208]
Urease–imprinted ultrathin TiO_2 films	$8.0x10^{-6}$ - $3.0x10^{-3}$	$5.0x10^{-6}$	30 days	Urine	[209]
Urease Covalent bonded to PVC–COOH polymer	$1.0x10^{-4}$ - $1.0x10^{-2}$	$1.0x10^{-4}$	20 days	Urine	[210]
Urease/γ–aluminum oxide matrix	$3.0x10^{-5}$ - $1.4x10^{-2}$	$1.0x10^{-5}$	90 days	Urine	[211]
Urease/BSA-Polypyrrole/Indium Tin Oxide	$6.6x10^{-6}$ - $7.5x10^{-4}$	Not reported	2 month	Aqueous solution	[212]
Urease/nylon + Ammonium ISE	$1.6x10^{-5}$ - $3.3x10^{-4}$	Not reported	29 days	Environmental	[213]

Herein, a customized urease-based bioreactor was designed and applied to urea potentiometric determination in an online flow configuration for real time monitoring of urea in wastewater. The immobilized enzyme is contained in a small reactor in a flow system. Controlled pore amino-functionalized glass beads were used as support materials for urease immobilization. The effluent from the bioreactor, containing the ammonium ions produced by the enzyme-promoted hydrolysis of urea, is passed into a flow-through cell housing an NH_4^+ potentiometric sensor. The bioreactor is operated under such conditions that the substrate is converted to the product with maximum efficiency. A fine tuning of the different parameters involved in bioreactor assembly was performed by using a chemometric approach, based on Design of Experiment (DoE) and Response Surface Methodology (RSM), in order to maximize the signal output and minimize the amount of the reagents used [214,215]. To the

best of our knowledge, it is the first time that an RSM approach has been used for the optimization of a urease-based bioreactor coupled to a potentiometric sensor for online flow monitoring of urea levels in wastewaters.

After a preliminary investigation of the analytical performances of the potentiometric sensor, the best experimental conditions for urea determination were optimized. Particular attention was devoted to the selection of the measuring buffer, which must be carefully selected based on the type of samples to be analyzed. Finally, the developed bioreactor was tested for urea determination in wastewater samples. The obtained results demonstrate that such an approach could be useful for addressing the growing environmental challenges posed by urea contamination, offering a means for a real time assessment of the quality of the aquatic ecosystems and wastewaters.

2.2. Materials and methods

2.1.1. Reagents

$NaH_2PO_4 \cdot 2H_2O$, Urea, NaOH, ($CaCl_2 \cdot 2H_2O$, $MgCl_2 \cdot 6H_2O$, NaCl, Na_2SO_4, KH_2PO_4, KCl, NH_4Cl, Peptone from soybean (enzymatic digest) suitable for microbiology, Glutaraldehyde Grade I (25 % in H_2O) were purchased by Merck (Milan, Italy). Urease TCI from Jack Bean (EC 3.5.1.5, 300 units/mg) was purchased from VWR (Milan, Italy). Controlled Pore Glass AminoPropyl beads (lot. 168982, reported pore diameter of 500 Å, particles size 120–200 mesh, amine content 139 μmol/g) were purchased from LGC Biosearch Technologies (Hoddesdon, United Kingdom).

Peristaltic pump model MINIPULS3 was purchased from Gilson (Milan, Italy). Potentiometer model HI-5222 double channel was purchased from Hanna Instruments (Milan, Italy). Ion-selective combined ammonium

electrode (NH_4^+-ISE) model 3051 was purchased from DirectION (Dover, UK). Plastic cylinders (length 40 mm, inner diameter 5 mm, outer diameter 13 mm), mesh-equipped caps, connections for bioreactor assembly, and the polymethyl methacrylate-based flow cell used for in-flow NH_4^+ measurements were designed and produced in-house.

2.1.2. Samples

Four wastewater samples were collected from the same location at the inlet of an Italian treatment plant processing urban and municipal wastes. After collection, each sample was stored in 0.5 L polyethylene bottles and immediately refrigerated at +4 °C until analysis, to minimize chemical and biological alterations.

Urea-free synthetic human urine was used to simulate analysis in urine samples. Once prepared, synthetic urine was fractioned, filtered to remove the suspended protein fraction, diluted 1:50 in 500 mM sodium phosphate buffer pH 7.0 and spiked with different urea concentrations.

2.1.3. Software

MODDE Pro Version 13.0.2 software (Sartorius Data Analytics, Göttingen, Germany) was employed for planning 3-level Full Factorial Design (FFD) used in the optimization step and for the related data treatment in RSM. The experiments described in FFD experimental plan were run in a randomized order.

2.1.4. Measurements set-up & bioreactor assembly

A block scheme of the measurement set-up is reported in **Figure 12a**. A peristaltic pump is used to introduce the sample in the bioreactor, where urea

is hydrolyzed by urease to produce NH_4^+ and CO_2. The NH_4^+ produced is potentiometrically measured by the NH_4^+-ISE. **Figure 12b** shows a scheme of the bioreactor. The measurement is performed in a customized flow cell (**Figure 12c**); the potential value is recorded vs. time (**Figure 12d**). The ΔmV is the analytical data which is proportional to the urea content.

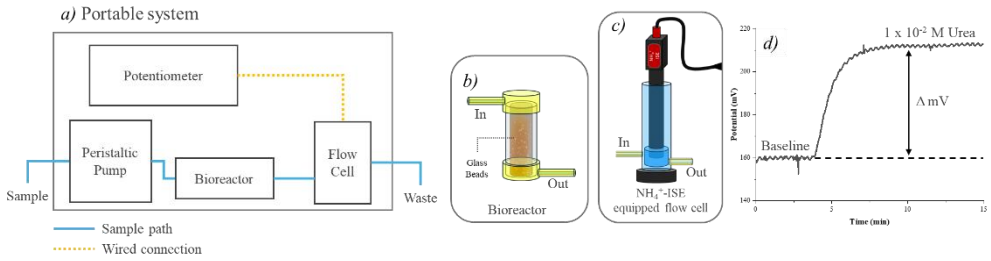

Figure 12. *Experimental set-up: a) Schematic representation of the instrumental set-up for urea online flow measurements; b) bioreactor; c) flow cell; d) example of potential vs. time signal.*

The protocol for the preparation of the bioreactors involves two main steps: a) activation of glass beads; b) beads functionalization with the enzyme. Both are performed using an in-flow setup. Regarding step a): plastic cylinders are filled with 120 mg of aminopropyl glass beads and a volume of solution containing glutaraldehyde prepared in a 100 mM phosphate buffer pH = 7.0. The two ends of each cylinder are then closed with mesh-equipped caps, connected to the fittings and placed in-flow at a flow rate of 0.2 mL min^{-1} for 1h 30 min. After this period of time, each cylinder is then washed with 50 mL 100 mM phosphate buffer pH = 7.0 (flow rate 0.2 mL min^{-1}) before passing to the next step. To carry on step b): a solution containing a fixed concentration of urease prepared in a 100 mM phosphate buffer pH = 7.0 is introduced in the cylinder containing the activated beads and placed in flow in a closed loop overnight at the flow rate of 0.2 mL min^{-1}.

Finally, the obtained bioreactor is washed by flushing it with 500 mM phosphate buffer pH = 7.0 at a flow rate of 0.2 mL min^{-1} for 30 min. The bioreactor can then be stored for subsequent use.

2.1.5. Response Surface Methodology for parameters optimization

An RSM study was carried out to optimize the parameters for the preparation of the bioreactor, making it possible to draw a detailed map of the predicted response throughout the experimental domain and thus to obtain the combination of settings that gave the best performance [216]. To perform the experiment, a 1.0 M urea solution (prepared in 500 mM phosphate buffer pH 7.0) was left to run in the bioreactor at a flow rate of 0.2 mL min^{-1}. Then, the outlet solution was collected and diluted 1:30 in the same buffer for the potentiometric measurement. The output potential value obtained for each reactor was considered as a response to carry out this study.

The considered factors were glutaraldehyde concentration and urease amount, which were studied in the following experimental domain: glutaraldehyde, 0.5–2.5 % v/v; urease, 3.0 - 9.0 mg mL^{-1}. The hypothesized relationship between the factors (x_i) and the response (y) consisted of a polynomial quadratic model, represented by Equation (19):

$$y = \beta_0 + \beta_1 x_1 + \beta_2 x_2 + \beta_{11} x_1^2 + \beta_{22} x_2^2 + \beta_{12} x_1 x_2 + \varepsilon \quad (19)$$

where y is the response (potential), β_0 is the intercept, β_1 and β_2 are the linear terms, β_{11} and β_{22} are the quadratic terms, β_{12} is the interaction term, ε is the experimental error and the factors are designated by x_1 (glutaraldehyde) and x_2 (urease).

In order to estimate the model coefficients, a 3-level FFD was used [217]. In this kind of design, the matrix includes every combination of factors' levels, and the number of experiments is $3^k + n$, where k is the number of factors to be studied, and n is the number of replicates at the center of the experimental domain for the estimate of the experimental variance.

2.3. Results and discussion

The coupling of the urease-based bioreactor with the potentiometric NH_4^+-ISE sensor for the determination of urea in wastewaters is described in **Figure 12**. The wastewater is sampled and introduced in the bioreactor, where urea is hydrolyzed by urease with the formation of NH_4^+ and CO_2. The NH_4^+ produced is potentiometrically measured. Preliminary experiments were devoted to evaluate the best experimental conditions to perform the measurements.

2.2.1. NH_4^+-ISE sensor performances

The NH_4^+ potentiometric response obtained for the ISE sensor is reported in **Figure 13**. The sensor shows a quasi-Nernstian behavior, with a slope of 51.3 ± 0.2 mV/decade in deionized water, and a linear response within a concentration range from $1.0 \cdot 10^{-5}$ to 1.0 M ($R^2 = 0.996$). A similar experiment was carried out for Na^+, K^+ and Ca^{2+}, respectively. These ions are common components of wastewater matrices and could act as interferents for the potentiometric measurements of NH_4^+. As shown in **Figure 13**, the response of the sensor to Na^+ and Ca^{2+} does not increase up to $1.0 \cdot 10^{-2}$ M and 0.5 M, respectively. A different behavior is observed for K^+; in this case, the sensor shows a not negligible response in the concentration range from $1.0 \cdot 10^{-5}$ to 1.0 M. This is also confirmed by the values of the selectivity coefficients (calculated using the separate solution method [218]) that are (8.79 ±

1476 0.08)·10^{-2}, (5.28 ± 0.05)·10^{-4}, and <1.0·10^{-4}, for K^+, Na^+ and Ca^{2+},
1477 respectively. Therefore, while K^+ can constitute an important interferent in the
1478 determination of the NH_4^+, Na^+ and especially Ca^{2+} have a more limited effect
1479 and only at very high concentrations.

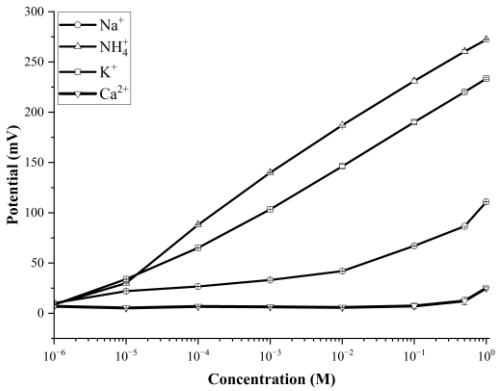

1480

1481 ***Figure 13.*** *Potentiometric response of the NH_4^+-ISE sensor for NH_4^+ in deionized water in the*
1482 *concentration range 1.0 · 10^{-6} - 1.0 M. A comparison with potentiometric responses for major interfering*
1483 *ions as Na^+, K^+ and Ca^{2+} in the same concentration range is also reported. The error bars correspond*
1484 *to the standard deviation (n = 3).*

1485 The NH_4^+-ISE sensor was then applied to the determination of NH_4^+ levels in
1486 four samples of municipal wastewater entering a water treatment and
1487 purification plant. For each sample, the NH_4^+ content was quantified, without
1488 applying any pretreatment, by using the Standard Addition Method [219]; the
1489 obtained results were compared with those obtained with a standard
1490 spectrophotometric reference method [220]. As it can be seen from **Table 7**,
1491 the NH_4^+ concentration values obtained with the two different methods are in
1492 good agreement. The Pearson correlation coefficient [221] was calculated to
1493 be 0.998, p-value = 0.13, n = 3.

Table 7. *NH_4^+ content in four samples of municipal wastewater analyzed using the standard spectrophotometric method and the NH_4^+-ISE sensor.*

Sample n.	Standard spectrophotometric method (mM)	NH_4^+-ISE sensor (mM)
1	2.0 ± 0.2	2.11 ± 0.03
2	2.7 ± 0.3	2.90 ± 0.04
3	4.5 ± 0.5	4.48 ± 0.03
4	4.1 ± 0.5	4.08 ± 0.05

2.2.2. Influence of the buffer composition

The ionic strength is a crucial parameter in potentiometric measurements, as it influences the activity of the ions to be measured. For this reason, it is convenient to keep it controlled and constant during the analysis. Furthermore, for urea determination, the pH value plays an important role, since the NH_4^+ ions and the carbon dioxide produced influence the pH of the measuring solution, which must be kept in the range of 7.0 - 8.0 to retain the maximum urease activity [222]. Thus, the selection of a suitable measurement buffer is mandatory. Among the various possibilities, phosphate buffer is recognized as one of the best medium, as reported in literature [223]. Particular attention must be devoted to the choice of the counterion; being K^+ a strong interferent and avoiding Ca^{2+} ions (due to the low solubility of its phosphate salts), Na^+ was selected as counterion.

Figure 14a shows the influence that NH_4^+ concentrations have on the final pH value of different phosphate buffer compositions at pH 7.0. As can be observed, the higher the buffer concentration is, the lower is the effect of the added NH_4^+ on the final pH value. For all the tested buffers, the pH remains

stable in the NH_4^+ concentration range $1.0 \cdot 10^{-6}$ - $1.0 \cdot 10^{-2}$ M (unlike for deionized water). For NH_4^+ concentrations higher than $1.0 \cdot 10^{-2}$ M, the buffering capacity becomes more influencing. Indeed, in the case of the 500 mM phosphate buffer, NH_4^+ does not affect the pH for the full concentration range tested, whereas for 50 and 10 mM phosphate buffer a pH variation can be observed starting from an NH_4^+ concentration of $1.0 \cdot 10^{-2}$ M. This is an important finding, because it demonstrates how critical is the buffering capacity. In the case of samples with high urea content (for example samples from septic tanks or from animal effluents), a more concentrated buffer is necessary; conversely, for samples of wastewater in which urea contents will be lower (i.e. outlets), a lower buffering capacity could be suitable.

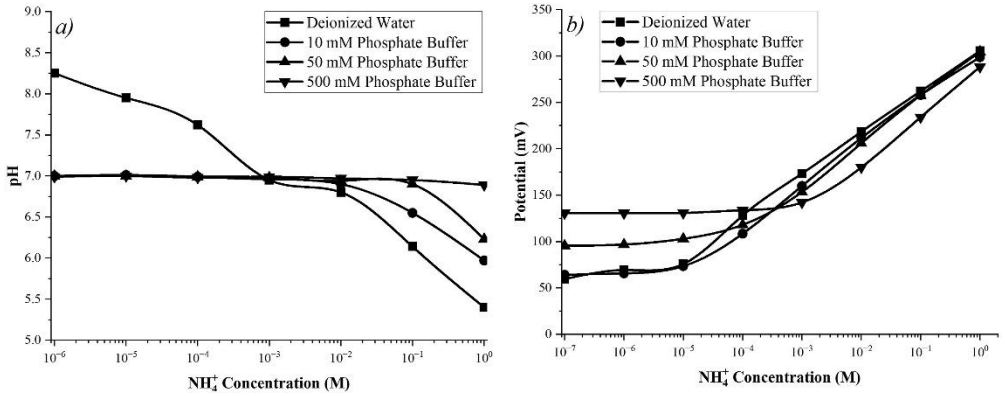

Figure 14. *Effect of NH_4^+concentration on the pH of the buffer: a) pH variation vs. added NH_4^+ in phosphate buffer at different concentrations (10, 50, 500 mM at pH 7.0); b) Calibration curves of NH_4^+ in different medium: deionized water, 10, 50 and 500 mM phosphate buffer pH 7.0.*

Buffer concentrations could also influence the detection limit of the measurements due to the Na^+ content, as demonstrated by the NH_4^+ calibration curves obtained in 10, 50 and 500 mM phosphate buffer (**Figure 14**). As can be observed, the slope of the linear portion remains unchanged, while the NH_4^+ detection limit shifts towards higher values, as the buffer (and therefore the

Na^+) concentration increases. In **Table 8**, the limits of detection (LOD) [224] and limits of quantification (LOQ) [225] for NH_4^+ are reported.

Table 8. *Linearity range, LOD, and LOQ evaluated for the NH_4^+-ISE in different mediums: deionized water and phosphate buffer pH 7.0 at different concentrations.*

Solution	Linearity range (M)	LOD (M)	LOQ (M)
Deionized water	$1.1 \cdot 10^{-5} – 1.0$	$3.4 \cdot 10^{-6}$	$1.1 \cdot 10^{-5}$
10 mM Phosphate buffer	$2.2 \cdot 10^{-5} – 1.0$	$6.7 \cdot 10^{-6}$	$2.2 \cdot 10^{-5}$
50 mM Phosphate buffer	$1.6 \cdot 10^{-4} – 1.0$	$4.8 \cdot 10^{-5}$	$1.6 \cdot 10^{-4}$
500 mM Phosphate buffer	$1.0 \cdot 10^{-3} – 1.0$	$2.6 \cdot 10^{-4}$	$8.7 \cdot 10^{-4}$

It can be observed that the LOD value in a 10 mM phosphate buffer is very close to that found in deionized water, whereas it increases by almost two orders of magnitude passing from 10 mM to 500 mM. This has to be carefully considered for the analysis of real samples. In wastewater samples for which the expected urea-derived NH_4^+ (urea-NH_4^+) content is low, such as drinking water [226], 10 mM phosphate buffer pH 7.0 turns out to be suitable for the quantification of NH_4^+. However, for samples with higher urea-NH_4^+ content, such as industrial [227], municipal [228] and animal farm wastewaters [229], a higher buffer concentration must be used.

2.2.3. Reagent optimization by DoE in bioreactor assembly

Once the analytical performances of the NH_4^+-ISE sensor were characterized, the bioreactors were assembled, by immobilizing the enzyme urease on controlled pores aminopropyl glass beads as solid support. Several requirements must be achieved for immobilizing an enzyme on a solid support:

a) the enzymatic activity should not be altered to any significant degree; b) the immobilized enzyme must be stable, so that the enzymatic activity will be preserved through several reaction cycles; c) the overall cost of the immobilization procedure must be affordable (i.e. significantly reduced or at least not increased). Controlled pore aminopropyl glass beads have been described extensively in literature as a solid support for enzymes in bioreactors [230]. The amine groups of the glass beads are susceptible to cross-linking with glutaraldehyde, a common crosslinking agent, that links the enzyme to glass beads. Nevertheless, an important issue is the control of the degree of cross-linking by controlling the amount of glutaraldehyde. In fact, the activity of the immobilized enzyme can be reduced excessively if too much cross-linking agent is used. On the other hand, if the amount of cross-linking agent is too low, a leakage of the enzyme is possible, and the lifetime of the bioreactor is reduced. Furthermore, the amount of cross-linking agent is related to the amount of enzyme used. By a proper selection of the amount of glutaraldehyde toward the amount of enzyme, it is possible to obtain a balance of high enzyme activity and long endurance, while achieving a high percentage of conversion of enzyme-substrate to the measurable product. In order to optimize the reagents involved in the bioreactor assembly, the effect of glutaraldehyde and enzyme amount was studied as a 2-factors system by using RSM chemometric approach. The experimental domain of the factors was selected on the basis of data reported in literature [230–232] and the results of preliminary experiments (data not shown). In particular, the experimental domain for glutaraldehyde was selected considering that values lower than 0.5 % v/v could compromise enzyme endurance and values higher than 2.5 % v/v might impair enzyme reaction efficiency. Conversely, the lower level for the enzyme was selected to ensure an efficient conversion of the enzyme-substrate to the end product,

while values higher than 9.0 were excluded for minimizing the cost of analysis. Due to the limited number of factors considered and the preliminary information already available, it was possible to directly define the experimental domain to be investigated by RSM.

To obtain the experimental data necessary for the study, several bioreactors were prepared by combining different urea and glutaraldehyde concentrations, according to the FFD shown in **Table 9**, for a total number of 12 combinations (9 experiments + 3 replicates at the center). In addition to them, two more bioreactors were prepared, one containing untreated glass beads while the second one was empty (blanks). Each bioreactor was then tested using a 1.0 M urea solution prepared in pH 7.0 sodium phosphate buffer at a concentration of 500 mM to have the greatest buffering capacity. In this way, by keeping constant urea concentration and flow rate, the variation in potential value can be only related to the combination of the bioreactor components. In **Table 9** the ΔmV measured vs. glutaraldehyde and urease concentrations are reported. Experiments performed with blanks gave negligible signals (lower than the background noise) and data are not shown.

Table 9. *Full Factorial Design (FFD) with the different combinations of urease and glutaraldehyde used to assemble the bioreactors. 12 combinations (9 experiments + 3 replicates) were finally tested.*

Exp. No.	*Glutaraldehyde (% v/v)*	*Urease concentration (mg mL^{-1})*	ΔmV
1	0.5	3.0	75.8
2	1.5	3.0	79.4
3	2.5	3.0	85.8
4	0.5	6.0	90.9
5	1.5	6.0	95.4

Exp. No.	*Glutaraldehyde (% v/v)*	*Urease concentration (mg mL^{-1})*	ΔmV
6	2.5	6.0	97.6
7	0.5	9.0	99.5
8	1.5	9.0	98.4
9	2.5	9.0	97.7
10	1.5	6.0	94.9
11	1.5	6.0	94.8
12	1.5	6.0	94.0

The response was statistically treated and the model was refined by deleting a non-significant quadratic term, resulting in the final calculated model:

$$y = 94.6 + 2.5x_1 + 9.1x_2 - 5.2x_2^2 - 3.0x_1x_2 \quad (20)$$

where y is the potential, x_1 is glutaraldehyde concentration (as v/v%) and x_2 is urease enzyme concentration (as mg mL^{-1}).

This model was found valid and significant by ANOVA and very good values of coefficient of determination R^2 and goodness of prediction Q^2 were found: $R^2 = 0.992$, $Q^2 = 0.959$, reproducibility = 0.994 [219]. The graphical analysis of coefficients is shown in **Figure 15a** and provides a visual representation of the model terms to determine their significance. Each bar corresponds to a term of the model and its length is proportional to the weight of the coefficient. A significant term is one that has an uncertainty level that does not extend across y = 0. A relevant positive linear effect and a negative quadratic effect of urease were noticed. The linear effect of glutaraldehyde was significant but of lower weight, and a negative interaction was found between glutaraldehyde and

urease. Contour plot is reported in **Figure 15b**, by plotting urease vs. glutaraldehyde. The maximization of ΔmV value is obtained in the red zone, at high levels of glutaraldehyde and urease. Anyway, it can be highlighted that values of ΔmV higher than 95.0 mV can be obtained also at medium levels of urease and at high levels of glutaraldehyde. Thus, with the aim of minimizing analysis cost while achieving high response, the value of urease was set at 6 mg mL^{-1}, while glutaraldehyde was fixed at the highest level, corresponding to 2.5 % v/v. Hence, applying these optimized conditions the measured ΔmV was 97.6 ± 0.7 mV (α = 0.025, n = 3), a value which fell inside the predicted interval (95.9 - 98.2 mV).

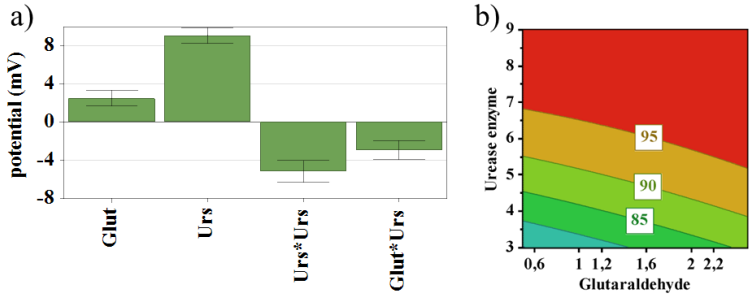

***Figure 15**. a) RSM graphical analysis of effects: Glutaraldehyde (Glut) concentration (v/v%); Urease (Urs) enzyme amount (mg mL^{-1}) b) RSM contour plot for potential obtained by plotting Urease enzyme amount (mg) vs. Glutaraldehyde concentration (v/v%).*

2.2.4. Flow rate optimization

Once optimized the reagent concentrations, the flow rate for online measurement was also evaluated. For this purpose, a $1.0 \cdot 10^{-3}$ M urea solution, prepared in 500 mM sodium phosphate buffer pH 7.0, was loaded into the system and left to flow until reaching a steady-state response condition; different flow rates were tested, from 0.1 to 3.0 mL min^{-1}. The results are reported in **Figure 16a–b**. In particular, **Figure 16a** shows the potential values obtained for the tested flow rates as a function of the measurement time. It can

be observed that the lower the flow rate, the longer the measurement takes to reach a steady-state condition. However, for flow rates in the range 0.1 – 1.0 mL min^{-1} the potential values at the steady-state are very similar. By contrast, they decrease for higher flow rates, probably because the contact time between the enzyme and the analyte is too short, as shown by the ΔmV vs. flow rate values reported in **Figure 16b**. Based on these experimental data, the flow rate of 1.0 mL min^{-1} was chosen to carry on further experiments.

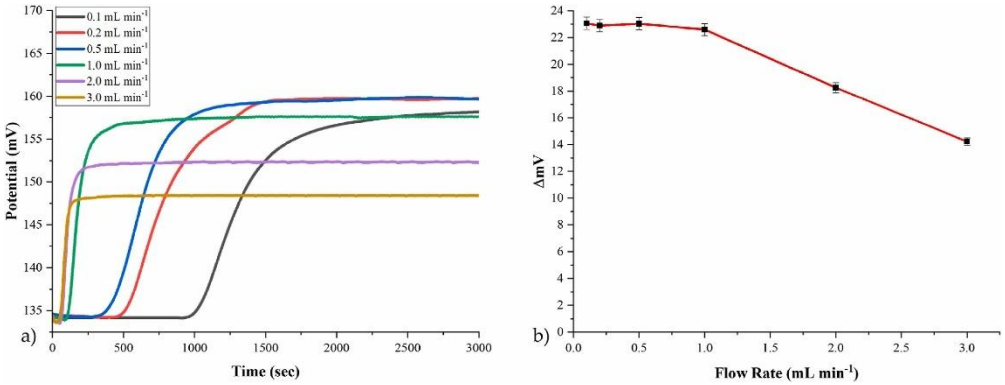

***Figure 16**. Flow rate optimization experiments: a) Potential values recorded vs. measurement time during the flowing of a 1.0 mM urea solution in 500 mM sodium phosphate buffer pH 7.0; b) ΔmV reported vs. flow rate. The error bars correspond to the standard deviation (n = 3).*

2.2.5. Calibration curves of urea in phosphate buffer

Once all critical parameters were optimized, calibration curves of urea in a concentration range from $1.0 \cdot 10^{-6}$ to 1.0 M were performed in sodium phosphate buffer. **Figure 17a** a shows the calibration curves obtained for different buffer concentrations, 10, 50 and 500 mM respectively. It can be observed that, as for the calibration curves for NH_4^+, there is a shift of the linearity range to higher urea concentrations, with the subsequent increase in the LOD values, from $8.9 \cdot 10^{-6}$ to $3.6 \cdot 10^{-4}$ M passing from 10 to 500 mM sodium phosphate buffer, respectively (**Table 10**).

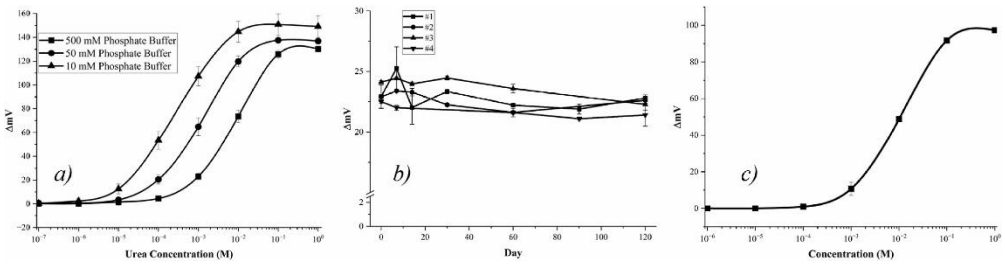

***Figure 17**. Urea calibration curves reported as ΔmV vs. urea concentration, performed in 500, 50 and 10 mM sodium phosphate buffer pH 7.0, respectively, b) Stability over time of four bioreactors; #1, #2 and #3 stored at 4 °C and #4 stored at room temperature. Tests were performed on 1 mM urea solution, c) Urea calibration curve obtained spiked synthetic urine solution obtained by plotting the signal vs. the added urea concentration.*

***Table 10**. Analytical performances of the proposed method in 10, 50 and 500 mM sodium phosphate buffers, pH 7.0.*

Phosphate buffer concentration (mM) pH = 7.0	Linearity range (M)	LOD (M)	LOQ (M)
10	$2.9 \cdot 10^{-5} – 1.0 \cdot 10^{-2}$	$8.9 \cdot 10^{-6}$	$3.0 \cdot 10^{-5}$
50	$1.3 \cdot 10^{-4} – 1.0 \cdot 10^{-2}$	$4.0 \cdot 10^{-5}$	$1.3 \cdot 10^{-4}$
500	$1.2 \cdot 10^{-3} – 1.0 \cdot 10^{-1}$	$3.6 \cdot 10^{-4}$	$1.2 \cdot 10^{-3}$

Therefore, as already mentioned, the buffer selection constitutes a critical point of the measurement and must be carefully selected considering the nature of the samples and the amount of urea to be determined.

The slope of the calibration curves in 500 mM phosphate buffers, pH 7.0 obtained for urea is 51.4 ± 0.4 mV/decade; considering the quasi-Nernstian behavior of the NH_4^+-ISE sensor, with a slope of 51.3 ± 0.2 mV/decade in deionized water, it is possible to conclude that the urea is converted to ammonia within the bioreactor with 100% efficiency over the corresponding linear range (**Table 10**). Indeed, the maximum efficiency of the bioreactor is strictly dependent on pH variation, so that this parameter must be checked for each type of sample.

The stability of the bioreactors was also evaluated, by testing four bioreactors over time using a $1.0 \cdot 10^{-3}$ M urea solution; three of them (named from #1 to #3) were stored at +4 °C, whereas one bioreactor (named as #4) was stored at room temperature in dark condition. The results are shown in **Figure 17b**; it can be seen that the potential response is similar for all the tested bioreactors (response average: 23 ± 1 mV), independently from the storage conditions. In particular, **Figure 17b** shows stability over time higher than 120 days without significant signal decay, confirming the robustness of the assembly methodology and the reproducibility of the functionalization process.

2.2.6. Application to real sample analysis

As already stated, the urea content in real samples can be very different, being strictly dependent on sample type (environmental vs. biological samples). The highest content is expected in urine samples. Some reported urea concentrations in urine from pigs are in the range 198 – 335 mM [233,234], and from around 153 to 763 mM [235]; in human urine, the average urea concentration is around 300 mM [236].

Considering that a possible application of the proposed analytical platform is the monitoring of the biofluid-septic tanks and the wastewater effluent from the farming settings, some preliminary experiments were performed to evaluate the analytical behavior of the bioreactor in this type of matrix. Indeed, urine contains various organic substances but also many inorganic salts, which could constitute an interference in the potentiometric measurements. Thus, a urea calibration curve in a diluted urea-free synthetic human urine [222]was performed (**Figure 17c**). In these experimental conditions, a linear response for urea in the concentration range $1.0 \cdot 10^{-3}$ - $1.0 \cdot 10^{-1}$ M was obtained (42.4 ± 0.5 mV/log[Urea], $R^2 = 0.998$), with a LOD of $6.8 \cdot 10^{-4}$ M. This is the

same linearity range obtained for the calibration curve in the 500 mM phosphate buffer; however, in this case a higher slope is observed (51.4 ± 0.5 mV/log[Urea]); this difference is probably due to a matrix effect related to the synthetic urine composition, as previously discussed. In any case, the approach is sensitive enough to be applied to the determination of urea in this kind of matrices.

Then, the measurements in the four inlet wastewater samples were carried out. To perform the experiments, the samples were filtered through a 0.45 μm filter to remove suspended matter, then spiked with urea in order to achieve a final concentration of 300 mM and finally diluted 1:10 in 500 mM sodium phosphate buffer at pH 7.0. The analysis was carried out by using the Standard Addition Method. **Table 11** shows the recovery results obtained for each sample.

Table 11. *Recovery values for Urea (300 mM) spiked in municipal wastewater samples.*

Sample n.	Observed Urea (mM)	Recovery %
1	295 ± 2	98 %
2	315 ± 3	105 %
3	299 ± 3	99 %
4	311 ± 4	104 %

As can be observed, a very high recovery percentage was obtained for all four samples, with a deviation from the added concentration of no more than 5 %. It is also interesting to note that the urea over- or underestimation does not depend on the NH_4^+ content of the sample, demonstrating that there is no effect of its presence on the urea quantification using the bioreactor-based system

coupled with a potentiometric NH_4^+ sensor. This is an interesting advantage of the proposed method over some colorimetric kits.

To better explain this concept, it should be noted that preliminary experiments aimed to characterize the wastewater for the urea content with commercially available colorimetric kits demonstrated that kits based on the reaction chaired by NADH, α-ketoglutarate and glutamate dehydrogenase are prone to the interference of NH_4^+ present in the wastewater, even in diluted samples. Sample turbidity could have also a detrimental effect on the colorimetric measurements. So, a careful selection of the analytical conditions has to be performed by using the colorimetric kits. The measurements performed with the proposed potentiometric platform are less prone to interference from turbidity and NH_4^+ contents. As a further remark, it should be noted that the NH_4^+ content (or any eventually interferents on the response of the potentiometric sensor) in the sample can be promptly evaluated by temporarily excluding the reactor during this operation by introducing a T-valve in the flow system. This approach is useful for monitoring and controlling NH_4^+ levels in real-time, while ensuring the continuity of the process. Subsequently, the measurement of urea can be carried out by restoring the flow within the reactor.

2.4.Conclusions

A potentiometric biocatalytic-based setup has been successfully developed for the analysis of urea in different types of wastewaters. Operational parameters for performing the measurements were optimized; particular attention was given to the selection of the measurement buffer, which was chosen to minimize potentiometric interferences with the sensor while maintaining adequate buffering capacity for the enzymatic activity. By varying the concentration and ionic strength of the buffer, it is possible to modulate the

linearity ranges and LODs, adapting them to the type of sample being analyzed. This versatility allows the system to be applied to samples with both high urea content (such as those from intensive livestock farms) and lower urea content (such as effluent from wastewater treatment plants). Moreover, in addition to being suitable for online measurements, the approach developed in this work has the advantage of not being affected by the presence of interferents such as NH_4^+, which is naturally present in wastewater samples, unlike most commercially available urea colorimetric kits. Finally, stability trials demonstrated that the optimized bioreactors can be used for more than 4 months without losing activity. This is an excellent premise for a possible application of the potentiometric biocatalytic-based platform for remote online monitoring of urea.

CHAPTER III

This chapter focuses on the industrial-driven optimization and integration of the continuous electrochemical sensing platform for real-time urea monitoring.

3. Industrial development and optimization

To further optimize the system, and considering that the project was also focused and financially supported by the private industrial partner Chemitec S.r.l., a stand-alone fluidic platform was developed, during over six months of work of the PhD candidate in the industrial plant, for remote-controlled measurement and monitoring, designed to be installed in situ when required for continuous urea quantification.

The optimization process involved two main aspects. The first consisted in the development of a cartridge-type bioreactor, designed to be easily replaceable once its performance began to deteriorate (**Figure 18**). The second step involved the design and optimization of the flow cell, for which three prototypes were sequentially developed (images not available due to industrial property restrictions).

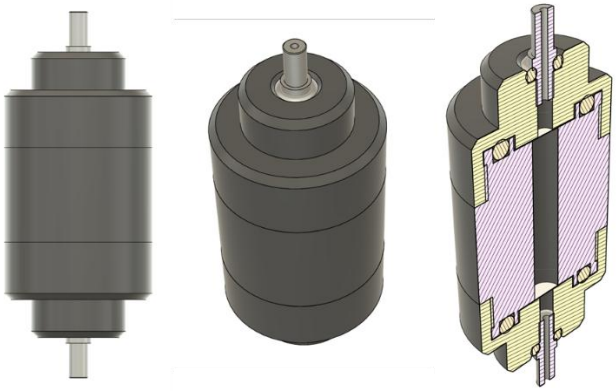

Figure 18. *Rendering and design of the bioreactor with cross-sectional view.*

The first prototype presented significant dead volumes exceeding 10 mL, resulting in slow response times. Moreover, due to the generation of CO_2 as a byproduct of urea hydrolysis, gas bubbles tended to accumulate on the electrode surface. This issue arose because the cell inlet was positioned directly

beneath the electrode, a configuration initially selected to enhance solution mixing. However, this geometry ultimately caused instability and poor reproducibility of the potentiometric response, as the electrode surface occasionally lost contact with the liquid phase due to gas bubble isolation.

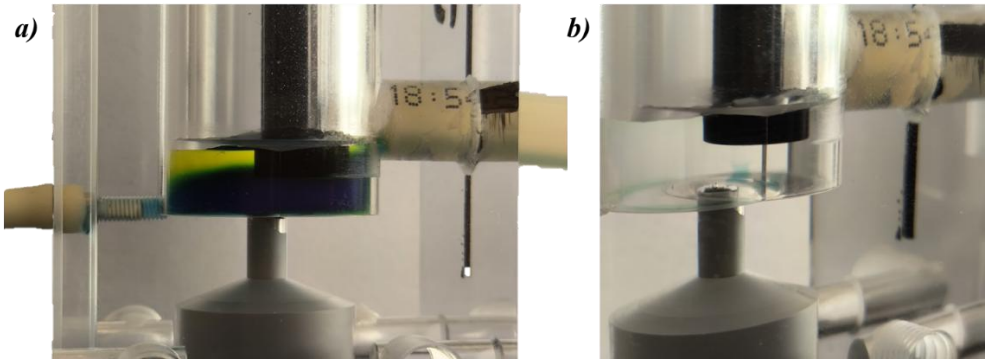

Figure 19. *Image of the flow cell containing two colored solutions illustrating: a) poor mixing between the solutions and stagnation zones; b) regions of turbulence and accumulation (in blue) inside the cell..*

In the second prototype, the flow cell was redesigned with a lateral inlet and an eccentrically positioned electrode, located farther from the inlet and closer to the outlet. These adjustments effectively prevented bubble accumulation on the electrode surface, resulting in a more stable and reproducible potential signal. Flow visualization studies were performed using colored solutions of identical density and temperature to evaluate the mixing efficiency within the cell. As shown in **Figure 19a**, the flow pattern exhibited poor homogenization and localized turbulence zones (**Figure 19b**), while the dead volume remained relatively high (≈ 8 mL).

These observations led to the development of the third prototype (**Figure 20**). In this design, the eccentric geometry of the combined ion-selective electrode was maintained to avoid bubble trapping, but the dead volume was minimized to approximately 3 mL, significantly improving the response time at equal flow rate (Data not shown).

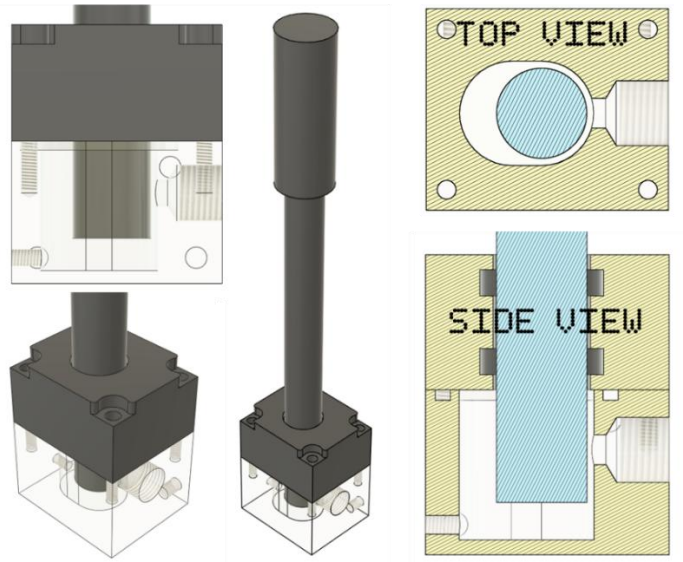

Figure 20. *Rendering of the flow cell with ion-selective electrode, showing top and side views in cross-section (ISE electrode shown in blue).*

The flow cell and the bioreactor were then integrated into a compact measurement station equipped with two peristaltic pumps: one for sample introduction and one for the delivery of a concentrated phosphate buffer solution at pH 7.0. The dual-pump configuration allows independent control of flow rates, enabling precise adjustment of the dilution factor. This feature makes it possible to operate within the linear dynamic range according to specific applications or expected urea concentrations in a given matrix (as discussed in **Section 2.2.5**).

The entire system is managed via an internet-connected control terminal, allowing for remote operation and real-time monitoring. The fully assembled prototype is shown in render **Figure 21**.

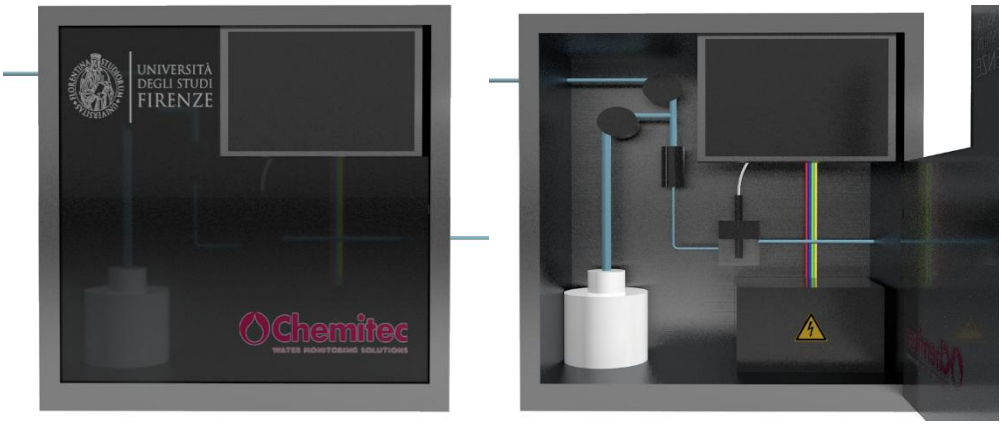

Figure 21. *Rendering of the prototype developed at Chemitec S.r.l., showing the fluidic sampling system, the reservoir containing the phosphate buffer, the peristaltic pumps, the flow cell with the ion-selective electrode, the power supply unit, and the instrument display.*

Following this stage of development, further efforts were directed toward assessing whether it was possible to eliminate the need for the phosphate buffer, thereby simplifying the overall system architecture. Additionally, particular attention was devoted to investigating the possibility of moving beyond the enzymatic approach, which, despite its selectivity, may be prone to heavy metal poisoning, loss of activity at temperatures above 40 °C, and other factors previously discussed.

For these reasons, the focus was shifted toward the synthesis of nanostructured materials for the development of printable electrodes suitable for in situ electrochemical measurements. This approach aimed to achieve a simpler, faster, and more efficient analytical platform while improving sensitivity, stability, and reproducibility compared to the enzymatic system.

The following section presents the research conducted on this topic, which explores the design, synthesis, and characterization of nickel-based nanomaterials and their integration into non-enzymatic electrochemical sensors for urea quantification.

CHAPTER IV

In this section the synthesis of nickel-based materials is proposed for the development of an amperometric sensor for urea quantification in wastewaters.

4. Nanostructured Ni-based sensors for urea determination: a simple and novel approach for wastewater monitoring

Urea is a major nitrogen pollutant in wastewater, contributing to eutrophication and ecosystem imbalance. Current enzymatic detection methods, while selective, are hindered by poor stability and high operational costs in complex matrices. Here, we present a simple, one-pot synthesis of nickel hydroxide nanoparticles (NiNPs) for the development of robust, non-enzymatic electrochemical sensors for urea monitoring. The mild chemical reduction strategy produces highly monodisperse NiNPs without the need for autoclaves or complex instrumentation, supporting scalability and cost-effectiveness.

The NiNPs were immobilized on glassy carbon and screen-printed carbon electrodes, enabling in situ formation of the catalytically active NiOOH phase. Amperometric sensing demonstrated a wide linear range and a low detection limit (165 – 1000 μM and 45.5 μM, respectively).

Validation against a commercial colorimetric kit in certified urine and municipal wastewater samples confirmed the robustness and accuracy of the Ni-based sensors, with recoveries of 95–120%.

This study, to the best of our knowledge, represents the first application of Ni-based sensors for direct wastewater analysis, providing a scalable and sustainable approach for real-time nitrogen pollution control.

3.1. Introduction

Urea ($CO(NH_2)_2$) plays a pivotal role in many industrial applications [237]. Furthermore, urea is the primary end-product of protein catabolism and nitrogen metabolism, synthesized in the liver and excreted via the kidneys [238]. Its concentration in physiological fluids such as blood, urine, and sweat serves as a critical biomarker for assessing renal and hepatic functions. In healthy individuals, blood urea levels typically range between 2.5 and 6.7 mM [239], while significantly elevated concentrations indicate possible pathological states such as chronic kidney disease, hepatic dysfunction, nephrotic syndrome, or urinary disorders [238]. In urine, urea concentration reaches approximately 342 ± 67 mM [240].

Environmental concerns arise from the widespread presence of urea in agricultural runoff, animal and human waste, and industrial effluents. Given its ubiquity, urea's impact on water quality has attracted significant scientific attention. Upon release into natural water bodies, urea undergoes microbial transformation into ammonia and nitrate, substances that contribute to eutrophication and threaten aquatic ecosystems as well as drinking water supplies [241]. These phenomena, intensified by anthropogenic activities, result in substantial ecological and economic burdens.

To mitigate these effects, advanced detection and remediation methodologies for urea have become increasingly important [202,242]. Electrochemical approaches stand out as promising solutions both for detection and remediation. Electrochemical sensors, due to their high sensitivity, scalability, and compatibility with real-time monitoring systems [202,242–244], have been used ever since for urea determination. Moreover, the electro-oxidation of urea has attracted growing interest not only for environmental remediation but also for energy-related applications such as hydrogen production and urea-powered fuel cells [196–198,245].

Recent advances have concentrated on enhancing the efficacy of urea oxidation using nanostructured catalysts. Among these, nickel-based nanomaterials have garnered significant attention owing to their low cost, excellent conductivity, and favorable catalytic activity towards urea oxidation [246]. Nickel nanoparticles, nanowires, and nanosheets exhibit high surface areas and tunable electronic properties, which facilitate urea decomposition at lower overpotentials compared to conventional noble metal catalysts [117,130,238,239,247].

The catalytic effect of Ni-based nanomaterials and the reaction with urea in alkaline environment is given in Equations 1-4 [245]:

$$CO(NH_2)_{2(aq)} + 6OH^- \rightarrow N_{2(g)} + 5H_2O_{(l)} + CO_{2(g)} + 6e^- \quad (21)$$

$$Ni(OH)_{2(s)} + OH^- \rightarrow NiOOH_{(s)} + H_2O_{(l)} + e^- \quad (22)$$

$$6H_2O_{(l)} + 6e^- \rightarrow 3H_{2(g)} + 6OH^- \quad (23)$$

$$CO(NH_2)_{2(aq)} + H_2O_{(l)} \rightarrow N_{2(g)} + 3H_{2(g)} + CO_{2(g)} \quad (24)$$

NiOOH has been employed as an efficient catalyst in various sensing applications, including glucose detection, underscoring its versatility and strong electrocatalytic properties [248–250].

Indeed, integrating such nanomaterials into electrochemical platforms offers a sustainable and economically viable pathway for urea sensing; however, only a few examples are reported in literature and a minority in biological fluids [251,252].

The current study aims to use a practical and straightforward approach using $Ni(OH)_2$ nanoparticle (NiNPs) for urea determination in wastewater. A single-step synthesis of NiNPs has been used to circumvent the need for expensive

instrumentation or commonly employed Teflon-lined autoclaves typically required for hydrothermal treatments [253–257]. By adopting a one-pot approach based on the chemical reduction with sodium borohydride in the presence of Pluronic® surfactants, the process enables the rapid and straightforward production of NiNPs under mild conditions. This methodology offers a practical and cost-effective synthesis for easy industrial, scalable, and environmentally conscious nanoparticle fabrication. Subsequently, the surface of glassy carbon (GC) electrodes and screen-printed carbon electrodes (SPCE) were modified using NiNPs embedded in a Nafion™ membrane to develop cost-effective amperometric sensors (Nf-NiNPs-GC and Nf-NiNPs-SPCE, respectively). The application of these sensors for urea quantification in wastewater was then assessed.

Following preliminary studies to evaluate NiNPs morphological characteristics, the analytical and operational performances of the developed sensors were evaluated, as key parameters including linearity range, potential interferents, limit of detection (LoD), and limit of quantification (LoQ). Finally, the sensors were tested in certified urine and real wastewater samples. The results were compared with those obtained using a commercially available kit for urea quantification. The data obtained demonstrate that this electrochemical approach holds significant promise for addressing the escalating environmental challenges posed by urea contamination, providing a means for real-time assessment of aquatic ecosystems and wastewater quality.

3.2.Materials and methods

3.2.1. Reagents

Urea, NaOH, $Ni(NO_3)_2 \cdot 6H_2O$, Pluronic® F-127, $NaBH_4$, Nafion™ (5 wt.%), Creatine, Oxalic Acid (OA), Uric Acid (UA), NaCl, KCl, NaOH, NH_4Cl,

$K_2Fe[Fe(CN)_6]$, $K_3Fe[Fe(CN)_6]$, and $[Ru(NH_3)_6]Cl_3$ were purchased by Merck (Milan, Italy). Liquichek Urine Chemistry Control (Level 1 #397, certified urea concentration 250 mM) was purchased by Bio-Rad (California, U.S.). Urea Assay Kit (KA1652) for comparison purposes was acquired from Abnova (Taipei, Taiwan).

Potentiostat model CH1140a was purchased from CH Instruments, Inc. (Texas, U.S.). Screen Printed Carbon electrode (SPCE) sensors model DropSens 110 were purchased from Metrohm Italiana S.R.L. (Origgio, Italy).

PalmSens4, assisted by PSTrace 5.11 (Palmsens BV, Houten, The Netherlands), was used to perform Chronocoulometry.

Zetasizer PRO Red Label was purchased from Malvern Panalytical S.R.L. (Milan, Italy).

3.2.2. Measurement set-up

Cyclic Voltammetry (CV) was performed in a three-electrode system setup. In the case of the GC electrode, the three-electrode configuration includes a modified GC working electrode, a stainless-steel counter electrode, and an Ag/AgCl (3 M KCl) reference electrode. For the SPCE, the system comprises a carbon-based modified working electrode, a carbon-based counter electrode, and an Ag/AgCl pseudo-reference electrode. Cyclic voltammetry experiments were conducted in the potential range: -0.5 – +0.6 V, with a scan rate of 50 mV/s.

Electrochemical impedance spectroscopy (EIS) measurements were performed with a sinusoidal voltage of 10 mV amplitude, at an open circuit potential (OCP) value, in a frequency range of 100 kHz to 10 mHz, in 5 mM $[Fe(CN)_6]^{3-/4-}$ in 0.1 M KCl. EIS measurements were then performed, and the spectra were

plotted as complex plane diagrams (Nyquist plots). The Randles-Ershler equivalent circuit parameters were then applied to fit the acquired data.

Chronocoulometric measurements were performed using the following parameters: time interval = 5 ms, potential step (E_1) = -0.5 V, and pulse duration (t_1) = 3 s. The redox probe used was 250 µM Ru(III) hexamine chloride ($RuHex^{3+}$) in 0.1 M KCl.

For amperometric measurements, the instrumental setup for the electrochemical measurement consists of a three-electrode system and a 10 mL glass electrochemical cell, equipped with a magnetic stirrer. In the case of the GC electrode, a stainless-steel counter electrode, and an Ag/AgCl (3 M KCl) reference electrode were used, while for the SPCE, a carbon-based counter electrode, and an Ag/AgCl pseudo-reference electrode were used. Measurements are carried out under continuous stirring, and the current is recorded over time. The current (i) serves as an analytical signal, and it is directly proportional to the urea concentration.

3.2.3. Samples

Seven wastewater samples were collected from the same location at the inlet of an Italian treatment plant processing urban and municipal wastes. After collection, each sample was stored in 0.5 L polyethylene bottle and immediately refrigerated at +4 °C until analysis, to minimize chemical and biological alterations.

Before the analysis the samples were filtered through a 0.45 µm PTFE membrane filter. The urea was then quantified using the standard addition method. An aliquot of 10 mL of the filtrate was collected, and NaOH was added to obtain a final concentration of 1.0 M NaOH. The current was then recorded as a function of time using amperometric detection at +0.48 V. Once the signal

reached a steady state, two successive additions of 100 µM urea were performed. The urea concentration in the sample was determined by linear regression of the current response versus the added concentration, according to the standard addition method.

The recovery was calculated as the ratio between the experimental and theoretical values obtained on a 100 µM urea spike under optimized experimental conditions described above.

3.2.4. NiNPs synthesis

In the proposed approach, a one-pot synthesis has been used to prepare the nanoparticles [257,258]. In this method, 8.1 mg of $Ni(NO_3)_2 \cdot 6H_2O$ and 5.0 mg of Pluronic® were added to 1.0 mL of distilled water in a vial under magnetic stirring (Sol1). Simultaneously, a solution is prepared containing 5.6 mg of $NaBH_4$, 995 µL of distilled water, and 5 µL of 1.0 M NaOH (Sol2). Once Sol1 becomes homogeneous and transparent, 100 µL of Sol2 is added. Within approximately ten seconds, this solution turns black, and the formation of gas bubbles can be observed. The color change indicates the reduction of Ni^{2+} and the subsequent formation of metallic Ni^0 nanoparticles (**Figure 22**).

The dispersion of Ni^0 nanoparticles is then transferred into a vial and centrifuged for 10 minutes at 14,000 rpm to remove the supernatant. Subsequently, 100 µL of distilled water is added for washing, and the mixture is redispersed using an ultrasonic bath for 10 minutes, followed by another centrifugation step and supernatant removal. Then, 100 µL of 1.0 M NaOH solution is added, and the nanoparticles are left at room temperature for 24 hours. After this period, the dispersion appears to be changed from black to an opalescent white color with greenish reflections (**Figure 22g**), indicating nanoparticle oxidation. Thus, the process is terminated, and the prepared

nanoparticles can be stored at +4 °C until use. Nanoparticles have been characterized through Dynamic Light Scattering (DLS) for sizing.

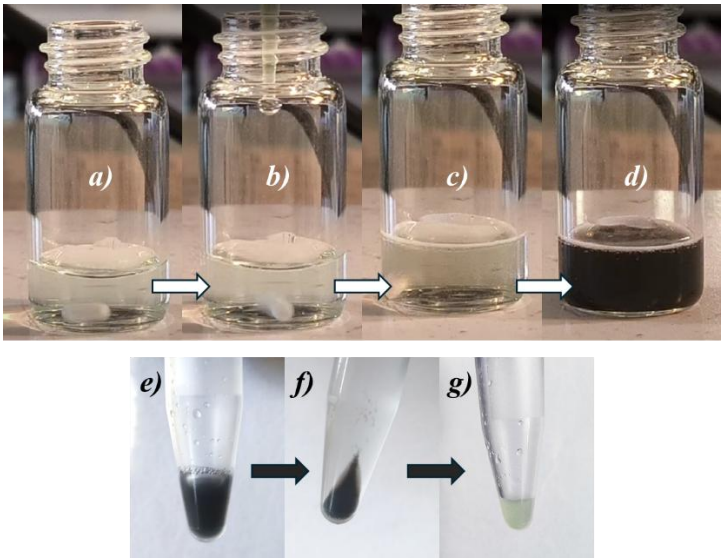

Figure 22. *Synthesis of NiNPs; a) solution containing $Ni(NO_3)_2$ and Pluronic®, b) addition of $NaBH_4$, c) solution after 5 sec, d) solution after 10 sec; e) solution containing the NiNPs, f) NiNPs precipitated by centrifugation, g) $Ni(OH)_2$ NPs obtained after 24h in 100 µL 1.0 M NaOH solution.*

For electrode preparation, 5 µL of the NiNPs dispersion is drop-cast onto the working electrode (GC or SPCE, respectively) and left to dry for 3 hours, followed by 10 µL of a 1% v/v Nafion™ (Nf) solution prepared in distilled water. The electrodes are then left to dry overnight. The electrode surface appears white, in agreement with literature reports that describe $Ni(OH)_2$ as a white compound [252].

Dynamic Light Scattering (DLS) analysis was employed to determine the hydrodynamic radius of the synthesized nanoparticles. This technique provides a rapid and non-invasive means to evaluate particle size distribution in colloidal suspensions. The hydrodynamic diameter obtained from DLS reflects not only the core size of the nanoparticles but also the solvation layer and any surface-bound species, offering critical insight into their colloidal stability,

degree of aggregation, and surface functionalization. As such, DLS serves as a valuable tool for assessing the physical characteristics of nanoparticles under physicochemical conditions relevant to their intended application. For the analysis, 50 μL of the final NiNPs dispersion was pipetted into a polystyrene cuvette (model DTS0012) and subsequently diluted with 550 μL of deionized water to ensure optimal particle count and scattering intensity. The sample was then subjected to DLS analysis under the instrumental conditions optimized by the manufacturer's instructions.

3.3.Results and discussion

3.3.1. NiNPs characterization

Following the synthesis process, an initial evaluation was performed to assess the efficiency and consistency of NiNPs formation. To determine the size distribution and colloidal stability of the NiNPs suspension, DLS measurements were carried out.

The measurements revealed an average hydrodynamic radius of 112 ± 6 nm, with a polydispersity index (PDI) of 0.07 ± 0.02 (data not shown). The narrow size distribution and low PDI indicate that the NiNPs suspension is highly monodispersed, with minimal size variation among particles. Such a low degree of polydispersity is indicative of a well-controlled synthesis process and suggests uniform nucleation and growth of the nanoparticles during the reaction. These characteristics are particularly desirable for applications where reproducibility and consistent particle behavior are critical, such as in catalysis, electrochemical systems, or biomedical formulations.

Nafion-NiNPs-modified GC (Nf-NiNPs-GC) and SPCE (Nf-NiNPs-SPCE) were then electrochemically characterized by CV and EIS. CV experiments

were performed from -0.5 to +0.6 V, with a scan rate of 50 mV/s, in a solution of 5 mM $Fe(CN)_6^{3-/4-}$ in 0.1 M KCl. As shown in **Figure 23a-b**, both the Nf-NiNPs-GC (**Figure 23a**) and Nf-NiNPs-SPCE (**Figure 23b**) exhibit a significant decrease in the redox peak current for $[Fe(CN)_6]^{3-/4-}$ with respect to the bare electrodes (GC blank and SPCE blank, respectively). This behavior is consistent with the modification of both bare-working electrode surfaces with $Ni(OH)_2$. EIS experiment shows an increase of R_{ct} at both electrode surfaces (**Figure 23c-d**), with noticeable differences from the blank for both electrodes. A CV scan was then performed in 1.0 M NaOH solution before and after urea addition to confirm the catalytic activity of the nanomaterial. **Figure 23e** shows CV scans performed in the range -0.2 to + 0.6 V, scan rate 50 mV/s, for both modified electrodes in the absence and in the presence of urea. In the presence of urea, a peak at +0.48 V is observed. This can be attributed to the redox transition from $Ni(OH)_2$ to NiOOH, with a color change from white ($Ni(OH)_2$) to black (NiOOH) [252]. **Figure 23f** shows an image of the electrode surfaces before and after SPCE activation and NiOOH formation.

As an additional investigation aimed at characterizing the electrode surface, the relative surface coverage parameter (Γ_{rel}) was studied for the SPCE-based sensor by using chronocoulometric measurements. For each sensor configuration (bare-, NiNPs-SPCE, and Nf-NiNPs-SPCE, respectively), a background chronocoulometric measurement in 0.1 M KCl, was performed followed by a measurement in the $RuHex^{3+}$ solution, under identical experimental conditions. Then, the surface coverage Γ was determined using a method based on plotting the charge vs. square root of time. The intercepts of these plots were then compared, for each type of sensor, and the difference was attributed to the faradaic charge (Γ_f) associated with the adsorbed electroactive species, effectively isolating it from the capacitive (Γ_c) background. The

correction Γ_f-Γ_c was applied for each electrode configuration, and the resulting values were then normalized by the correction for the bare electrode. The obtained values, Γ_{rel}, (3.4 ± 0.1 for NiNPs-SPCE and 9.2 ± 0.3 for Nf-NiNPs-SPCE) represent a relative surface coverage parameter that is dimensionless and useful for comparing the effect of the surface modification on the apparent amount of adsorbed species [259,260]. These data of the Γ_{rel} confirm the presence of the NiNPs on the electrode surface. The higher value of Γ_{rel} observed for the Nf-NiNPs-SPCE compared to the NiNPs-SPCE can be attributed not only to a possible increase in the electroactive surface area, but also to the electrostatic effects. In particular, the presence of sulfonic acid groups in Nafion™ creates an anionic environment on the electrode surface, which can attract cations such as $RuHex^{3+}$, used as a redox probe. This electrostatic interaction promotes a higher local concentration of the probe near the electrode interface, leading to an apparent increase in Γ_{rel} that is independent of the actual geometric expansion of the surface. A similar observation has been reported in studies on the interaction between Nafion™ films and redox cations [261], where it was shown that electrostatic accumulation of cations can significantly influence the extracted electrochemical parameters.

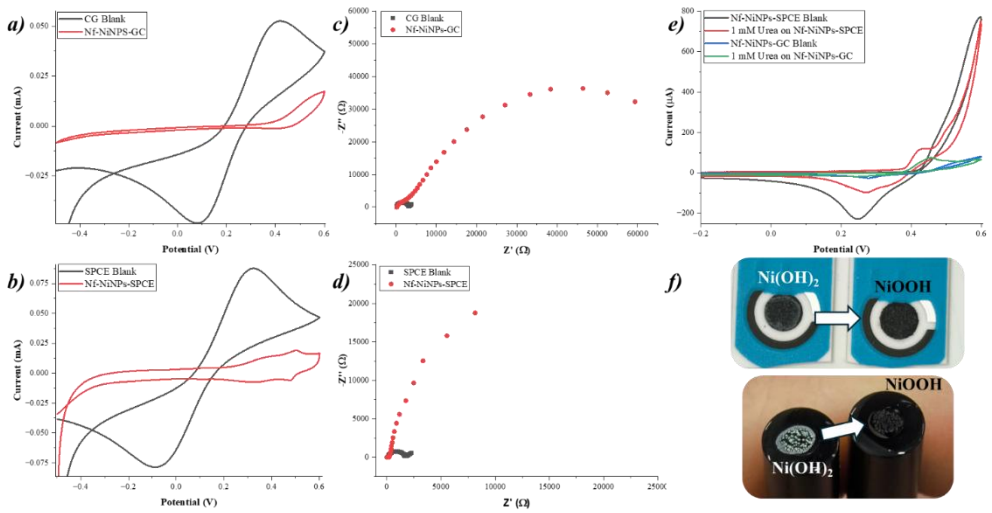

Figure 23. *CV scans, respectively of a) GC (Bare GC) and Nf-NiNPs-GC, and b) SPCE (Bare SPCE) and Nf-NiNPs-SPCE respectively, performed from -0.5 to +0.6 V, scan rate 50 mV/s in a solution of 5 mM $Fe(CN)_6^{3-/4-}$ prepared in 0.1 M KCl; c) and d) EIS measurements in 5 mM $Fe(CN)_6^{3-/4-}$ prepared in 0.1 M KCl solution at 0.01–100,000 Hz frequency range with amplitude 10 mV; e) Cyclic Voltammetry of Nf-NiNPs-GC and Nf-NiNPs-SPCE in 1.0 M NaOH with and without the presence of 1 mM of urea from -0.2 to +0.6 V, scan rate 50 mV/s; f) Nf-NiNPs-GC and Nf-NiNPs-SPCE electrodes surface before and after activation in 1.0 M NaOH solution at E_{app}: +0.48 V.*

3.3.2. Analytical performance for urea determination

Sensors were then applied to the analytical determination of urea by using amperometry at a constant potential of +0.48 V. **Figure 24a** shows the raw data obtained from the amperometric measurement performed with Nf-NiNPs-SPCEs. The red arrows indicate the time and the concentration of the addition. The time interval between two consecutive additions is 20 sec, whereas current values are recorded for 10 sec after each addition, allowing sufficient time for signal stabilization. As can be observed, no detectable signal is achieved for urea concentrations lower than 100 μM; for higher concentrations, it is possible to observe a correlation between the added urea and the recorded current. At urea concentrations higher than 10000 μM, a decrease in the current response is observed. This behavior may be attributed to the slow regeneration kinetics of the catalyst; this step involves the desorption of CO species adsorbed on the

electrode surface. The accumulation of CO/CO_2 can hinder the catalytic process by blocking active sites and thus slowing down the overall reaction rate [262].

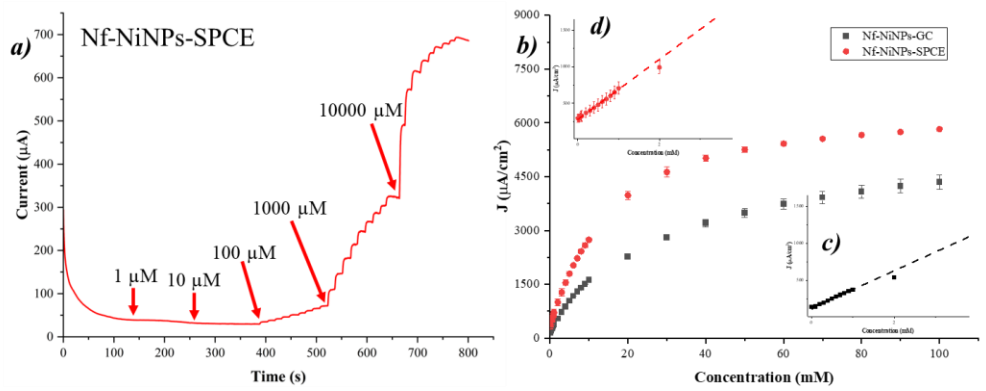

Figure 24. *a) Raw data from amperometric measurement obtained while performing a calibration curve for urea in 1.0 M NaOH solution obtained with the Nf-NiNPs-SPCE; additions were performed every 20 seconds. The current is sampled after 10 seconds; b) A comparison of the calibration curves obtained for urea in 1.0 M NaOH solution (reported as concentration (mM) vs. current density (j)) for both Nf-NiNPs-GC and Nf-NiNPs-SPCE. For Nf- NiNPs-GC (in black): Ag/AgCl (3 M KCl) reference electrode and stainless-steel counter electrode were used; for Nf-NiNPs-SPCE (in red): Ag/AgCl pseudoreference electrode and a carbon counter electrode; c) and d) dynamic linearity range and equation of Nf-NiNPs-GC and Nf-NiNPs-SPCE, respectively.*

Figure 24b shows a comparison of the calibration curves for urea obtained with both Nf-NiNPs-GC and Nf-NiNPs-SPCE in the range 0-100 mM, reported as current density *J*. Each calibration has been performed comparing the modified and bare electrode (data not shown**)**. For both, linear response ranges were identified (**Figure 24c-d**) and the LoD and LoQ values were calculated as 3.3σ/slope and 10σ/slope, respectively. Regarding Nf-NiNPs-GC, a linearity range (*J vs.* Concentration) was identified between 165 – 1000 μM of urea concentration ($y = (2.54 \pm 0.02)\cdot10^{-7}x + (1.26 \pm 0.01)\cdot10^{-4}$, $R^2 = 0.9996$), with a LoD and LoQ values of 45.5 and 165.0 μM, respectively. For Nf-NiNPs-SPCE, a linear response was achieved between 90 – 1000 μM of urea ($y = (4.10 \pm 0.09)\cdot10^{-7}x + (2.82 \pm 0.05)\cdot10^{-4}$, $R^2 = 0.9960$), whereas LoD and LoQ were found to be as 26.9 and 90.0 μM, respectively. Compared to

other urea sensors reported in literature based on Ni-nanomaterials ,the Nf-NiNPs-SPCE sensor exhibited a series of great performances, such as super sensitivity, wider linear range, even, for the majority, lower detection limit and has been the first one applied to wastewater (**Table 12**).

Table 12. *Comparison of analytical performances of other reported urea sensors.*

Material	Linear range (mM)	LOD	Matrices studied	DOI
Ni nanoparticles on glassy carbon	0.085 – 3.10	60 µM	Artificial urine, dialysate, hemodialysis wastewater	[263]
Ni–Co MOF conductive hydrogel	0.5 – 70	445 µM	Simulated tear fluid	[264]
NiONPs/Urease	0.83 – 16.65	830 µM	---	[265]
NiO on EggShell	0.05 – 2.5	~20 µM	---	[266]
Urease-MBs/GO/NiO	0.01 – 0.3	223 µM	---	[267]
Nf-NiNPs-SPCE	0.09 – 1.00	27 µM	Synthetic Urine, Wastewaters	This Work

Additionally, to assess the reproducibility of the sensor fabrication process, the response of different Nf-NiNPs-GC and Nf-NiNPs-SPCE sensors was evaluated upon the addition of 100 µM urea (data not shown). The interelectrode relative standard deviation (RSD%) was then calculated for both electrode types, resulting in values of 6.1% for Nf-NiNPs-GC (n = 9) and 10.5% for Nf-NiNPs-SPCE (n = 9).

3.3.3. Interferents

To evaluate the selectivity of the developed sensors, the response of the Nf-NiNPs electrodes to common species typically found in human urine but which can also be present in wastewater, such as creatinine, oxalic acid (OA), uric acid (UA), chloride ions (Cl^-), and ammonium ions (NH_4^+) was monitored in the presence of 1.0 mM of urea. In particular, 10 µM creatinine, 10 µM OA, 0.1 mM UA, 0.1 mM Cl^-, and 0.1 mM NH_4^+ were added in 1.0 M NaOH solution containing 1.0 mM of urea. The concentration values of the interferents were chosen considering their physiological level in human urine, which can be the worst-case scenario in wastewater samples [38]. Furthermore, some of these molecules, such as ammonium, are known to be interferents in enzymatic reactions that are the main reagents of some colorimetric commercially available kits for urea determination in clinical samples.

As can be seen from **Figure 25a-b**, no current increase for both Nf-NiNPs sensors is observed after the addition of any of the molecules evaluated as potential interferents. However, a current increase is shown after each 1.0 mM urea addition, demonstrating the excellent selectivity of the developed sensors.

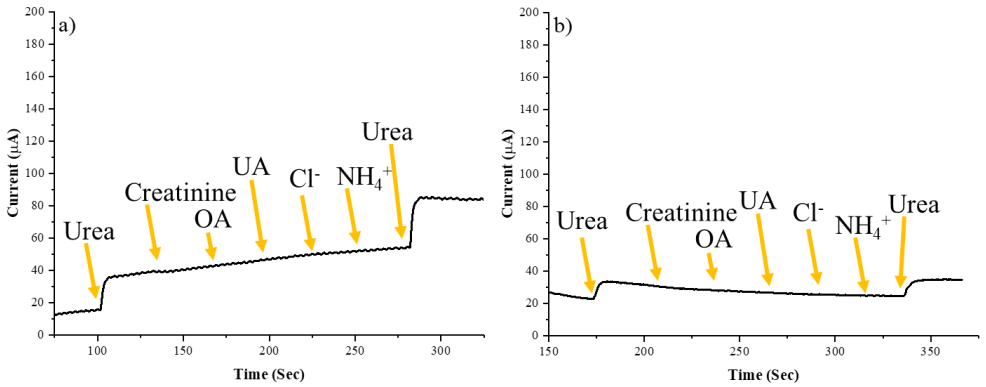

Figure 25. *Amperometric responses obtained at a) Nf-NiNPs-SPCE and b) Nf-NiNPs-GC electrodes to the addition of different interfering species (Creatinine 10 µM, Oxalic Acid (OA) 10 µM, Uric Acid (UA) 100 µM, Cl^- 0.1 mM, NH_4^+ 0.1 mM) or urea (1 mM). E_{app} = +0.48 vs. the respective (pseudo)reference electrode; supporting electrolyte: 1.0 M NaOH solution.*

To evaluate the performance of the sensor in real matrix, a certified urine sample was studied using the standard addition method. For this purpose, the urine sample was diluted 1:100 in 10 mL of 1.0 M NaOH. Then, two subsequent spikes were performed using 20 µL of a 500 mM urea solution prepared in 1.0 M NaOH, in order to obtain 1.0 µM of urea as the final concentration. By extrapolating the analysis data, the urea content obtained for the urine sample was evaluated as 224 ± 47 mM for the Nf-NiNPs-GC, and 255 ± 11 mM for the Nf-NiNPs-SPCE. Both results are comparable to the certified value of 250 mM, highlighting that both sensors are suitable for urea quantification in complex matrices. However, the sensor based on SPCE provides a compact (three electrodes on a strip) and miniaturized platform, more suitable for in-field screening use. Thus, wastewater samples were analyzed by using Nf-NiNPs-SPCE.

3.3.4. Application to wastewater sample analysis

Seven wastewater samples were collected at different positions from a municipal wastewater treatment plant. Sample #1 was collected at the inlet of the treatment plant, samples #2 and #3 were collected at the outlet of the plant, while samples #4–#7 were taken at the plant outlet after undergoing sand filtration.

All seven wastewater samples were first characterized by using a commercial colorimetric urea quantification kit; the results obtained showed that urea concentration was below the LoD of the kit (13 µM, as reported in the manufacturer's instructions) for six of the seven samples. The same samples were then analyzed by the sensor using the standard addition method. Before analysis, each sample was filtered through 0.45 µm membrane filters and added with NaOH to reach a final concentration of 1.0 M.

The results obtained by performing 3 replicates are reported in **Table 13**. As can be observed, samples #2–#7 showed urea concentrations below the sensor's LoD (26.9 µM). Notably, only sample #1 yielded a value of 162 ± 23 µM using the sensor, whereas when analyzed using the commercial kit, a urea concentration of 155 ± 15 µM was obtained. This demonstrates that the developed sensor can detect urea with good agreement with a commercially available kit, showing that it can be successfully applied to the analysis of environmental samples. Although the LOD of the Nf-NiNPs-SPCE sensor is slightly higher than that of the commercial colorimetric kit, the proposed platform provides notable advantages in terms of cost-effectiveness, simplicity, and portability. Unlike enzyme-based urea kits that require multiple reagents, controlled temperature, and long incubation times, the electrochemical sensor enables rapid measurements without enzymatic components or bulky instrumentation such as an ELISA microplate reader. Operated with a compact and affordable potentiostat, it is fully compatible with on-site or point-of-need testing, making it a practical and sustainable alternative for routine urea monitoring in environmental samples.

Table 13. *Concentration of urea obtained by using the commercial colorimetric kit and the Nf-NiNPs-SPCEs. Recovery values obtained after a 100 µM solution of urea was added in the samples*.

Sample	Urea Colorimetric Kit Concentration (µM)	NiNPs Sensor Concentration (µM)	Recovery %
1	155 ± 15	162 ± 23	---
2	<LOD	<LOD	116 ± 13
3	<LOD	<LOD	95 ± 7
4	<LOD	<LOD	96± 10
5	<LOD	<LOD	116 ± 13
6	<LOD	<LOD	120 ± 14
7	<LOD	<LOD	97 ± 12

The recovery parameter was calculated for samples #2–#7 after spiking a known urea concentration. Recovery percentages are reported in **Table 13**; as can be seen, they exhibit values from 95 to 120%. These values are found to be close to the theoretical 100% value, confirming the method's robustness as well as the sensor's reliability for the analysis of real environmental samples.

3.4. Conclusions

A facile, one-pot synthesis of nickel hydroxide nanoparticles (NiNPs) is presented. The mild chemical reduction strategy produces highly monodisperse NiNPs without the need for autoclaves or complex instrumentation, supporting scalability and cost-effectiveness. These were then used to develop robust, non-enzymatic electrochemical sensors for urea monitoring, employing glassy carbon (Nf-NiNPs-GC) and screen-printed carbon electrodes (Nf-NiNPs-SPCE). The amperometric sensors demonstrated broad linear ranges and low detection limits. Interference studies confirmed high selectivity for urea against common compounds that can be found in co-presence. The performance of the developed Nf-NiNPs-SPCE was compared against a standard commercially available colorimetric kit for urea determination, obtaining a good agreement between the methods.

To the best of our knowledge, this is the first example of a modified Nf-iNPs-SPCEs applied to the analysis of wastewater samples for urea quantification, thereby opening new perspectives in environmental analysis.

The electrochemical platform demonstrated analytical reliability, with advantages in terms of operational simplicity, cost-efficiency, and portability which is not possible with the colorimetric kit, which required ex-situ handling and a microplate reader. Thus, Nf-NiNPs-SPCEs sensor represents a promising

tool for online monitoring applications in municipal and industrial wastewater treatment facilities, where rapid and reliable in-situ analysis is critical.

CHAPTER V

This section addresses the general conclusions, the advantages and limitations of the two systems, as well as their potential applications and future developments.

5. Final Conclusions

The present dissertation was dedicated to the development and critical evaluation of electrochemical strategies for urea quantification in complex matrices, with particular emphasis on wastewater monitoring. Two complementary approaches were explored: (i) a potentiometric biocatalytic flow system based on urease as a recognition element, and (ii) an amperometric non-enzymatic sensor based on nickel nanostructures as electrocatalysts for the urea oxidation reaction. Each system was optimized, validated, and assessed in terms of analytical performance, stability, and applicability.

A comparative discussion highlights the advantages and limitations of both systems, drawing on experimental results as well as insights from the state of the art.

From the enzymatic side, the potentiometric biocatalytic system offers remarkable specificity. The urease-based “lock-and-key” mechanism ensures selective recognition of urea, thereby reducing the impact of interfering species. Indeed, in our tests, potentiometric detection showed good resilience to common interferents. However, this advantage is counterbalanced by intrinsic limitations of enzymatic activity: variations in pH, the presence of heavy metals, or other inhibitory compounds may compromise enzyme efficiency. In long-term use, enzyme deactivation remains a critical issue, imposing constraints on sensor durability and cost-effectiveness. Moreover, the potentiometric platform exhibited relatively higher LOD, which may preclude its use in highly diluted samples such as drinking water. Nevertheless, its wide linearity range makes it well suited for applications involving

wastewater or industrial effluents, where urea concentrations are typically elevated.

On the other hand, the amperometric Ni-based system relies on the direct electro-oxidation of urea at the electrode surface, eliminating the need for a biorecognition element. The absence of enzymes might ensure longer-term stability, lower cost of fabrication, and higher robustness under varying environmental conditions. Experimental tests confirmed that the system maintained reliable performance in the presence of typical interferents, including compounds commonly found in urine and wastewater, with no evidence of severe cross-reactivity. However, the specificity of the amperometric sensor is inherently lower than that of the enzymatic approach, since the catalytic mechanism is not exclusive to urea. Although careful material engineering mitigates this drawback, the possibility of interference from electroactive species cannot be fully excluded. From an analytical standpoint, the amperometric system displayed lower detection limits compared to the potentiometric counterpart, rendering it attractive for applications in environmental monitoring of diluted samples, where urea levels may be close to regulatory thresholds.

Taken together, these observations underscore the complementary nature of the two strategies. The potentiometric urease-based system excels in specificity and linearity, and is particularly well adapted to monitoring wastewater streams or industrial discharges with high urea content, provided that enzyme stability can be maintained or cost-effective replacement strategies are implemented. In contrast, the nickel-based amperometric sensor demonstrates sensitivity, robustness, and versatility, which makes it promising for broader environmental and even clinical applications, particularly when lower concentration ranges are of interest. The trade-off between selectivity and

sensitivity is a defining feature of the comparison: while the enzyme ensures selective recognition at the expense of robustness, the non-enzymatic catalyst provides long-term durability and low LODs at the expense of molecular specificity.

Beyond this dual comparison, the thesis also provides broader reflections on the future directions of urea sensing. Advances in nanomaterials will further enhance the catalytic activity and stability of non-enzymatic sensors, potentially narrowing the gap in selectivity with enzyme-based approaches. Conversely, progress in enzyme stabilization strategies, such as immobilization in advanced matrices, encapsulation, or genetic engineering, may significantly prolong the lifetime and robustness of urease-based devices. Moreover, the integration of electrochemical sensors into microfluidic and lab-on-chip platforms is expected to improve automation, reduce reagent consumption, and enable multiplexed analysis. Coupling these systems with wearable technologies could open new avenues for real-time monitoring of urea in sweat or other biological fluids, relevant to personalized healthcare. Finally, the application of artificial intelligence and chemometric methods will be instrumental in addressing selectivity issues, correcting for environmental variations, and enhancing data interpretation in complex samples.

In conclusion, this doctoral work provides both a critical review of the state of the art and original contributions to the design and validation of innovative electrochemical systems for urea quantification. By comparing enzymatic and non-enzymatic strategies, it demonstrates that no single solution is universally superior; rather, the choice of approach must be guided by the analytical context and the concentration range of interest. Potentiometric enzymatic sensors remain valuable tools for high-concentration samples where selectivity is paramount, while nickel-based amperometric systems represent a promising

alternative for low-concentration monitoring requiring high sensitivity and robustness. Together, these contributions enrich the toolbox of bioanalytical chemistry, paving the way toward sustainable and practical solutions for monitoring a molecule of central relevance to human health, agriculture, and the environment.

Bibliography

[1] I.Y. Wong, The History of Urea and Its Use in the Modern Fertilizer Industry, in: Proceedings of the 4th International Conference on Biotechnology and Biomedicine, SCITEPRESS - Science and Technology Publications, 2022: pp. 435–439. https://doi.org/10.5220/0012032100003633.

[2] Urea, its history and applications, Mark Brouwer (2009).

[3] D.S. Dimski, Ammonia Metabolism and the Urea Cycle: Function and Clinical Implications, J Vet Intern Med 8 (1994) 73–78. https://doi.org/10.1111/j.1939-1676.1994.tb03201.x.

[4] M.C. Korrapati, H.M. Mehendale, Urea, in: Encyclopedia of Toxicology, Elsevier, 2014: pp. 885–888. https://doi.org/10.1016/B978-0-12-386454-3.00357-2.

[5] C.S. Pundir, S. Jakhar, V. Narwal, Determination of urea with special emphasis on biosensors: A review, Biosens Bioelectron 123 (2019) 36–50. https://doi.org/10.1016/j.bios.2018.09.067.

[6] B. Yang, L. Bankir, Urea and urine concentrating ability: new insights from studies in mice, American Journal of Physiology-Renal Physiology 288 (2005) F881–F896. https://doi.org/10.1152/ajprenal.00367.2004.

[7] I.M. Washington, G. Van Hoosier, Clinical Biochemistry and Hematology, in: The Laboratory Rabbit, Guinea Pig, Hamster, and Other Rodents, Elsevier, 2012: pp. 57–116. https://doi.org/10.1016/B978-0-12-380920-9.00003-1.

[8] S.N. Botewad, D.K. Gaikwad, N.B. Girhe, H.N. Thorat, P.P. Pawar, Urea biosensors: A comprehensive review, Biotechnol Appl Biochem 70 (2023) 485–501. https://doi.org/10.1002/bab.2168.

[9] C.S. Pundir, S. Jakhar, V. Narwal, Determination of urea with special emphasis on biosensors: A review, Biosens Bioelectron 123 (2019) 36–50. https://doi.org/10.1016/j.bios.2018.09.067.

[10] J.V. Leonard, A.A.M. Morris, Urea cycle disorders, Seminars in Neonatology 7 (2002) 27–35. https://doi.org/10.1053/siny.2001.0085.

[11] S.M. Laville, A. Couturier, O. Lambert, M. Metzger, N. Mansencal, C. Jacquelinet, M. Laville, L. Frimat, D. Fouque, C. Combe, B.M. Robinson, B. Stengel, S. Liabeuf, Z.A. Massy, C. Ayav, S. Briançon, D. Cannet, C. Combe, D. Fouque, L. Frimat, Y.-E. Herpe, C. Jacquelinet, M. Laville, Z.A. Massy,

C. Pascal, B.M. Robinson, B. Stengel, C. Lange, K. Legrand, S. Liabeuf, M. Metzger, E. Speyer, T. Hannedouche, B. Moulin, S. Mailliez, G. Lebrun, E. Magnant, G. Choukroun, B. Deroure, A. Lacraz, G. Lambrey, J. Philippe, Bourdenx, M. Essig, T. Lobbedez, R. Azar, H. Sekhri, M. Smati, M. Jamali, A. Klein, M. Delahousse, C. Combe, S. Martin, I. Landru, E. Thervet, Z.A. Massy, P. Lang, X. Belenfant, P. Urena, C. Vela, L. Frimat, D. Chauveau, V. Panescu, C. Noel, F. Glowacki, M. Hoffmann, M. Hourmant, D. Besnier, A. Testa, F. Kuentz, P. Zaoui, C. Chazot, L. Juillard, S. Burtey, A. Keller, N. Kamar, D. Fouque, M. Laville, Urea levels and cardiovascular disease in patients with chronic kidney disease, Nephrology Dialysis Transplantation 38 (2023) 184–192. https://doi.org/10.1093/ndt/gfac045.

[12] D.S. Dimski, Ammonia Metabolism and the Urea Cycle: Function and Clinical Implications, J Vet Intern Med 8 (1994) 73–78. https://doi.org/10.1111/j.1939-1676.1994.tb03201.x.

[13] K. Nichols, I.P.C. de Carvalho, R. Rauch, J. Martín-Tereso, Review: Unlocking the limitations of urea supply in ruminant diets by considering the natural mechanism of endogenous urea secretion, Animal 16 (2022) 100537. https://doi.org/10.1016/j.animal.2022.100537.

[14] G.B. Huntington, S.L. Archibeque, Practical aspects of urea and ammonia metabolism in ruminants, J Anim Sci 77 (2000) 1. https://doi.org/10.2527/jas2000.77E-Suppl1y.

[15] S. Kojima, A. Bohner, N. von Wirén, Molecular Mechanisms of Urea Transport in Plants, J Membr Biol 212 (2006) 83–91. https://doi.org/10.1007/s00232-006-0868-6.

[16] A. Sirko, R. Brodzik, Plant ureases: roles and regulation., Acta Biochim Pol 47 (2000) 1189–1195. https://doi.org/10.18388/abp.2000_3972.

[17] C.-P. Witte, Urea metabolism in plants, Plant Science 180 (2011) 431–438. https://doi.org/10.1016/j.plantsci.2010.11.010.

[18] J.F.T. Berliner, Crystal Urea: Industrial Development and Properties, Ind Eng Chem 28 (1936) 517–522. https://doi.org/10.1021/ie50317a003.

[19] Production of urea worldwide from 2009 to 2022, (n.d.).

[20] L. Shi, L. Liu, B. Yang, G. Sheng, T. Xu, Evaluation of Industrial Urea Energy Consumption (EC) Based on Life Cycle Assessment (LCA), Sustainability 12 (2020) 3793. https://doi.org/10.3390/su12093793.

[21] S. Qureshi, M. Mumtaz, F.K. Chong, A. Mukhtar, S. Saqib, S. Ullah, M. Mubashir, K.S. Khoo, P.L. Show, A review on sensing and catalytic activity of nano-catalyst for synthesis of one-step ammonia and urea: Challenges and perspectives, Chemosphere 291 (2022) 132806. https://doi.org/10.1016/j.chemosphere.2021.132806.

[22] M. Xia, C. Mao, A. Gu, A.A. Tountas, C. Qiu, T.E. Wood, Y.F. Li, U. Ulmer, Y. Xu, C.J. Viasus, J. Ye, C. Qian, G. Ozin, Solar Urea: Towards a Sustainable Fertilizer Industry, Angewandte Chemie International Edition 61 (2022). https://doi.org/10.1002/anie.202110158.

[23] I. Santos Mesquita, P. Albuquerque Melo, A. Resende Secchi, Novel pathways for urea synthesis decarbonization: An analytical review from Bosch–Meiser to electroreduction processes, Appl Energy 400 (2025) 126527. https://doi.org/10.1016/j.apenergy.2025.126527.

[24] J. Ding, R. Ye, Y. Fu, Y. He, Y. Wu, Y. Zhang, Q. Zhong, H.H. Kung, M. Fan, Direct synthesis of urea from carbon dioxide and ammonia, Nat Commun 14 (2023) 4586. https://doi.org/10.1038/s41467-023-40351-5.

[25] I. Santos Mesquita, P. Albuquerque Melo, A. Resende Secchi, Novel pathways for urea synthesis decarbonization: An analytical review from Bosch–Meiser to electroreduction processes, Appl Energy 400 (2025) 126527. https://doi.org/10.1016/j.apenergy.2025.126527.

[26] J. Meessen, Urea synthesis, Chemie Ingenieur Technik 86 (2014) 2180–2189. https://doi.org/10.1002/cite.201400064.

[27] P.M. Glibert, J. Harrison, C. Heil, S. Seitzinger, Escalating Worldwide use of Urea – A Global Change Contributing to Coastal Eutrophication, Biogeochemistry 77 (2006) 441–463. https://doi.org/10.1007/s10533-005-3070-5.

[28] M. Canle L, S. Rodríguez, L.F. Rodríguez Vázquez, J.A. Santaballa, S. Steenken, First stages of photodegradation of the urea herbicides Fenuron, Monuron and Diuron, J Mol Struct 565–566 (2001) 133–139. https://doi.org/10.1016/S0022-2860(00)00940-6.

[29] Q. Sun, C. Hse, T.F. Shupe, Effect of different catalysts on urea–formaldehyde resin synthesis, J Appl Polym Sci 131 (2014). https://doi.org/10.1002/app.40644.

[30] A. Nuryawan, I. Risnasari, T. Sucipto, A. Heri Iswanto, R. Rosmala Dewi, Urea-formaldehyde resins: production, application, and testing, IOP Conf Ser

Mater Sci Eng 223 (2017) 012053. https://doi.org/10.1088/1757-899X/223/1/012053.

[31] E. Berardesca, N. Cameli, Non-invasive assessment of urea efficacy: A review, Int J Clin Pract 74 (2020). https://doi.org/10.1111/ijcp.13603.

[32] E. Campione, T. Cosio, M. Di Prete, A. Piccolo, C. Lanna, P. Lombardo, L. Diluvio, E. Dika, F. Baciorri, A. Orlandi, L. Bianchi, Effectiveness of a cosmetic device containing a combination of alpha- and beta-hydroxy acids, urea, and thuja for the treatment of seborrheic keratoses, J Cosmet Dermatol 21 (2022) 2113–2119. https://doi.org/10.1111/jocd.14346.

[33] T. Lauer, Preparation of Ammonia from Liquid AdBlue – Modeling Approaches and Future Challenges, Chemie Ingenieur Technik 90 (2018) 783–794. https://doi.org/10.1002/cite.201700107.

[34] J.W. Erisman, M.A. Sutton, J. Galloway, Z. Klimont, W. Winiwarter, How a century of ammonia synthesis changed the world, Nat Geosci 1 (2008) 636–639. https://doi.org/10.1038/ngeo325.

[35] J.M. Bremner, Recent research on problems in the use of urea as a nitrogen fertilizer, Fertilizer Research 42 (1995) 321–329. https://doi.org/10.1007/BF00750524.

[36] K.L. Sahrawat, Control of urea hydrolysis and nitrification in soil by chemicals—Prospects and problems, Plant Soil 57 (1980) 335–352. https://doi.org/10.1007/BF02211691.

[37] Rocky Lemus, https://extension.msstate.edu/publications/urea-based-fertilizers-forage-production, Publication 2678 (POD-10-24) (2011).

[38] B. Azeem, K. KuShaari, Z.B. Man, A. Basit, T.H. Thanh, Review on materials & methods to produce controlled release coated urea fertilizer, Journal of Controlled Release 181 (2014) 11–21. https://doi.org/10.1016/j.jconrel.2014.02.020.

[39] R. Zhao, J. Liu, N. Xu, T. He, J. Meng, Z. Liu, Urea hydrolysis in different farmland soils as affected by long-term biochar application, Front Environ Sci 10 (2022). https://doi.org/10.3389/fenvs.2022.950482.

[40] Clain A. JonesRichard T. KoenigJason W. EllsworthShow all 5 authorsGrant D. Jackson, Management of Urea Fertilizer to Minimize Volatilization, (2007).

[41] S. Seitzinger, J.A. Harrison, J.K. Böhlke, A.F. Bouwman, R. Lowrance, B. Peterson, C. Tobias, G. Van Drecht, Denitrification across Landscapes and Waterscapes: A Synthesis, 2006.

[42] D. Matczuk, A. Siczek, Effectiveness of the use of urease inhibitors in agriculture: a review, Int Agrophys 35 (2021) 197–208. https://doi.org/10.31545/intagr/139714.

[43] S.-J. Hwang, Eutrophication and the Ecological Health Risk, Int J Environ Res Public Health 17 (2020) 6332. https://doi.org/10.3390/ijerph17176332.

[44] R.A. Copeland, ENZYMES A Practical Introduction to Structure, Mechanism, and Data Analysis SECOND EDITION, n.d.

[45] V.B. Urlacher, K. Koschorreck, Enzyme Structure and Function, in: 2024: pp. 19–38. https://doi.org/10.1007/978-3-031-42999-6_2.

[46] T.D.H. Bugg, Introduction to Enzyme and Coenzyme Chemistry, (n.d.) 7–12.

[47] I. D'Agostino, S. Carradori, Urease, in: Metalloenzymes, Elsevier, 2024: pp. 393–410. https://doi.org/10.1016/B978-0-12-823974-2.00035-8.

[48] K. STINGL, Staying alive overdosed: How does control urease activity?, International Journal of Medical Microbiology 295 (2005) 307–315. https://doi.org/10.1016/j.ijmm.2005.06.006.

[49] J.L. Boer, S.B. Mulrooney, R.P. Hausinger, Nickel-dependent metalloenzymes, Arch Biochem Biophys 544 (2014) 142–152. https://doi.org/10.1016/j.abb.2013.09.002.

[50] J.L. Boer, S.B. Mulrooney, R.P. Hausinger, Nickel-dependent metalloenzymes, Arch Biochem Biophys 544 (2014) 142–152. https://doi.org/10.1016/j.abb.2013.09.002.

[51] B. Nagel, H. Dellweg, L.M. Gierasch, Glossary for chemists of terms used in biotechnology (IUPAC Recommendations 1992), Pure and Applied Chemistry 64 (1992) 143–168. https://doi.org/10.1351/pac199264010143.

[52] D.R. Thévenot, K. Toth, R.A. Durst, G.S. Wilson, Electrochemical biosensors: recommended definitions and classification1International Union of Pure and Applied Chemistry: Physical Chemistry Division, Commission I.7 (Biophysical Chemistry); Analytical Chemistry Division, Commission V.5 (Electroanalytical Chemistry).1, Biosens Bioelectron 16 (2001) 121–131. https://doi.org/10.1016/S0956-5663(01)00115-4.

[53] A. Pasquarelli, Catalytic Biosensors, 2021.

[54] Chapter 4 Affinity Biosensors, in: 1992: pp. 253–290. https://doi.org/10.1016/S0167-9244(08)70036-2.

[55] Varnakavi. Naresh, N. Lee, A Review on Biosensors and Recent Development of Nanostructured Materials-Enabled Biosensors, Sensors 21 (2021) 1109. https://doi.org/10.3390/s21041109.

[56] I. Palchetti, Affinity Biosensors for Tumor-Marker Analysis, Bioanalysis 6 (2014) 3417–3435. https://doi.org/10.4155/bio.14.247.

[57] N.J. Ronkainen, H.B. Halsall, W.R. Heineman, Electrochemical biosensors, Chem Soc Rev 39 (2010) 1747. https://doi.org/10.1039/b714449k.

[58] J.A.L.B. Yunus S, Potentiometric Biosensors, Encyclopedia of Biophysics. Springer Berlin Heidelberg, Berlin, Heidelberg (2013) 1941–1946.

[59] Sadeghi SJ, Amperometric Biosensors, Encyclopedia of Biophysics, Springer Berlin Heidelberg, Berlin, Heidelberg (2013) 61–67.

[60] R.H. Radecki J, Voltammetric Biosensors in Bioanalysis, Handbook of Bioanalytics. Springer International Publishing, Cham (2022) 747–760.

[61] E.B. Bahadır, M.K. Sezgintürk, A review on impedimetric biosensors, Artif Cells Nanomed Biotechnol 44 (2016) 248–262. https://doi.org/10.3109/21691401.2014.942456.

[62] J.-R.N. Dzyadevych S, Conductometric biosensors. In: Biological Identification, 2014.

[63] Z. Li, M. Xiao, C. Jin, Z. Zhang, Toward the Commercialization of Carbon Nanotube Field Effect Transistor Biosensors, Biosensors (Basel) 13 (2023) 326. https://doi.org/10.3390/bios13030326.

[64] J. Häberle, N. Boddaert, A. Burlina, A. Chakrapani, M. Dixon, M. Huemer, D. Karall, D. Martinelli, P. Crespo, R. Santer, A. Servais, V. Valayannopoulos, M. Lindner, V. Rubio, C. Dionisi-Vici, Suggested guidelines for the diagnosis and management of urea cycle disorders, Orphanet J Rare Dis 7 (2012) 32. https://doi.org/10.1186/1750-1172-7-32.

[65] https://www.esamed.it/en/products/human-line/point-of-care-testing-en/automatic-dry-biochemical-analyzer-sd1/ (accessed on 30/05/2023), (n.d.).

[66] https://lifetest.dk/en/product/insight-minichem-analyser-si-units-urea-mmol-l-ua-umol-l-crea-umol-l/ (Accessed on 30/05/2023), (n.d.).

[67] https://it.lysunbio.com/ (Accessed on 30/05/2023), (n.d.).

[68] https://www.globalpointofcare.abbott/en/index.html (Accessed on 30/05/2023), (n.d.).

[69] R. Larcher, M. Lottelier, S. Badiou, A.-M. Dupuy, A.-S. Bargnoux, J.-P. Cristol, Analytical Performances of the Novel i-STAT Alinity Point-of-Care Analyzer, Diagnostics 13 (2023) 297. https://doi.org/10.3390/diagnostics13020297.

[70] https://www.siemens-healthineers.com/blood-gas/blood-gas-systems/epoc-blood-analysis-system (Accessed on 30/05/2023), (n.d.).

[71] https://www.edan.com/product/e/i15_Blood_Gas_and_Chemistry_Analysis_System.html (Accessed on 30/05/2023), (n.d.).

[72] https://www.radiometer.com/en/products/blood-gas-testing/abl90-flex-plus-blood-gas-analyzer (Accessed on 30/05/2023), (n.d.).

[73] A.-S. Bargnoux, N. Kuster, T. Sutra, L. Laroche, A. Rodriguez, M. Morena, L. Chenine, L. Chalabi, A.-M. Dupuy, S. Badiou, J.-P. Cristol, Evaluation of a new point-of-care testing for creatinine and urea measurement, Scand J Clin Lab Invest 81 (2021) 290–297. https://doi.org/10.1080/00365513.2021.1914344.

[74] C.J. Saatkamp, M.L. de Almeida, J.A.M. Bispo, A.L.B. Pinheiro, A.B. Fernandes, L. Silveira, Quantifying creatinine and urea in human urine through Raman spectroscopy aiming at diagnosis of kidney disease, J Biomed Opt 21 (2016) 037001. https://doi.org/10.1117/1.JBO.21.3.037001.

[75] Z. Zhao, J. Xiao, X. Zhang, J. Jiang, M. Zhang, Y. Li, T. Li, J. Wang, A thread-based micro device for continuous electrochemical detection of saliva urea, Microchemical Journal 190 (2023) 108634. https://doi.org/10.1016/j.microc.2023.108634.

[76] D.J. Saldanha, A. Cai, N.-M. Dorval Courchesne, The Evolving Role of Proteins in Wearable Sweat Biosensors, ACS Biomater Sci Eng 9 (2023) 2020–2047. https://doi.org/10.1021/acsbiomaterials.1c00699.

[77] P. Schimmel, L. Kleinjans, R.S. Bongers, J. Knol, C. Belzer, Breast milk urea as a nitrogen source for urease positive *Bifidobacterium infantis*, FEMS Microbiol Ecol 97 (2021). https://doi.org/10.1093/femsec/fiab019.

[78] W.D. Gould, C. Hagedorn, R.G.L. McCready, Urea Transformations and Fertilizer Efficiency in Soil, in: 1986: pp. 209–238. https://doi.org/10.1016/S0065-2113(08)60283-7.

[79] B. Gagnon, N. Ziadi, C. Grant, Urea fertilizer forms affect grain corn yield and nitrogen use efficiency, Can J Soil Sci 92 (2012) 341–351. https://doi.org/10.4141/cjss2011-074.

[80] V. Dhanushkodi, T.B. Priyadharshini, M. Baskar, S. Meena, K. Senthil, T.U. Maheshwari, Slow and Controlled Release Nitrogen Fertilizers: Options for Improving Rice Productivity: A Review, Int J Plant Soil Sci (2022) 970–981. https://doi.org/10.9734/ijpss/2022/v34i242726.

[81] M. Pan, G. Heinecke, S. Bernardo, C. Tsui, J. Levitt, Urea: a comprehensive review of the clinical literature, Dermatol Online J 19 (2013). https://doi.org/10.5070/D31911020392.

[82] T.A. Currier, D.W. Bohnert, S.J. Falck, S.J. Bartle, Daily and alternate day supplementation of urea or biuret to ruminants consuming low-quality forage: I. Effects on cow performance and the efficiency of nitrogen use in wethers1,2, J Anim Sci 82 (2004) 1508–1517. https://doi.org/10.2527/2004.8251508x.

[83] M. Xia, C. Mao, A. Gu, A.A. Tountas, C. Qiu, T.E. Wood, Y.F. Li, U. Ulmer, Y. Xu, C.J. Viasus, J. Ye, C. Qian, G. Ozin, Solar Urea: Towards a Sustainable Fertilizer Industry, Angewandte Chemie 134 (2022). https://doi.org/10.1002/ange.202110158.

[84] D. Weerakoon, B. Bansal, L.P. Padhye, A. Rachmani, L. James Wright, G. Silyn Roberts, S. Baroutian, A critical review on current urea removal technologies from water: An approach for pollution prevention and resource recovery, Sep Purif Technol 314 (2023) 123652. https://doi.org/10.1016/j.seppur.2023.123652.

[85] P.M. Glibert, T.M. Trice, B. Michael, L. Lane, Urea in the Tributaries of the Chesapeake and Coastal Bays of Maryland, Water Air Soil Pollut 160 (2005) 229–243. https://doi.org/10.1007/s11270-005-2546-1.

[86] M. Latkar, T. Chakrabarti, Performance of upflow anaerobic sludge blanket reactor carrying out biological hydrolysis of urea, Water Environment Research 66 (1994) 12–15. https://doi.org/10.2175/WER.66.1.3.

[87] Y. Chen, H. Chen, Z. Chen, H. Hu, C. Deng, X. Wang, The benefits of autotrophic nitrogen removal from high concentration of urea wastewater through a process of urea hydrolysis and partial nitritation in sequencing batch reactor, J Environ Manage 292 (2021) 112762. https://doi.org/10.1016/j.jenvman.2021.112762.

[88] P.S. Francis, S.W. Lewis, K.F. Lim, Analytical methodology for the determination of urea: current practice and future trends, TrAC Trends in Analytical Chemistry 21 (2002) 389–400. https://doi.org/10.1016/S0165-9936(02)00507-1.

[89] W.T. Bolleter, C.J. Bushman, P.W. Tidwell, Spectrophotometric Determination of Ammonia as Indophenol, Anal Chem 33 (1961) 592–594. https://doi.org/10.1021/ac60172a034.

[90] O. Özbek, C. Berkel, Ö. Isildak, I. Isildak, Potentiometric urea biosensors, Clinica Chimica Acta 524 (2022) 154–163. https://doi.org/10.1016/j.cca.2021.11.011.

[91] M.K. Reay, C.A. Yates, P.J. Johnes, C.J. Arthur, D.L. Jones, R.P. Evershed, High resolution HPLC-MS confirms overestimation of urea in soil by the diacetyl monoxime (DAM) colorimetric method, Soil Biol Biochem 135 (2019) 127–133. https://doi.org/10.1016/j.soilbio.2019.04.015.

[92] J. Zhou, C. Liu, Y. Chen, X. Luo, D. Deng, Determination of Urea in Swimming Pool Water Using High-Performance Liquid Chromatography with Online Postcolumn Derivatization by Xanthydrol, J Chromatogr Sci 61 (2023) 339–346. https://doi.org/10.1093/chromsci/bmac025.

[93] E. Reynoso, E. Torres, F. Bettazzi, I. Palchetti, Trends and Perspectives in Immunosensors for Determination of Currently-Used Pesticides: The Case of Glyphosate, Organophosphates, and Neonicotinoids, Biosensors (Basel) 9 (2019) 20. https://doi.org/10.3390/bios9010020.

[94] P.S. Sfragano, G. Moro, F. Polo, I. Palchetti, The Role of Peptides in the Design of Electrochemical Biosensors for Clinical Diagnostics, Biosensors (Basel) 11 (2021) 246. https://doi.org/10.3390/bios11080246.

[95] I. Palchetti, C. Upjohn, A.P.F. Turner, M. Mascini, Disposable Screen-Printed Electrodes (Spe) Mercury-Free for Lead Detection, Anal Lett 33 (2000) 1231–1246. https://doi.org/10.1080/00032710008543119.

[96] G.G. Guilbault, J.G. Montalvo, Urea-specific enzyme electrode, J Am Chem Soc 91 (1969) 2164–2165. https://doi.org/10.1021/ja01036a083.

[97] G.G. Guilbault, E. Hrabankova, Electrode for determination of amino acids, Anal Chem 42 (1970) 1779–1783. https://doi.org/10.1021/ac50160a052.

[98] G.G. Guilbault, J.G. Montalvo, Enzyme electrode for the substrate urea, J Am Chem Soc 92 (1970) 2533–2538. https://doi.org/10.1021/ja00711a052.

[99] P.H. Weiner, J.F. Parcher, Improved urea electrode, Anal Chem 45 (1973) 417–419. https://doi.org/10.1021/ac60324a053.

[100] G.G. Guilbault, F.R. Shu, Enzyme electrodes based on the use of a carbon dioxide sensor. Urea and L-tyrosine electrodes, Anal Chem 44 (1972) 2161–2166. https://doi.org/10.1021/ac60321a023.

[101] M. Mascini, G.G. Guilbault, Urease coupled ammonia electrode for urea determination in blood serum, Anal Chem 49 (1977) 795–798. https://doi.org/10.1021/ac50014a031.

[102] C. Eggenstein, M. Borchardt, C. Diekmann, Bernd Gründig, C. Dumschat, K. Cammann, M. Knoll, Friedrich Spener, A disposable biosensor for urea determination in blood based on an ammonium-sensitive transducer, Biosens Bioelectron 14 (1999) 33–41. https://doi.org/10.1016/S0956-5663(98)00103-1.

[103] F. Silva, Potentiometric determination of urea by sequential injection using Jack bean meal crude extract as a source of urease, Talanta 53 (2000) 331–336. https://doi.org/10.1016/S0039-9140(00)00490-2.

[104] T. Anfält, A. Graneli, D. Jagner, A Urea Electrode Based on the Ammonia Probe, Anal Lett 6 (1973) 969–975. https://doi.org/10.1080/00032717308058175.

[105] A. Senillou, N. Jaffrezic-Renault, C. Martelet, S. Cosnier, A miniaturized urea sensor based on the integration of both ammonium based urea enzyme field effect transistor and a reference field effect transistor in a single chip, Talanta 50 (1999) 219–226. https://doi.org/10.1016/S0039-9140(99)00122-8.

[106] M. SINGH, N. VERMA, A. GARG, N. REDHU, Urea biosensors, Sens Actuators B Chem 134 (2008) 345–351. https://doi.org/10.1016/j.snb.2008.04.025.

[107] D.A. Daramola, D. Singh, G.G. Botte, Dissociation Rates of Urea in the Presence of NiOOH Catalyst: A DFT Analysis, J Phys Chem A 114 (2010) 11513–11521. https://doi.org/10.1021/jp105159t.

[108] F. Guo, K. Ye, M. Du, X. Huang, K. Cheng, G. Wang, D. Cao, Electrochemical impedance analysis of urea electro-oxidation mechanism on nickel catalyst in alkaline medium, Electrochim Acta 210 (2016) 474–482. https://doi.org/10.1016/j.electacta.2016.05.149.

[109] V. Vedharathinam, G.G. Botte, Experimental Investigation of Potential Oscillations during the Electrocatalytic Oxidation of Urea on Ni Catalyst in

Alkaline Medium, The Journal of Physical Chemistry C 118 (2014) 21806–21812. https://doi.org/10.1021/jp5052529.

[110] V. Vedharathinam, G.G. Botte, Direct evidence of the mechanism for the electro-oxidation of urea on Ni(OH)2 catalyst in alkaline medium, Electrochim Acta 108 (2013) 660–665. https://doi.org/10.1016/j.electacta.2013.06.137.

[111] S. Singh, M. Sharma, G. Singh, Recent advancements in urea biosensors for biomedical applications, IET Nanobiotechnol 15 (2021) 358–379. https://doi.org/10.1049/nbt2.12050.

[112] H.D. Mai, G.Y. Sung, H. Yoo, Fabrication of nickel oxide nanostructures with high surface area and application for urease-based biosensor for urea detection, RSC Adv 5 (2015) 78807–78814. https://doi.org/10.1039/C5RA14103F.

[113] D. Zhu, H. Zhang, J. Miao, F. Hu, L. Wang, Y. Tang, M. Qiao, C. Guo, Strategies for designing more efficient electrocatalysts towards the urea oxidation reaction, J Mater Chem A Mater 10 (2022) 3296–3313. https://doi.org/10.1039/D1TA09989B.

[114] X. Wang, J. Li, Y. Duan, J. Li, H. Wang, X. Yang, M. Gong, Electrochemical Urea Oxidation in Different Environment: From Mechanism to Devices, ChemCatChem 14 (2022). https://doi.org/10.1002/cctc.202101906.

[115] K.J. Babu, N. Senthilkumar, A.R. Kim, G.G. kumar, Freestanding and binder free PVdF-HFP/Ni-Co nanofiber membrane as a versatile platform for the electrocatalytic oxidation and non-enzymatic detection of urea, Sens Actuators B Chem 241 (2017) 541–551. https://doi.org/10.1016/j.snb.2016.10.069.

[116] S. Amin, A. Tahira, A. Solangi, V. Beni, J.R. Morante, X. Liu, M. Falhman, R. Mazzaro, Z.H. Ibupoto, A. Vomiero, A practical non-enzymatic urea sensor based on $NiCo_2O_4$ nanoneedles, RSC Adv 9 (2019) 14443–14451. https://doi.org/10.1039/C9RA00909D.

[117] C. Bao, Q. Niu, Z.-A. Chen, X. Cao, H. Wang, W. Lu, Ultrathin nickel-metal–organic framework nanobelt based electrochemical sensor for the determination of urea in human body fluids, RSC Adv 9 (2019) 29474–29481. https://doi.org/10.1039/C9RA05716A.

[118] J. Yoon, Y.S. Yoon, D.-J. Kim, Silver-Nanoparticle-Decorated NiOOH Nanorods for Electrocatalytic Urea Sensing, ACS Appl Nano Mater 3 (2020) 7651–7658. https://doi.org/10.1021/acsanm.0c01279.

[119] Y.-T. Chen, P.-Y. Chen, S.-P. Ju, Preparation of Ni nanotube-modified electrodes via galvanic displacement on sacrificial Zn templates: Solvent effects and attempts for non-enzymatic electrochemical detection of urea, Microchemical Journal 158 (2020) 105172. https://doi.org/10.1016/j.microc.2020.105172.

[120] T.S. Sunil Kumar Naik, S. Saravanan, K.N. Sri Saravana, U. Pratiush, P.C. Ramamurthy, A non-enzymatic urea sensor based on the nickel sulfide / graphene oxide modified glassy carbon electrode, Mater Chem Phys 245 (2020) 122798. https://doi.org/10.1016/j.matchemphys.2020.122798.

[121] T.Q.N. Tran, S.W. Yoon, B.J. Park, H.H. Yoon, CeO2-modified LaNi0.6Fe0.4O3 perovskite and MWCNT nanocomposite for electrocatalytic oxidation and detection of urea, Journal of Electroanalytical Chemistry 818 (2018) 76–83. https://doi.org/10.1016/j.jelechem.2018.04.003.

[122] T.Q.N. Tran, G. Das, H.H. Yoon, Nickel-metal organic framework/MWCNT composite electrode for non-enzymatic urea detection, Sens Actuators B Chem 243 (2017) 78–83. https://doi.org/10.1016/j.snb.2016.11.126.

[123] R. Sha, K. Komori, S. Badhulika, Graphene–Polyaniline composite based ultra-sensitive electrochemical sensor for non-enzymatic detection of urea, Electrochim Acta 233 (2017) 44–51. https://doi.org/10.1016/j.electacta.2017.03.043.

[124] J. Yoon, M. Sim, T.-S. Oh, Y.S. Yoon, D.-J. Kim, Flexible Electrochemical Sensor Based on NiCu(OOH) for Monitoring Urea in Human Sweat, J Electrochem Soc 168 (2021) 117510. https://doi.org/10.1149/1945-7111/ac34ca.

[125] F. Cui, Y. Yue, Y. Zhang, Z. Zhang, H.S. Zhou, Advancing Biosensors with Machine Learning, ACS Sens 5 (2020) 3346–3364. https://doi.org/10.1021/acssensors.0c01424.

[126] H. Chen, E. Kätelhön, R.G. Compton, Machine learning in fundamental electrochemistry: Recent advances and future opportunities, Curr Opin Electrochem 38 (2023) 101214. https://doi.org/10.1016/j.coelec.2023.101214.

[127] B. Zambelli, F. Musiani, S. Benini, S. Ciurli, Chemistry of Ni^{2+} in Urease: Sensing, Trafficking, and Catalysis, Acc Chem Res 44 (2011) 520–530. https://doi.org/10.1021/ar200041k.

[128] M.S. Ghauri, J.D.R. Thomas, Evaluation of an ammonium ionophore for use in poly(vinyl chloride) membrane ion-selective electrodes: solvent mediator effects, Analyst 119 (1994) 2323. https://doi.org/10.1039/an9941902323.

[129] P. Kumar, P. Ramulu Lambadi, N. Kumar Navani, Non-enzymatic detection of urea using unmodified gold nanoparticles based aptasensor, Biosens Bioelectron 72 (2015) 340–347. https://doi.org/10.1016/j.bios.2015.05.029.

[130] Y.L. Liu, R. Liu, Y. Qin, Q.F. Qiu, Z. Chen, S.B. Cheng, W.H. Huang, Flexible Electrochemical Urea Sensor Based on Surface Molecularly Imprinted Nanotubes for Detection of Human Sweat, Anal Chem 90 (2018) 13081–13087. https://doi.org/10.1021/acs.analchem.8b04223.

[131] G. Palleschi, M. Mascini, E. Martinez-fabregas, S. Alegret, Urea Determination in Human Sera With an Ammonium Ion Selective Electrode Made With Solid Inner Electric Contact and Immobilised Urease, Anal Lett 21 (1988) 1115–1129. https://doi.org/10.1080/00032718808055500.

[132] I. Wałcerz, R. Koncki, E. Leszczyńska, B. Salamonowicz, S. Głąb, Urea Biosensors Based on PVC Membrane Ion-Selective Electrodes, Anal Lett 29 (1996) 1939–1953. https://doi.org/10.1080/00032719608000800.

[133] Y. Kan, An All-Solid-State Ammonium Ion-Selective Electrode Based on Polyaniline as Transducer and Poly (o-phenylenediamine) as Sensitive Membrane, Int J Electrochem Sci (2016) 9928–9940. https://doi.org/10.20964/2016.12.03.

[134] J. Hu, A. Stein, P. Bühlmann, Rational design of all-solid-state ion-selective electrodes and reference electrodes, TrAC Trends in Analytical Chemistry 76 (2016) 102–114. https://doi.org/10.1016/j.trac.2015.11.004.

[135] M.E. Meyerhoff, Polymer membrane electrode based potentiometric ammonia gas sensor, Anal Chem 52 (1980) 1532–1534. https://doi.org/10.1021/ac50059a037.

[136] K.A. Erickson, P. Wilding, Evaluation of a novel point-of-care system, the i-STAT portable clinical analyzer, Clin Chem 39 (1993) 283–287. https://doi.org/10.1093/clinchem/39.2.283.

[137] P.S. Sfragano, S. Laschi, I. Palchetti, Sustainable Printed Electrochemical Platforms for Greener Analytics, Front Chem 8 (2020). https://doi.org/10.3389/fchem.2020.00644.

[138] S. Laschi, I. Palchetti, G. Marrazza, M. Mascini, Development of disposable low density screen-printed electrode arrays for simultaneous electrochemical

measurements of the hybridisation reaction, Journal of Electroanalytical Chemistry 593 (2006) 211–218. https://doi.org/10.1016/j.jelechem.2006.04.015.

[139] C.S. Kushwaha, P. Singh, N.S. Abbas, S.K. Shukla, Self-activating zinc oxide encapsulated polyaniline-grafted chitosan composite for potentiometric urea sensor, Journal of Materials Science: Materials in Electronics 31 (2020) 11887–11896. https://doi.org/10.1007/s10854-020-03743-7.

[140] S. Jakhar, C.S. Pundir, Preparation, characterization and application of urease nanoparticles for construction of an improved potentiometric urea biosensor, Biosens Bioelectron 100 (2018) 242–250. https://doi.org/10.1016/j.bios.2017.09.005.

[141] Y.-H. Nien, T.-Y. Su, C.-S. Ho, J.-C. Chou, C.-H. Lai, P.-Y. Kuo, Z.-X. Kang, Z.-X. Dong, T.-Y. Lai, C.-H. Wang, The Analysis of Potentiometric Flexible Arrayed Urea Biosensor Modified by Graphene Oxide and γ-Fe_2O_3 Nanoparticles, IEEE Trans Electron Devices 67 (2020) 5104–5110. https://doi.org/10.1109/TED.2020.3023067.

[142] B. Öndeş, F. Akpınar, M. Uygun, M. Muti, D. Aktaş Uygun, High stability potentiometric urea biosensor based on enzyme attached nanoparticles, Microchemical Journal 160 (2021) 105667. https://doi.org/10.1016/j.microc.2020.105667.

[143] H.J.N.P.D. Mello, M. Mulato, Enzymatically functionalized polyaniline thin films produced with one-step electrochemical immobilization and its application in glucose and urea potentiometric biosensors, Biomed Microdevices 22 (2020). https://doi.org/10.1007/s10544-020-00478-4.

[144] F. Kuralay, H. Özyörük, A. Yıldız, Potentiometric enzyme electrode for urea determination using immobilized urease in poly(vinylferrocenium) film, Sens Actuators B Chem 109 (2005) 194–199. https://doi.org/10.1016/j.snb.2004.12.043.

[145] M. Gutiérrez, S. Alegret, M. del Valle, Potentiometric bioelectronic tongue for the analysis of urea and alkaline ions in clinical samples, Biosens Bioelectron 22 (2007) 2171–2178. https://doi.org/10.1016/j.bios.2006.10.007.

[146] D. Chirizzi, C. Malitesta, Potentiometric urea biosensor based on urease immobilized by an electrosynthesized poly(o-phenylenediamine) film with buffering capability, Sens Actuators B Chem 157 (2011) 211–215. https://doi.org/10.1016/j.snb.2011.03.051.

[147] S.M.U. Ali, Z.H. Ibupoto, S. Salman, O. Nur, M. Willander, B. Danielsson, Selective determination of urea using urease immobilized on ZnO nanowires, Sens Actuators B Chem 160 (2011) 637–643. https://doi.org/10.1016/j.snb.2011.08.041.

[148] S.V. Marchenko, I.S. Kucherenko, A.N. Hereshko, I.V. Panasiuk, O.O. Soldatkin, A.V. El'skaya, A.P. Soldatkin, Application of potentiometric biosensor based on recombinant urease for urea determination in blood serum and hemodialyzate, Sens Actuators B Chem 207 (2015) 981–986. https://doi.org/10.1016/j.snb.2014.06.136.

[149] B. Liu, R. Hu, J. Deng, Studies on a potentiometric urea biosensor based on an ammonia electrode and urease, immobilized on a γ-aluminum oxide matrix, Anal Chim Acta 341 (1997) 161–169. https://doi.org/10.1016/S0003-2670(96)00553-3.

[150] S.K. Jha, A. Topkar, S.F. D'Souza, Development of potentiometric urea biosensor based on urease immobilized in PVA–PAA composite matrix for estimation of blood urea nitrogen (BUN), J Biochem Biophys Methods 70 (2008) 1145–1150. https://doi.org/10.1016/j.jprot.2007.12.006.

[151] X. Chen, Z. Yang, S. Si, Potentiometric urea biosensor based on immobilization of urease onto molecularly imprinted TiO2 film, Journal of Electroanalytical Chemistry 635 (2009) 1–6. https://doi.org/10.1016/j.jelechem.2009.07.005.

[152] T. Ahuja, D. Kumar, N. Singh, A.M. Biradar, Rajesh, Potentiometric urea biosensor based on multi-walled carbon nanotubes (MWCNTs)/silica composite material, Materials Science and Engineering: C 31 (2011) 90–94. https://doi.org/10.1016/j.msec.2010.08.001.

[153] K. Saeedfar, L. Heng, T. Ling, M. Rezayi, Potentiometric Urea Biosensor Based on an Immobilised Fullerene-Urease Bio-Conjugate, Sensors 13 (2013) 16851–16866. https://doi.org/10.3390/s131216851.

[154] R.O. Flores, L. Maria, C. Silva, A.F. Melo, A.M. Salgado, Analysis of Potential Applicability of the Potentiometric Urea Biosensor to Real Samples, in: 2013. www.aidic.it/cet.

[155] W. Prissanaroon-Ouajai, A. Sirivat, P.J. Pigram, N. Brack, Potentiometric Urea Biosensor Based on a Urease-Immobilized Polypyrrole, Macromol Symp 354 (2015) 334–339. https://doi.org/10.1002/masy.201400087.

[156] R. Ramesh, P. Puhazhendi, J. Kumar, M.K. Gowthaman, S.F. D'Souza, N.R. Kamini, Potentiometric biosensor for determination of urea in milk using

immobilized Arthrobacter creatinolyticus urease, Materials Science and Engineering: C 49 (2015) 786–792. https://doi.org/10.1016/j.msec.2015.01.048.

[157] A.N. Reshetilov, Y. V. Plekhanova, S.A. Tikhonenko, A. V. Dubrovskii, Polyelectrolyte microcapsules with urease and paramagnetic particles as a basis for a potentiometric biosensor for determining urea, Journal of Analytical Chemistry 70 (2015) 1368–1372. https://doi.org/10.1134/S1061934815110131.

[158] J. MagalhÃ£es, Urea potentiometric biosensor based on urease immobilized on chitosan membranes, Talanta 47 (1998) 183–191. https://doi.org/10.1016/S0039-9140(98)00066-6.

[159] M.-J. Syu, Y.-S. Chang, Ionic effect investigation of a potentiometric sensor for urea and surface morphology observation of entrapped urease/polypyrrole matrix, Biosens Bioelectron 24 (2009) 2671–2677. https://doi.org/10.1016/j.bios.2009.01.036.

[160] P. Pandey, Tetraphenylborate doped polyaniline based novel pH sensor and solid-state urea biosensor, Talanta 55 (2001) 773–782. https://doi.org/10.1016/S0039-9140(01)00505-7.

[161] S. Komaba, M. Seyama, T. Momma, T. Osaka, Potentiometric biosensor for urea based on electropolymerized electroinactive polypyrrole, Electrochim Acta 42 (1997) 383–388. https://doi.org/10.1016/S0013-4686(96)00226-5.

[162] Rajesh, V. Bisht, W. Takashima, K. Kaneto, Development of a potentiometric urea biosensor based on copolymer poly(N-3-aminopropyl pyrrole-co-pyrrole) film, React Funct Polym 62 (2005) 51–59. https://doi.org/10.1016/j.reactfunctpolym.2004.08.009.

[163] T. AHUJA, I. MIR, D. KUMAR, RAJESH, Potentiometric urea biosensor based on BSA embedded surface modified polypyrrole film, Sens Actuators B Chem 134 (2008) 140–145. https://doi.org/10.1016/j.snb.2008.04.020.

[164] U.B. Trivedi, D. Lakshminarayana, I.L. Kothari, N.G. Patel, H.N. Kapse, K.K. Makhija, P.B. Patel, C.J. Panchal, Potentiometric biosensor for urea determination in milk, Sens Actuators B Chem 140 (2009) 260–266. https://doi.org/10.1016/j.snb.2009.04.022.

[165] B. Lakard, D. Magnin, O. Deschaume, G. Vanlancker, K. Glinel, S. Demoustier-Champagne, B. Nysten, A.M. Jonas, P. Bertrand, S. Yunus, Urea potentiometric enzymatic biosensor based on charged biopolymers and

electrodeposited polyaniline, Biosens Bioelectron 26 (2011) 4139–4145. https://doi.org/10.1016/j.bios.2011.04.009.

[166] L.T.M. Nguyen, H.H. Yoon, Potentiometric Urea Biosensor Based on Carbon Nanotubes and Polyion Complex Film, J Nanosci Nanotechnol 15 (2015) 1150–1153. https://doi.org/10.1166/jnn.2015.9327.

[167] X. Mei, J. Yang, J. Liu, Y. Li, Wearable, nanofiber-based microfluidic systems with integrated electrochemical and colorimetric sensing arrays for multiplex sweat analysis, Chemical Engineering Journal 454 (2023) 140248. https://doi.org/10.1016/j.cej.2022.140248.

[168] G. Ibáñez-Redín, G. Rosso Cagnani, N. O. Gomes, P.A. Raymundo-Pereira, S.A. S. Machado, M.A. Gutierrez, J.E. Krieger, O.N. Oliveira, Wearable potentiometric biosensor for analysis of urea in sweat, Biosens Bioelectron 223 (2023) 114994. https://doi.org/10.1016/j.bios.2022.114994.

[169] J. Ping, J. Wu, Y. Wang, Y. Ying, Simultaneous determination of ascorbic acid, dopamine and uric acid using high-performance screen-printed graphene electrode, Biosens Bioelectron 34 (2012) 70–76. https://doi.org/10.1016/j.bios.2012.01.016.

[170] F. Bettazzi, C. Ingrosso, P.S. Sfragano, V. Pifferi, L. Falciola, M.L. Curri, I. Palchetti, Gold nanoparticles modified graphene platforms for highly sensitive electrochemical detection of vitamin C in infant food and formulae, Food Chem 344 (2021) 128692. https://doi.org/10.1016/j.foodchem.2020.128692.

[171] J. Ping, Y. Wang, J. Wu, Y. Ying, F. Ji, Determination of ascorbic acid levels in food samples by using an ionic liquid–carbon nanotube composite electrode, Food Chem 135 (2012) 362–367. https://doi.org/10.1016/j.foodchem.2012.05.013.

[172] E. Dervisevic, M. Dervisevic, J.N. Nyangwebah, M. Şenel, Development of novel amperometric urea biosensor based on Fc-PAMAM and MWCNT bio-nanocomposite film, Sens Actuators B Chem 246 (2017) 920–926. https://doi.org/10.1016/j.snb.2017.02.122.

[173] A.K. Singh, M. Singh, N. Verma, Electrochemical preparation of Fe3O4/MWCNT-polyaniline nanocomposite film for development of urea biosensor and its application in milk sample, Journal of Food Measurement and Characterization 14 (2020) 163–175. https://doi.org/10.1007/s11694-019-00278-2.

[174] V. Sanko, A. Şenocak, S.O. Tümay, E. Demirbas, A novel comparative study for electrochemical urea biosensor design: Effect of different ferrite nanoparticles (MFe2O4, M: Cu, Co, Ni, Zn) in urease immobilized composite system, Bioelectrochemistry 149 (2023) 108324. https://doi.org/10.1016/j.bioelechem.2022.108324.

[175] V. Kumar, I. Kaur, S. Arora, R. Mehla, K. Vellingiri, K.-H. Kim, Graphene nanoplatelet/graphitized nanodiamond-based nanocomposite for mediator-free electrochemical sensing of urea, Food Chem 303 (2020) 125375. https://doi.org/10.1016/j.foodchem.2019.125375.

[176] K. Kim, J. Lee, B.M. Moon, Y.B. Seo, C.H. Park, M. Park, G.Y. Sung, Fabrication of a urea biosensor for real-time dynamic fluid measurement, Sensors (Switzerland) 18 (2018). https://doi.org/10.3390/s18082607.

[177] D. Fapyane, D. Berillo, J.-L. Marty, N.P. Revsbech, Urea Biosensor Based on a CO_2 Microsensor, ACS Omega 5 (2020) 27582–27590. https://doi.org/10.1021/acsomega.0c04146.

[178] H.S. Magar, R.Y.A. Hassan, A. Mulchandani, Electrochemical Impedance Spectroscopy (EIS): Principles, Construction, and Biosensing Applications, Sensors 21 (2021) 6578. https://doi.org/10.3390/s21196578.

[179] A. Bose, K. Biswas, Impedimetry-Based Disposable Sensor for the Detection of Urea in Aqueous Media, IEEE Sens J 23 (2023) 4185–4192. https://doi.org/10.1109/JSEN.2022.3232377.

[180] R. Rahmanian, S.A. Mozaffari, H.S. Amoli, M. Abedi, Development of sensitive impedimetric urea biosensor using DC sputtered Nano-ZnO on TiO2 thin film as a novel hierarchical nanostructure transducer, Sens Actuators B Chem 256 (2018) 760–774. https://doi.org/10.1016/j.snb.2017.10.009.

[181] S.S. An, H.H. Yoon, G. Das, Amperometric urea biosensors based on sulfonated graphene/polyaniline nanocomposite, Int J Nanomedicine (2015) 55. https://doi.org/10.2147/IJN.S88315.

[182] O.Y. Saiapina, V.M. Pyeshkova, O.O. Soldatkin, V.G. Melnik, B.A. Kurç, A. Walcarius, S.V. Dzyadevych, N. Jaffrezic-Renault, Conductometric enzyme biosensors based on natural zeolite clinoptilolite for urea determination, Materials Science and Engineering: C 31 (2011) 1490–1497. https://doi.org/10.1016/j.msec.2011.06.003.

[183] M. Tak, V. Gupta, M. Tomar, Zinc oxide–multiwalled carbon nanotubes hybrid nanocomposite based urea biosensor, J Mater Chem B 1 (2013) 6392. https://doi.org/10.1039/c3tb20935k.

[184] J. Das, P. Sarkar, Enzymatic electrochemical biosensor for urea with a polyaniline grafted conducting hydrogel composite modified electrode, RSC Adv 6 (2016) 92520–92533. https://doi.org/10.1039/C6RA12159D.

[185] R. Rahmanian, S.A. Mozaffari, M. Abedi, Disposable urea biosensor based on nanoporous ZnO film fabricated from omissible polymeric substrate, Materials Science and Engineering: C 57 (2015) 387–396. https://doi.org/10.1016/j.msec.2015.08.004.

[186] S.A. Mozaffari, R. Rahmanian, M. Abedi, H.S. Amoli, Urea impedimetric biosensor based on reactive RF magnetron sputtered zinc oxide nanoporous transducer, Electrochim Acta 146 (2014) 538–547. https://doi.org/10.1016/j.electacta.2014.08.105.

[187] M. de L.S. Vasconcellos, L.R.G. Silva, C.S. Lee, A.S. Fajardo, S. Garcia-Segura, J. Ribeiro, Dimensionally stable anode based sensor for urea determination via linear sweep voltammetry, Sensors 21 (2021). https://doi.org/10.3390/s21103450.

[188] Z. Zhou, L. Wang, J. Wang, C. Liu, T. Xu, X. Zhang, Machine Learning with Neural Networks to Enhance Selectivity of Nonenzymatic Electrochemical Biosensors in Multianalyte Mixtures, ACS Appl Mater Interfaces 14 (2022) 52684–52690. https://doi.org/10.1021/acsami.2c17593.

[189] H. Rezk, A.G. Olabi, M.A. Abdelkareem, E.T. Sayed, Artificial intelligence as a novel tool for enhancing the performance of urine fed microbial fuel cell as an emerging approach for simultaneous power generation and wastewater treatment, J Taiwan Inst Chem Eng (2023) 104726. https://doi.org/10.1016/j.jtice.2023.104726.

[190] J. Parab, M. Sequeira, M. Lanjewar, C. Pinto, G. Naik, Backpropagation Neural Network-Based Machine Learning Model for Prediction of Blood Urea and Glucose in CKD Patients, IEEE J Transl Eng Health Med 9 (2021) 1–8. https://doi.org/10.1109/JTEHM.2021.3079714.

[191] Z. Jiang, S. Yang, X. Chen, Q. Pang, Y. Xu, S. Qi, W. Yu, H. Dai, Controlled release urea improves rice production and reduces environmental pollution: a research based on meta-analysis and machine learning, Environmental Science and Pollution Research 29 (2022) 3587–3599. https://doi.org/10.1007/s11356-021-15956-2.

[192] H. Wang, X. Zheng, L. Fang, S. Lu, Urea Electrooxidation in Alkaline Environment: Fundamentals and Applications, ChemElectroChem 10 (2023). https://doi.org/10.1002/celc.202300138.

[193] S. Shen, B. Li, M. Li, J. Fan, Z. Zhao, Removal of urea from wastewater by heterogeneous catalysis, Desalination Water Treat 55 (2015) 70–76. https://doi.org/10.1080/19443994.2014.911116.

[194] P.O. Lee, J.A. Cherry, J.W. Edmonds, Organic Nitrogen Runoff in Coastal Marshes: Effects on Ecosystem Denitrification, Estuaries and Coasts 40 (2017) 437–446. https://doi.org/10.1007/s12237-016-0161-6.

[195] R. Ranjan, S.P. Singh, Removal of Urea and Ammonia from Wastewater, in: 2023: pp. 335–353. https://doi.org/10.1007/978-981-99-2062-4_14.

[196] E.T. Sayed, T. Eisa, H.O. Mohamed, M.A. Abdelkareem, A. Allagui, H. Alawadhi, K.-J. Chae, Direct urea fuel cells: Challenges and opportunities, J Power Sources 417 (2019) 159–175. https://doi.org/10.1016/j.jpowsour.2018.12.024.

[197] S. Nangan, Y. Ding, A.Z. Alhakemy, Y. Liu, Z. Wen, Hybrid alkali-acid urea-nitrate fuel cell for degrading nitrogen-rich wastewater, Appl Catal B 286 (2021) 119892. https://doi.org/10.1016/j.apcatb.2021.119892.

[198] W. Xu, Z. Wu, S. Tao, Urea-Based Fuel Cells and Electrocatalysts for Urea Oxidation, Energy Technology 4 (2016) 1329–1337. https://doi.org/10.1002/ente.201600185.

[199] W. Yan, D. Wang, L.A. Diaz, G.G. Botte, Nickel nanowires as effective catalysts for urea electro-oxidation, Electrochim Acta 134 (2014) 266–271. https://doi.org/10.1016/j.electacta.2014.03.134.

[200] D. Wang, W. Yan, G.G. Botte, Exfoliated nickel hydroxide nanosheets for urea electrolysis, Electrochem Commun 13 (2011) 1135–1138. https://doi.org/10.1016/j.elecom.2011.07.016.

[201] D. Wang, W. Yan, S.H. Vijapur, G.G. Botte, Enhanced electrocatalytic oxidation of urea based on nickel hydroxide nanoribbons, J Power Sources 217 (2012) 498–502. https://doi.org/10.1016/j.jpowsour.2012.06.029.

[202] L. Quadrini, S. Laschi, C. Ciccone, F. Catelani, I. Palchetti, Electrochemical methods for the determination of urea: Current trends and future perspective, TrAC Trends in Analytical Chemistry 168 (2023) 117345. https://doi.org/10.1016/j.trac.2023.117345.

[203] S. Laschi, P.S. Sfragano, F. Tadini-Buoninsegni, N. Guigues, I. Palchetti, Development of a flow system for decentralized electrochemical analysis of heavy metals using screen-printed electrodes: the importance of sensor stability, Analyst 149 (2024) 4239–4249. https://doi.org/10.1039/D4AN00616J.

[204] S.K. Vishwakarma, A. Bardia, C. Lakkireddy, N. Raju, S.A.B. Paspala, Md.A. Habeeb, A.A. Khan, Intraperitoneal transplantation of bioengineered humanized liver grafts supports failing liver in acute condition, Materials Science and Engineering: C 98 (2019) 861–873. https://doi.org/10.1016/j.msec.2019.01.045.

[205] D. Jung, H. Biggs, J. Erikson, P.U. Ledyard, New Colorimetric Reaction for End-Point, Continuous-Flow, and Kinetic Measurement of Urea, Clin Chem 21 (1975) 1136–1140. https://doi.org/10.1093/clinchem/21.8.1136.

[206] B. Lakard, D. Magnin, O. Deschaume, G. Vanlancker, K. Glinel, S. Demoustier-Champagne, B. Nysten, A.M. Jonas, P. Bertrand, S. Yunus, Urea potentiometric enzymatic biosensor based on charged biopolymers and electrodeposited polyaniline, Biosens Bioelectron 26 (2011) 4139–4145. https://doi.org/10.1016/j.bios.2011.04.009.

[207] K. Saeedfar, L. Heng, T. Ling, M. Rezayi, Potentiometric Urea Biosensor Based on an Immobilised Fullerene-Urease Bio-Conjugate, Sensors 13 (2013) 16851–16866. https://doi.org/10.3390/s131216851.

[208] A. Mulyasuryani, A. Roosdiana, A. Srihardyastutie, THE POTENTIOMETRIC UREA BIOSENSOR USING CHITOSAN MEMBRANE, Indonesian Journal of Chemistry 10 (2010) 162–166. https://doi.org/10.22146/ijc.21454.

[209] X. Chen, Z. Yang, S. Si, Potentiometric urea biosensor based on immobilization of urease onto molecularly imprinted TiO2 film, Journal of Electroanalytical Chemistry 635 (2009) 1–6. https://doi.org/10.1016/j.jelechem.2009.07.005.

[210] M. Gutiérrez, S. Alegret, M. del Valle, Potentiometric bioelectronic tongue for the analysis of urea and alkaline ions in clinical samples, Biosens Bioelectron 22 (2007) 2171–2178. https://doi.org/10.1016/j.bios.2006.10.007.

[211] B. Liu, R. Hu, J. Deng, Studies on a potentiometric urea biosensor based on an ammonia electrode and urease, immobilized on a γ-aluminum oxide matrix, Anal Chim Acta 341 (1997) 161–169. https://doi.org/10.1016/S0003-2670(96)00553-3.

[212] T. AHUJA, I. MIR, D. KUMAR, RAJESH, Potentiometric urea biosensor based on BSA embedded surface modified polypyrrole film, Sens Actuators B Chem 134 (2008) 140–145. https://doi.org/10.1016/j.snb.2008.04.020.

[213] A. Medeiros, L. Maria, M.A. Zarur Coelho, Development of Potentiometric Urea Biosensor based on Canavalia ensiformis Urease, in: Biosensors - Emerging Materials and Applications, InTech, 2011. https://doi.org/10.5772/20163.

[214] F. Bettazzi, S. Orlandini, L. Zhang, S. Laschi, M.M. Nilsen, A. Krolicka, T. Baussant, I. Palchetti, A simple and selective electrochemical magneto-assay for sea lice eDNA detection developed with a Quality by Design approach, Science of The Total Environment 791 (2021) 148111. https://doi.org/10.1016/j.scitotenv.2021.148111.

[215] L. Quadrini, E. Salvadori, S. Laschi, M. Verrucchi, A. Gnerucci, A. Cagnini, I. Palchetti, Characterization of corrosion products on contemporary bronze artwork by using voltammetry of microparticles and PCA, Microchemical Journal 200 (2024) 110330. https://doi.org/10.1016/j.microc.2024.110330.

[216] G. Hancu, S. Orlandini, L.A. Papp, A. Modroiu, R. Gotti, S. Furlanetto, Application of Experimental Design Methodologies in the Enantioseparation of Pharmaceuticals by Capillary Electrophoresis: A Review, Molecules 26 (2021) 4681. https://doi.org/10.3390/molecules26154681.

[217] E.J.N.K.-W.C.W.S.W. L. Eriksson, Design of Experiments – Principles and Applications, 3rd ed., Umetrics Academy, Umeå, 2008.

[218] Y. Umezawa, P. Bühlmann, K. Umezawa, K. Tohda, S. Amemiya, Potentiometric Selectivity Coefficients of Ion-Selective Electrodes. Part I. Inorganic Cations (Technical Report), Pure and Applied Chemistry 72 (2000) 1851–2082. https://doi.org/10.1351/pac200072101851.

[219] Standard Addition Method, (n.d.). https://facultystaff.richmond.edu/~cstevens/301/Resources/Tutorial_SAM4.pdf (accessed October 22, 2024).

[220] APAT, Istituto di ricerca sulle acque, Metodi analitici per le acque - Volume Secondo , Italia, 2003.

[221] V.A. Profillidis, G.N. Botzoris, Statistical Methods for Transport Demand Modeling, in: Modeling of Transport Demand, Elsevier, 2019: pp. 163–224. https://doi.org/10.1016/B978-0-12-811513-8.00005-4.

[222] B. Krajewska, S. Ciurli, Jack bean (Canavalia ensiformis) urease. Probing acid–base groups of the active site by pH variation, Plant Physiology and Biochemistry 43 (2005) 651–658. https://doi.org/10.1016/j.plaphy.2005.05.009.

[223] H.-H. Deng, G.-L. Hong, F.-L. Lin, A.-L. Liu, X.-H. Xia, W. Chen, Colorimetric detection of urea, urease, and urease inhibitor based on the peroxidase-like activity of gold nanoparticles, Anal Chim Acta 915 (2016) 74–80. https://doi.org/10.1016/j.aca.2016.02.008.

[224] M. Mazloum-Ardakani, M.A. Sheikh-Mohseni, Carbon Nanotubes in Electrochemical Sensors, in: Carbon Nanotubes - Growth and Applications, InTech, 2011. https://doi.org/10.5772/20604.

[225] LoQ Calculating Protocol, (n.d.). https://food.ec.europa.eu/system/files/2017-05/animal-feed-guidance_document_lod_en.pdf (accessed October 22, 2024).

[226] EFSA Guideline for ammonium in water, (n.d.). https://efsa.onlinelibrary.wiley.com/doi/pdf/10.2903/j.efsa.2012.2918#:~:text=ionised%20to%20ammonium.-,For%20ammonium%20in%20drinking%20water%2C%20an%20indicator%20parameter%20of%200.50,higher%20than%200.50%20mg%2FL. (accessed October 22, 2024).

[227] K. Marek, K. Pawęska, A. Bawiec, Treatment of Wastewater with High Ammonium Nitrogen Concentration, Journal of Ecological Engineering 22 (2021) 224–231. https://doi.org/10.12911/22998993/134079.

[228] A. Malovanyy, H. Sakalova, Y. Yatchyshyn, E. Plaza, M. Malovanyy, Concentration of ammonium from municipal wastewater using ion exchange process, Desalination 329 (2013) 93–102. https://doi.org/10.1016/j.desal.2013.09.009.

[229] I.R. Phillips, Nutrient leaching losses from undisturbed soil cores following applications of piggery wastewater, Soil Research 40 (2002) 515. https://doi.org/10.1071/SR01058.

[230] G. Johansson, L. Ögren, An enzyme reactor electrode for urea determinations, Anal Chim Acta 84 (1976) 23–29. https://doi.org/10.1016/S0003-2670(01)82834-8.

[231] M. Jurkiewicz, S. Alegret, E. Fàbregas, Comparison of flow injection analytical biosystems based on open-tube and packed-bed enzyme reactors,

Anal Chim Acta 370 (1998) 47–58. https://doi.org/10.1016/S0003-2670(98)00234-7.

[232] C. Capannesi, I. Palchetti, M. Mascini, A. Parenti, Electrochemical sensor and biosensor for polyphenols detection in olive oils, Food Chem 71 (2000) 553–562. https://doi.org/10.1016/S0308-8146(00)00211-9.

[233] T.T. Canh, M.W. Verstegen, A.J. Aarnink, J.W. Schrama, Influence of dietary factors on nitrogen partitioning and composition of urine and feces of fattening pigs., J Anim Sci 75 (1997) 700. https://doi.org/10.2527/1997.753700x.

[234] X. Dai, H. Karring, A Determination and Comparison of Urease Activity in Feces and Fresh Manure from Pig and Cattle in Relation to Ammonia Production and pH Changes, PLoS One 9 (2014) e110402. https://doi.org/10.1371/journal.pone.0110402.

[235] N. Edouard, M. Hassouna, P. Robin, P. Faverdin, Low degradable protein supply to increase nitrogen efficiency in lactating dairy cows and reduce environmental impacts at barn level, Animal 10 (2016) 212–220. https://doi.org/10.1017/S1751731115002050.

[236] B.K. Boggs, R.L. King, G.G. Botte, Urea electrolysis: direct hydrogen production from urine, Chemical Communications (2009) 4859. https://doi.org/10.1039/b905974a.

[237] S.K. Masjedi, A. Kazemi, M. Moeinnadini, E. Khaki, S.I. Olsen, Urea production: An absolute environmental sustainability assessment, Science of The Total Environment 908 (2024) 168225. https://doi.org/10.1016/j.scitotenv.2023.168225.

[238] J. Yoon, M. Sim, T.-S. Oh, Y.S. Yoon, D.-J. Kim, Flexible Electrochemical Sensor Based on NiCu(OOH) for Monitoring Urea in Human Sweat, J Electrochem Soc 168 (2021) 117510. https://doi.org/10.1149/1945-7111/ac34ca.

[239] S. Lu, Z. Gu, M. Hummel, Y. Zhou, K. Wang, B. Bin Xu, Y. Wang, Y. Li, X. Qi, X. Liu, Nickel Oxide Immobilized on the Carbonized Eggshell Membrane for Electrochemical Detection of Urea, J Electrochem Soc 167 (2020) 106509. https://doi.org/10.1149/1945-7111/ab9c80.

[240] L. Liu, H. Mo, S. Wei, D. Raftery, Quantitative analysis of urea in human urine and serum by ^{1}H nuclear magnetic resonance, Analyst 137 (2012) 595–600. https://doi.org/10.1039/C2AN15780B.

[241] D.B. Donald, M.J. Bogard, K. Finlay, P.R. Leavitt, Comparative effects of urea, ammonium, and nitrate on phytoplankton abundance, community composition, and toxicity in hypereutrophic freshwaters, Limnol Oceanogr 56 (2011) 2161–2175. https://doi.org/10.4319/lo.2011.56.6.2161.

[242] L. Quadrini, S. Orlandini, S. Laschi, C. Ciccone, F. Catelani, I. Palchetti, Development of a flow biocatalytic-based platform for electrochemical monitoring of urea in wastewater, Talanta 289 (2025). https://doi.org/10.1016/j.talanta.2025.127755.

[243] I. Palchetti, C. Upjohn, A.P.F. Turner, M. Mascini, Disposable Screen-Printed Electrodes (Spe) Mercury-Free for Lead Detection, Anal Lett 33 (2000) 1231–1246. https://doi.org/10.1080/00032710008543119.

[244] S. Laschi, P.S. Sfragano, F. Tadini-Buoninsegni, N. Guigues, I. Palchetti, Development of a flow system for decentralized electrochemical analysis of heavy metals using screen-printed electrodes: the importance of sensor stability, Analyst 149 (2024) 4239–4249. https://doi.org/10.1039/D4AN00616J.

[245] B.K. Boggs, R.L. King, G.G. Botte, Urea electrolysis: direct hydrogen production from urine, Chemical Communications (2009) 4859. https://doi.org/10.1039/b905974a.

[246] Y. Ma, C. Ma, Y. Wang, K. Wang, Advanced Nickel-Based Catalysts for Urea Oxidation Reaction: Challenges and Developments, Catalysts 12 (2022) 337. https://doi.org/10.3390/catal12030337.

[247] S. Lu, Q. Wang, L. Fang, X. Zheng, F. Yin, H. Liu, Bimetallic Platinum–Nickel Nanoparticles Modified on the Screen-Printed Electrode for Highly Sensitive Urea Determination, IEEE Sens J 24 (2024) 4221–4227. https://doi.org/10.1109/JSEN.2023.3345948.

[248] C. FENG, Z. CHEN, H. YIN, J. GONG, H. WANG, C. WANG, L. WANG, Sensitive Electrochemical Sensors for Glucose Detection Based on Ni(OH)₂/Nickel-Dimethylglyoxime Composite Nanotubes, Electrochemistry 92 (2024) 24–00018. https://doi.org/10.5796/electrochemistry.24-00018.

[249] N. Pal, S. Banerjee, A. Bhaumik, A facile route for the syntheses of Ni(OH)2 and NiO nanostructures as potential candidates for non-enzymatic glucose sensor, J Colloid Interface Sci 516 (2018) 121–127. https://doi.org/10.1016/j.jcis.2018.01.027.

[250] C.-Y. Ko, J.-H. Huang, S. Raina, W.P. Kang, A high performance non-enzymatic glucose sensor based on nickel hydroxide modified nitrogen-incorporated nanodiamonds, Analyst 138 (2013) 3201. https://doi.org/10.1039/c3an36679k.

[251] N. Ezzat, M.A. Hefnawy, S.A. Fadlallah, R.M. El-Sherif, S.S. Medany, Synthesis of nickel-sphere coated Ni-Mn layer for efficient electrochemical detection of urea, Sci Rep 14 (2024) 14818. https://doi.org/10.1038/s41598-024-64707-z.

[252] J. Yoon, Y.S. Yoon, D.-J. Kim, Silver-Nanoparticle-Decorated NiOOH Nanorods for Electrocatalytic Urea Sensing, ACS Appl Nano Mater 3 (2020) 7651–7658. https://doi.org/10.1021/acsanm.0c01279.

[253] A. Ungureanu, B. Dragoi, A. Chirieac, S. Royer, D. Duprez, E. Dumitriu, Synthesis of highly thermostable copper-nickel nanoparticles confined in the channels of ordered mesoporous SBA-15 silica, J Mater Chem 21 (2011) 12529. https://doi.org/10.1039/c1jm10971e.

[254] O. Karaagac, S. Atmaca, H. Kockar, A Facile Method to Synthesize Nickel Ferrite Nanoparticles: Parameter Effect, J Supercond Nov Magn 30 (2017) 2359–2369. https://doi.org/10.1007/s10948-016-3796-4.

[255] N.-D. Jaji, M.B.H. Othman, H.L. Lee, M.H. Hussin, D. Hui, One-pot solvothermal synthesis and characterization of highly stable nickel nanoparticles, Nanotechnol Rev 10 (2021) 318–329. https://doi.org/10.1515/ntrev-2021-0019.

[256] K. Nejati, R. Zabihi, Preparation and magnetic properties of nano size nickel ferrite particles using hydrothermal method, Chem Cent J 6 (2012) 23. https://doi.org/10.1186/1752-153X-6-23.

[257] H. Chen, J. Yan, H. Wu, Y. Zhang, S. (Frank) Liu, One-pot fabrication of NiFe 2 O 4 nanoparticles on α-Ni(OH) 2 nanosheet for enhanced water oxidation, J Power Sources 324 (2016) 499–508. https://doi.org/10.1016/j.jpowsour.2016.05.075.

[258] D. Soto, V. Serafín, M. Pedrero, J.M. Pingarrón, S. Campuzano, J. Orozco, Hierarchical Au@Pt nanoparticle/amino benzoic acid polymer-based hybrid material for labeled and label-free detection of interleukin-6: a comparative assessment, Microchimica Acta 191 (2024) 683. https://doi.org/10.1007/s00604-024-06745-y.

[259] D. Voccia, F. Bettazzi, G. Baydemir, I. Palchetti, Alkaline-Phosphatase-Based Nanostructure Assemblies for Electrochemical Detection of microRNAs, J

Nanosci Nanotechnol 15 (2015) 3378–3384.
https://doi.org/10.1166/jnn.2015.10201.

[260] A.B. Steel, T.M. Herne, M.J. Tarlov, Electrochemical Quantitation of DNA Immobilized on Gold, Anal Chem 70 (1998) 4670–4677.
https://doi.org/10.1021/ac980037q.

[261] Y. Zeng, S. Xiang, S. Lu, X. Qi, Structural Design of Nickel Hydroxide for Efficient Urea Electrooxidation, Materials 17 (2024) 2617.
https://doi.org/10.3390/ma17112617.

[262] X. Wang, J. Li, Y. Duan, J. Li, H. Wang, X. Yang, M. Gong, Electrochemical Urea Oxidation in Different Environment: From Mechanism to Devices, ChemCatChem 14 (2022). https://doi.org/10.1002/cctc.202101906.

[263] G.F. de Oliveira, J.C. de Souza, J.L. da Silva, M.V. Boldrin Zanoni, Non-Enzymatic Electrochemical Sensor Modified by Nickel Nanoparticles for Urea Determination in Biological Fluids, Processes 13 (2025) 1306.
https://doi.org/10.3390/pr13051306.

[264] G. Mukundan, S. Badhulika, Nickel-cobalt metal-organic frameworks based flexible hydrogel as a wearable contact lens for electrochemical sensing of urea in tear samples, Microchimica Acta 191 (2024) 252.
https://doi.org/10.1007/s00604-024-06339-8.

[265] M. Tyagi, M. Tomar, V. Gupta, NiO nanoparticle-based urea biosensor, Biosens Bioelectron 41 (2013) 110–115.
https://doi.org/10.1016/j.bios.2012.07.062.

[266] S. Lu, Z. Gu, M. Hummel, Y. Zhou, K. Wang, B. Bin Xu, Y. Wang, Y. Li, X. Qi, X. Liu, Nickel Oxide Immobilized on the Carbonized Eggshell Membrane for Electrochemical Detection of Urea, J Electrochem Soc 167 (2020) 106509. https://doi.org/10.1149/1945-7111/ab9c80.

[267] J.-C. Chou, C.-Y. Wu, P.-Y. Kuo, C.-H. Lai, Y.-H. Nien, Y.-X. Wu, S.-H. Lin, Y.-H. Liao, The Flexible Urea Biosensor Using Magnetic Nanoparticles, IEEE Trans Nanotechnol 18 (2019) 484–490.
https://doi.org/10.1109/TNANO.2019.2895137.

La borsa di dottorato è cofinanziata con risorse dell'Unione europea – *NextGenerationEU*
Piano Nazionale di Ripresa e Resilienza – Missione 4 – Componente 2 "Dalla ricerca all'impresa" – Investimento 3.3 "Introduzione di dottorati innovativi che rispondono ai fabbisogni di innovazione delle imprese" – D.M. 352/2022
CUP: B12B22000660007